Schlumberger
Carbon Services

Kevin Dome
Static Model Development Final Report

Wade Zaluski

16 February 2018

CS1801-005-WZ

Any interpretation, research, analysis, data, results, estimates, or recommendation furnished with the services or otherwise communicated by Schlumberger to the customer at any time in connection with the services are opinions based on inferences from measurements, empirical relationships and/or assumptions, which inferences, empirical relationships and/or assumptions are not infallible, and with respect to which professionals in the industry may differ. Accordingly, Schlumberger cannot and does not warrant the accuracy, correctness or completeness of any such interpretation, research, analysis, data, results, estimates or recommendation. Customer acknowledges that it is accepting the services "as is", that Schlumberger makes no representation or warranty, express or implied, of any kind or description in respect thereto. Specifically, customer acknowledges that Schlumberger does not warrant that any interpretation, research, analysis, data, results, estimates, or recommendation is fit for a particular purpose, including but not limited to compliance with any government request or regulatory requirement. Customer further acknowledges that such services are delivered with the explicit understanding and agreement that any action taken based on the services received shall be at its own risk and responsibility and no claim shall be made against Schlumberger as a consequence thereof.

Table of Contents

1 Executive Summary

As one of seven Regional Carbon Sequestration Partnerships, the Big Sky Carbon Sequestration Partnership (BSCSP) is supported through a cooperative agreement with the U.S. Department of Energy (DOE). BSCSP's goal is to demonstrate that Kevin Dome is a safe and viable location for the long-term storage of carbon dioxide (CO_2).

One component of this project was the continued development of a geomodel that was used to characterize the CO_2 storage complex. A geomodel was developed to represent the Upper Duperow (seal), the Middle Duperow (reservoir), overlying formations and underlying formations. Schlumberger Carbon Services was contracted to develop this geological model of Kevin Dome and the surrounding region. This geomodel used well data, well fracture interpretation, core, 2D seismic, 3D seismic and 3D seismic inversion products to statistically map the lateral heterogeneity of porosity and permeability within the storage complex. Now that the geomodel is completed, it is to be used as the primary input for reservoir simulations of CO_2 migration in the Duperow.

The purpose of this report is to summarize the geomodeling work completed in 2017 for the BSCSP, which will be used to support reservoir engineering efforts that is being conducted by BSCSP project partners. Petrel* E&P software platform is a key component for site characterization throughout the Kevin Dome geological modeling. This report focuses on data and processes used to develop the BSCSP geomodel, the challenges encountered, and the solutions that were applied.

2 Site Location and Geology

2.1 Site Location

The Kevin Dome Project is in northern Montana (Figure 1). The projects objective was to inject up to one million tonnes of CO_2 into the regionally extensive Duperow carbonate formation. The project infrastructure includes a CO_2 production well (Danielson) that was to produce CO_2 from a natural accumulation in the Duperow. The CO_2 would have been transported via pipeline to the CO_2 injection well (Wallewein) where it was to be injected into the Duperow Formation. The projects injection plan was cancelled primarily because there was insufficient CO_2 that could have been produced from the Duperow formation and because the water quality at the injection well was considered to be fresh.

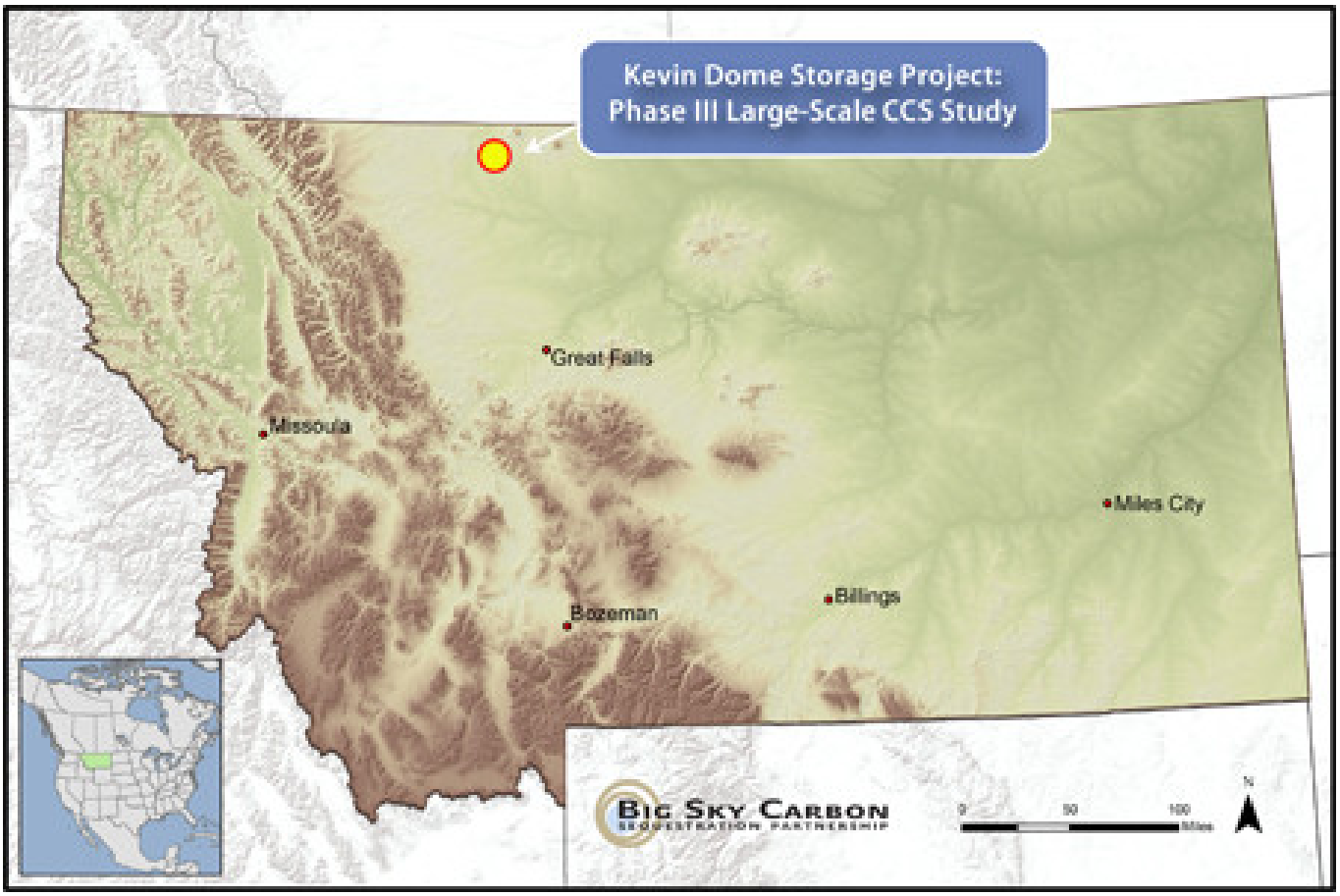

Figure 1: Site location

2.2 Geology

Figure 2 is a stratigraphic column of the Kevin Dome area. The injection formation is the Middle Duperow (limestone/dolomite) with the overlying caprock being the Upper Duperow (dolomite), Nisku (dolomite), and Potlach (anhydrite).

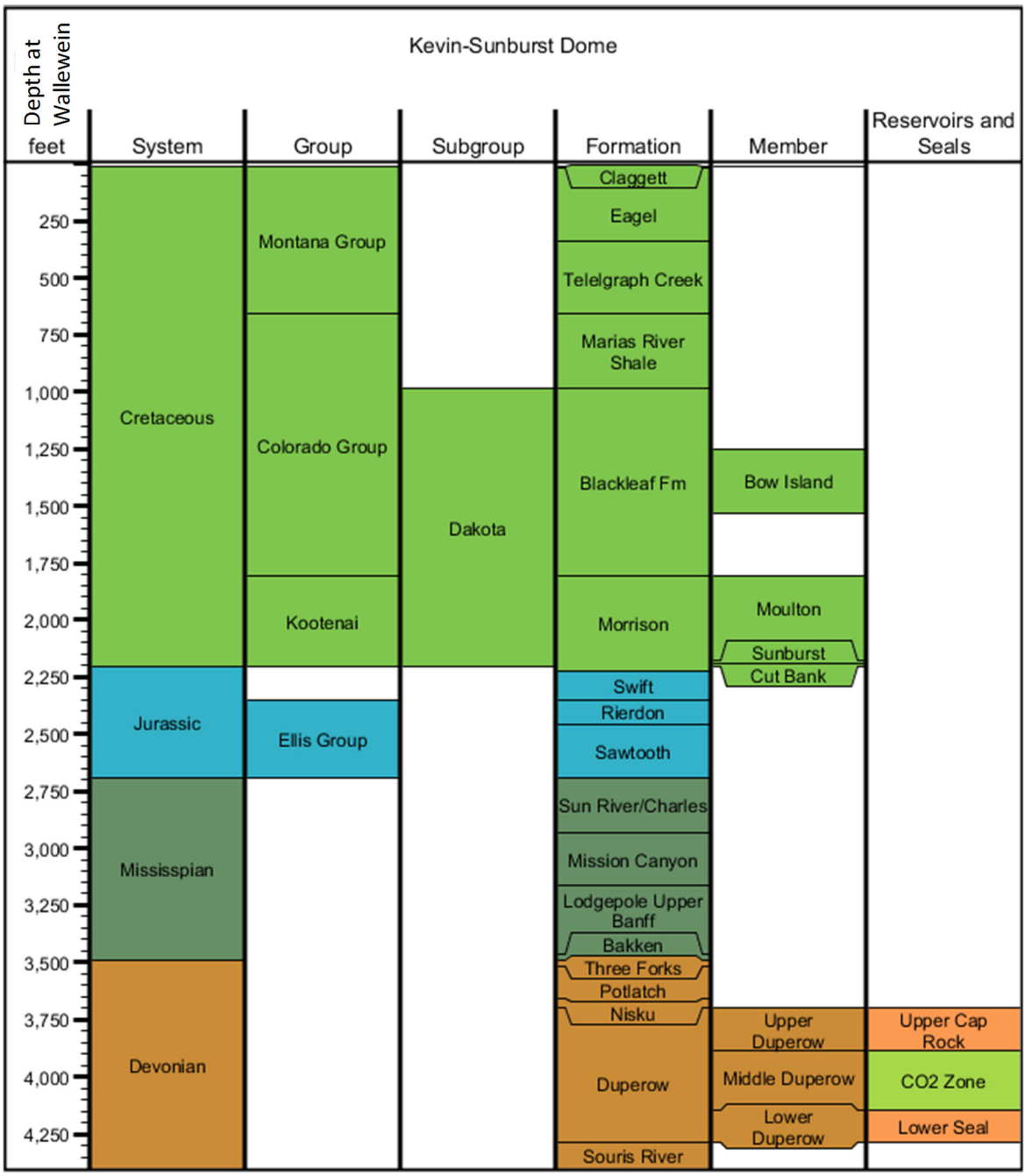

Figure 2: Stratigraphic column

3 Geomodel Framework

3.1 Geomodel Versions

Montana State University (MSU) requested that Schlumberger Carbon Services construct a geomodel for a large regional area and then a version of the model with refined detail closer to the Wallewein injector well. A geomodel was developed using Petrel* which was used to incorporate available well and seismic data. There are three different versions of the geomodel associated with the Kevin Dome Project as summarized in the following points, Figure 3 and in Table 1.

Geomodel Version 1

- Geomodel Version 1 was a preliminary model that incorporated all data available in late 2014.
- This model was built to cover a larger regional area.
- This was to be a preliminary version of the model until the 3D seismic data could be incorporated.
- The horizontal extent of the model is 64 miles east to west and 44 miles north to south.
- Porosity and permeability interpolation was based only on variogram analysis from the upscaled well logs.
- Geomodel Version 1 was delivered to MSU in 2015.

Geomodel Version 2

- Geomodel Version 2 includes model development as of January 2017 when it was delivered. Geomodel Version 2 was generated and developed based on the framework from Geomodel Version 1.
- The horizontal extent of the model is based on the limits of the 3D seismic footprint, which is six miles in the east west direction and eight miles in the north south direction (Figure 3). This extent was considered as suitable for modeling the simulated injection around the Wallewein well.
- The purpose of Geomodel Version 2 was to incorporate depth window averaged map based elastic attributes (P-impedance, S-impedance, and density) from the 3D seismic survey (shown in Table 2), updated well tops, and open fractures into the model. The interpolation of porosity for Geomodel Version 1 was based only on variogram analysis from the upscaled well logs. This was useful at the time; however, much was unknown about the spatial variation of porosity between the wells. When the map based seismic inversion attributes became available, they were used to guide the interpolation of porosity and fracture intensity within the model domain. Two methods of porosity interpolation were completed for this project.
    - The first method used extracted variogram parameters from the 3D seismic elastic inversion products to guide the porosity interpolation.
    - The second method (Section 4.6) used a lithology analysis and prediction rock physics based workflow that integrates well logs, seismic inversion, and geological modeling to provide an estimate of the most probable lithology in the inter-well geologic model space, and the likelihood associated with the prediction. Litho analysis is a fully Bayesian approach that integrates different measurements at different scales.

Geomodel Version 3

- Geomodel Version 3 which is the final high-resolution version of the model was delivered in December 2017. It incorporates the above described items; however, this version is much improved because it includes the integration of 3D elastic attributes (P-impedance, S-impedance, and density). The higher resolution seismic scale model is also extended to a 20km*20km model domain centered at the Wallewein injection well. In Geomodel Version 2, the elastic properties were 2D map based averages, the 3D attributes provided vertical resolution that greatly improves the models detail.
- During the development of Geomodel Version 2, the TWT 3D seismic data revealed vertical features that likely are related to faulting. These features could not be added into Geomodel Version 2 because the depth converted 3D seismic data set was not available. Vecta Oil and Gas provided the 3D data set and the 3D TVD elastic attributes (P-impedance, S-impedance, and density) in 2017. With these data available, these potential faulting features were incorporated into the model.

- Two versions of porosity and permeability were generated based on two different facies models. The first facies model, originally as part of Geomodel 2, uses a 3-Rock Type facies classification (dolomite, calcite and anhydrite). The second method (8-Rock Type) uses an 8 class depositional environment classification core log which was provided by Dave Bowen. A version of the 8-Rock Types models was also generated that excludes the integration of the elastic of 3D elastic attributes and uses only the variogram ranges to interpolate properties between the wells.
- Because there was uncertainty with regards to the interpreted faults, a version of the model without the faults was generated. The surfaces, lithology prediction workflow and fracture model without the faults were all regenerated without the faults. This can be used for reservoir simulations to generate a no fault scenario.
- A coarser resolution model was also generated that extrapolates the facies, porosity, permeability and fracture properties from the detailed model domain to cover the Kevin Dome. The surface area of the model covers the Kevin Dome limited to the spill point of the Intermediate Duperow. This coarser model only covers the Middle Duperow and Middle Duperow_B and contains only a million cells.

Table 1: Kevin Dome geomodel versions

Geomodel Version	Elemental Analysis	Well Tops	2D Seismic	3D Seismic	East to West Dimension	Fracture model	Facies, Porosity and Permeability Interpolation	Delivered
Geomodel Version 1	35 wells	MSU Well Tops	15 lines	4 horizons	64 miles by 44 miles (orange polygon Figure 3)	No	Interpolates using variograms from well logs	Jan 2015
Geomodel Version 2	8 wells	Updated Well tops	Lines not in model domain	4 extended horizons	6 miles by 8 miles (blue polygon Figure 3)	yes	Interpolates with the 3 facies class method (Section 4.6) and uses only depth window averaged map based seismic inversion products	Jan 2017
Geomodel Version 3 Seismic Scale (high resolution)	8 wells	Updated Well tops	Lines not in model domain	4 extended horizons	20 km by 20km (purple polygon Figure 3)	Yes. Uses 3D seismic inversion products for fracture driver	Interpolates porosity with the 3 Rock Type method and the 8-Rock Type method (Section 4.6). These methods use the full 3D elastic property based seismic inversion products	Dec 2017
Geomodel Version 3 Kevin Dome Scale (low resolution)	35 wells	Updated Well tops	15 lines	4 extended horizons	Limited to the spill point of the Intermediate Duperow. 39 miles by 42 miles (red polygon Figure 3)	Yes	Interpolates based on the geostatics of the seismic scale model	Dec 2017

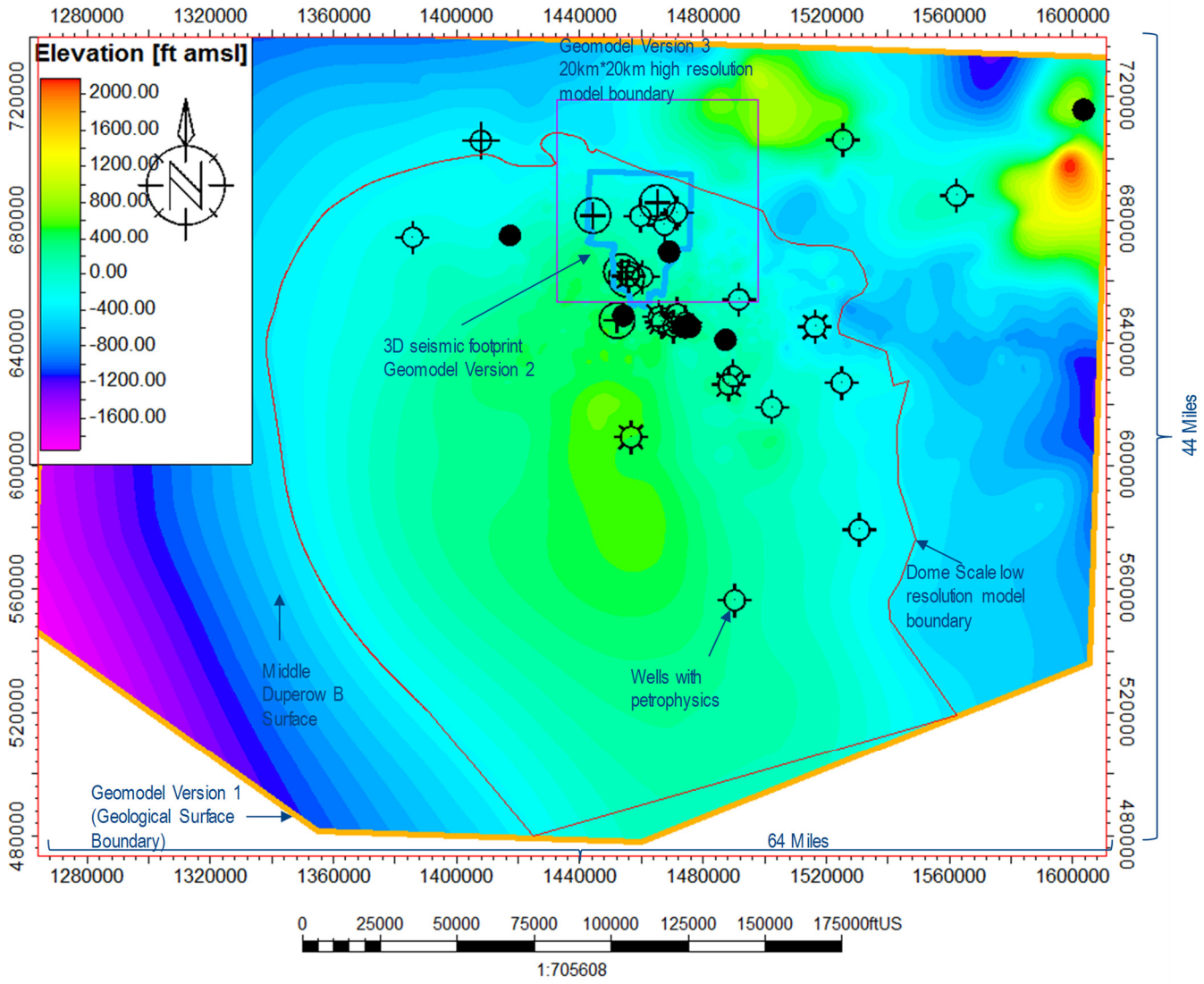

Figure 3: Model Domains

3.2 Input data

3.2.1 Well Data

To develop the geological model up to and including Geomodel Version 3, the following well data were used:

- Well location data for 2,038 wells with X, Y and Z locations (Figure 4).
- MSU geologist Dave Bowen provided a list of well tops personally picked for the Danielson, Wallewein, and surrounding key wells.
- Well log data wells (gamma ray, resistivity, neutron, density etc.).
- Core plug analysis (porosity and permeability) data from the Wallewein and Danielson.
- ELAN Elemental Analysis was completed on 35 wells (porosity, permeability, lithology fraction etc.) (Black symbols in Figure 3).
- On the Danielson and Wallewein, FMI* fullbore formation microimager logs were used to understand sedimentary bedding planes, associated facies, and fractures.
- Sonic Scanner* acoustic scanning platform was run in the Danielson and Wallewein to understand the mechanical properties of the formations.
- Vecta Oil and Gas synthesized and supplied dipole sonic log data from wells Pace 11-28 and Midland_10.
- As part of a seismic well tie process, Vecta Oil and Gas supplied the time-depth relationships (TDR) used for the Wallewein, Danielson, Pace 11-28 and Midland_10.
- MSU geologist Dave Bowen produced an 8 class depositional environment interpretation log along the available slabbed core.

3.2.2 Seismic Survey Data

To develop the geological model up to and including Geomodel Version 3, the following 2D and 3D seismic data were incorporated (Table 2).

Table 2: Seismic surveys

Seismic Survey	
2D Seismic	Fifteen 2D seismic surveys were made available by MSU (Figure 4). These surveys were in the depth domain. Once imported into the model, the Madison, Potlach, Middle Duperow and Cambrian were interpreted by Schlumberger and used in formation surface modeling.
3D Seismic	A 3D 9-component seismic survey was conducted over the site (Figure 4). Vecta Oil and Gas processed the data and provided the following data to be used in the geological model construction: • Two-way-time (TWT) and true-vertical-depth (TVD) interpretation of the Bow Island, Swift, Potlach and Intermediate Duperow. • 3D TWT seismic volume in SGY format. • 3D TVD seismic volume in SGY format (made available in early 2017) • 3D TVD elastic attributes (P-impedance, S-impedance, and density) (made available in early 2017)

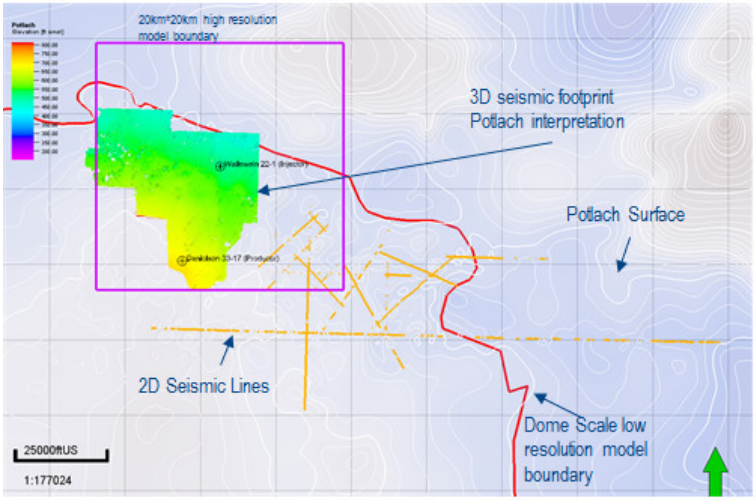

Formation (Zone)	Number of Well Tops	3D Seismic Interpretation	2D Seismic Interpretation
Blackleaf	952		
Bow_Island	1264	Bow_Island	
Kootenai	1398		
Sunburst	1526		
Morrison_Fm	1639		
Swift	1612	Swift	
Rierdon	1625		
Sawtooth	1330		
Madison	647		Madison
Banff_Fm_Lodgepole	105		
Bakken	108		
Three_Forks	110		
Potlatch	110	Potlatch	Potlatch
Nisku	110		
Upper_Duperow	105		
Middle_Duperow	47		Middle_Duperow
Middle_Duperow_B	12		
Intermediate_Duperow	39	Intermediate_Duperow	
Lower_Duperow	36		
Souris_River	26		
Cambrian	14		Cambrian
Precambrian	8		

Figure 4: Available Data

3.3 Structural and Stratigraphic Framework

The following section describes the process used to generate formation horizons used as the structural and stratigraphic framework for the petrophysical model at the time of the development of Geomodel Version 3. MSU requested that formation surfaces be modeled from the surface down to the Precambrian basement. Generating formation surfaces for the model area was challenging because the high number of wells (2,338) and incomplete or inconsistent formation top lists required an automated approach. Only 35 of these wells had log data to interpret formation tops. 2D and 3D seismic data were also used to generate formation surfaces.

The surface generation process began using well tops provided by Dave Bowen in 2016 as template to interpret the well tops for offset wells around the 3D seismic survey area. Surfaces were generated using these well tops and seismic interpretation, where available. Because of gaps in well top data and the lack of wells penetrating deeper formations, surface correction approaches were used to fill in data gaps. The following two steps describe the workflow that was used to generate representative surfaces.

1. Formation surfaces were generated using available well tops and seismic interpretation (Figure 4). Surfaces are generated upward from the Madison Formation trending the surface to the underlying formation. Surfaces were generated down from the Madison Formation trending the surface to the overlying formation. This trending process helps capture any known structural variation observed in overlying or underlying formations.
2. Surfaces are generated from Step 1; however, they are not representative of the actual structure because there are many places where surfaces cross one another. For deeper formations such as the Souris River, there are less than 30 well

tops; therefore, there was not enough data to properly generate a surface that reflected the actual structure under the Kevin Dome.

   a. To solve these problems at each well, isochore points were generated for each formation. The minimum thickness observed from all of the well tops was extracted.
   b. Using the formation surfaces from Step 1, isochore maps were generated. Where these isochore maps were less than the minimum thickness extracted from the point well data, the isochore maps were replaced with that value. This method assumes that this is the minimum thickness of each formation in the area.
   c. Surfaces were re-generated by taking the formation surface and adding the isochore map below to generate the surface for the underlying formation.
   d. This process is repeated for each formation.

3. The 3D seismic data revealed vertical features that likely are related to faulting (Figure 5). These potential faulting features (blue) reach up above the Potlach and could be conduits for upward fluid migration. These faulting feature can be seen in the edge detection attribute on the seismic horizon interpretations. These faults were incorporated into the surface generation process.
4. A digital elevation model, provided by Dave Bowen was also incorporated into the model (Figure 6).

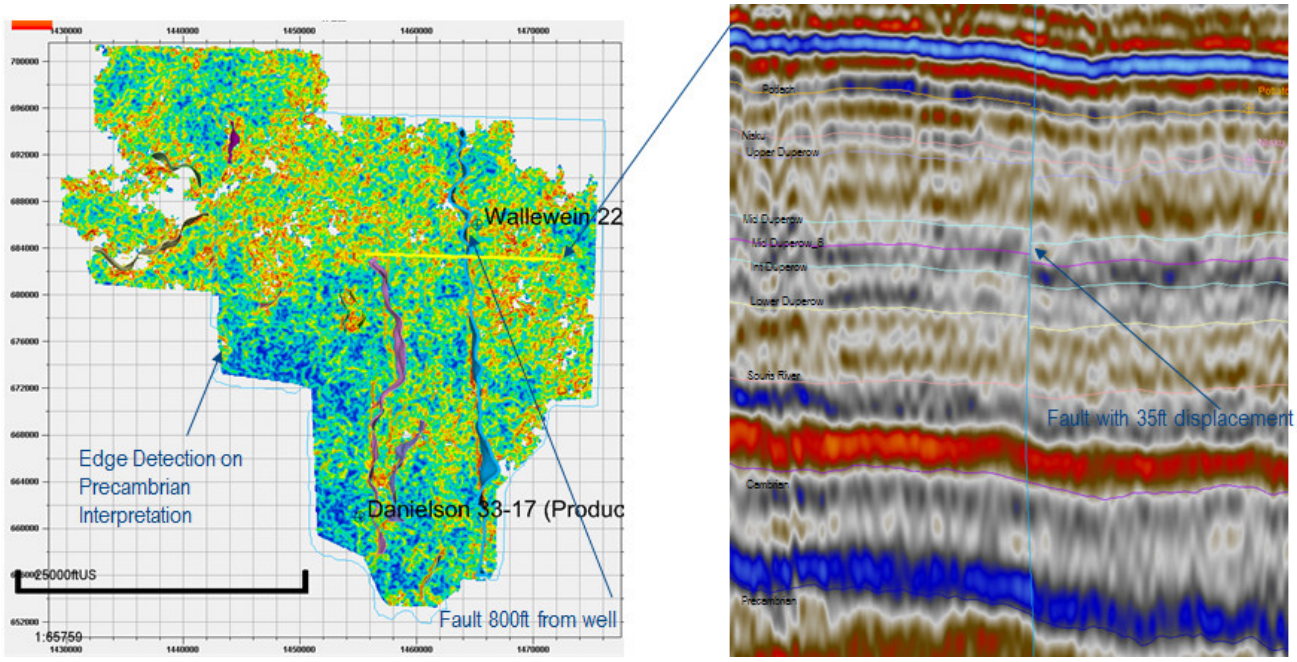

Figure 5: Observed faulting in the 3D Seismic.

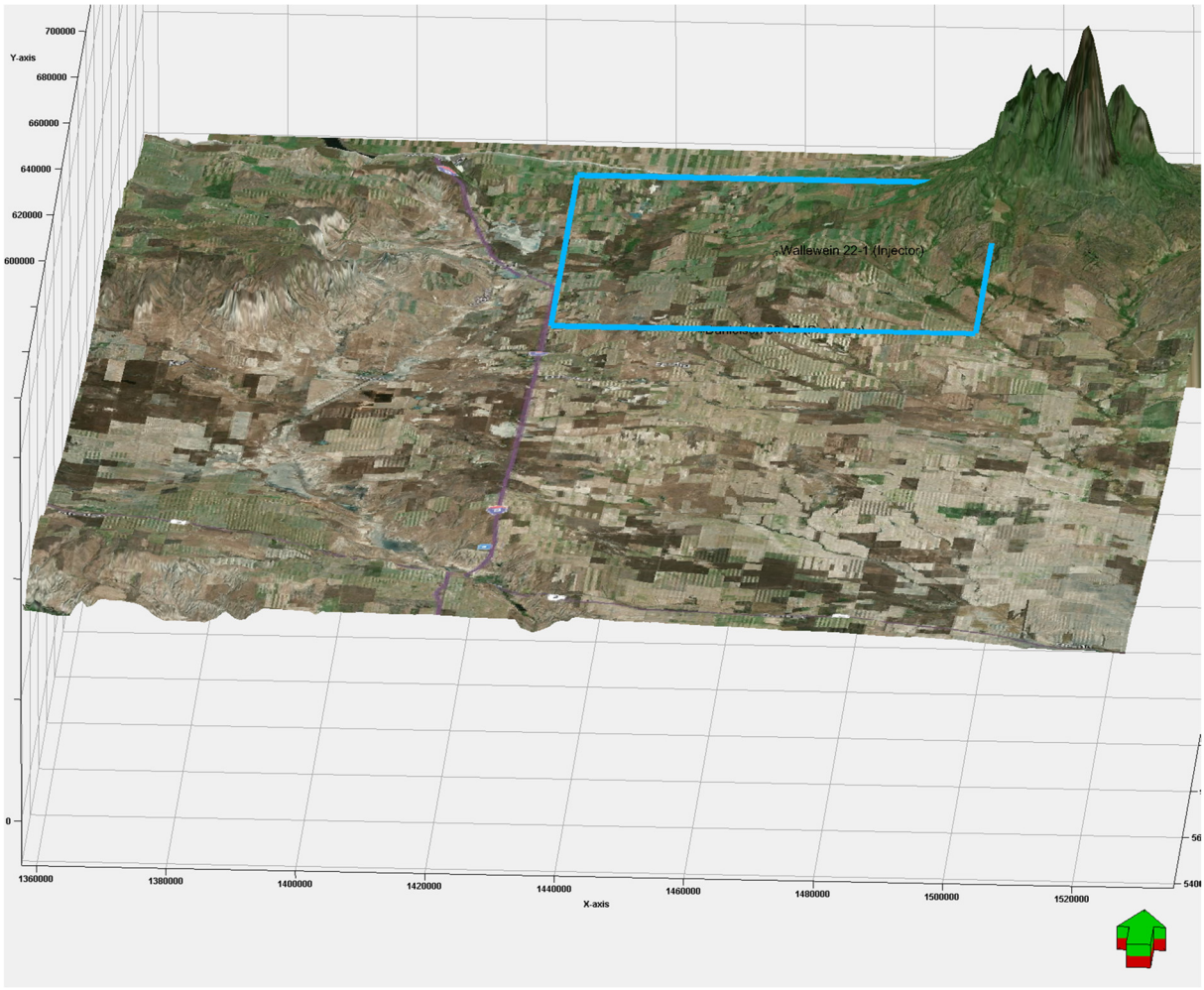

Figure 6: Digital elevation model of the ground surface

4 Geomodel 3 Property Modeling Seismic Scale Model

Geomodel Version 3 was generated in 2017 and was developed based on the framework from Geomodel Version 1 and Geomodel Version 2. The purpose of Geomodel Version 3 was to incorporate elastic 3D attributes (P-impedance, S-impedance, and density) from the 3D seismic survey and open fractures into the model. The interpolation of porosity for Geomodel Version 1 was based only on variogram analysis from the upscaled well logs. Geomodel Version 2 used depth window averaged elastic attributes. This was useful at the time; however, much was unknown about the spatial variation of porosity between the wells. When the 3D seismic inversion attributes became available, they were used to guide the spatial variation interpolation of porosity and fracture intensity within the model domain.

4.1 Geocellular Grid Development

Geomodel Version 3 has a horizontal cell size of 300ft by 300ft and was created for the formations listed following (Table 3). The formation surfaces were used to make model zones and were layered as outlined in Table 3 (Figure 7 and Figure 8). The horizontal extent of the model is 20km*20km. This extent was considered as a suitable for modeling around the simulated injection around the Wallewein. As mentioned above, potential faults were observed during the development of Geomodel Version 2. These 11 faults were incorporated into the model into Geomodel Version 3.

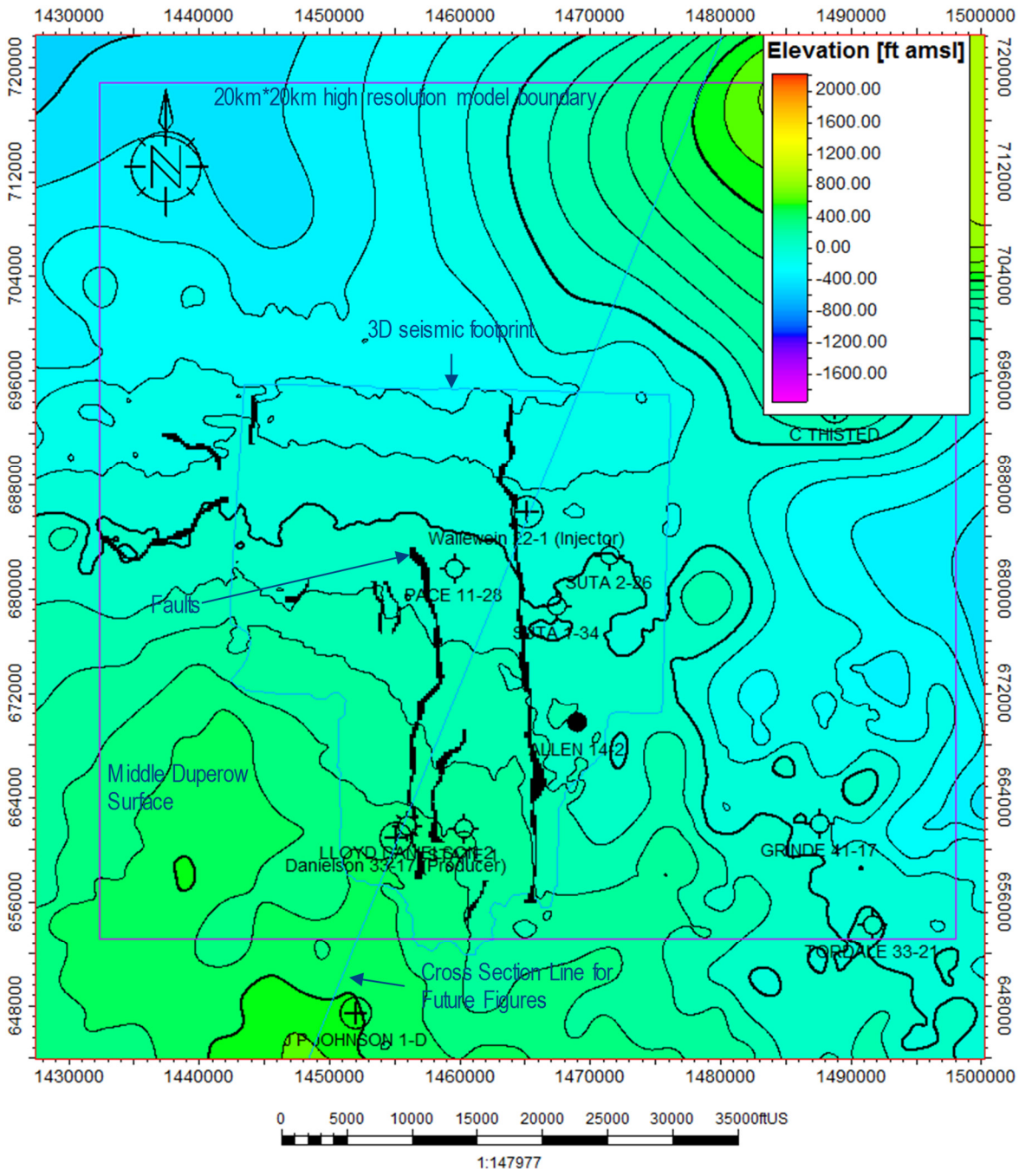

Figure 7: Extent of Geomodel Version 3

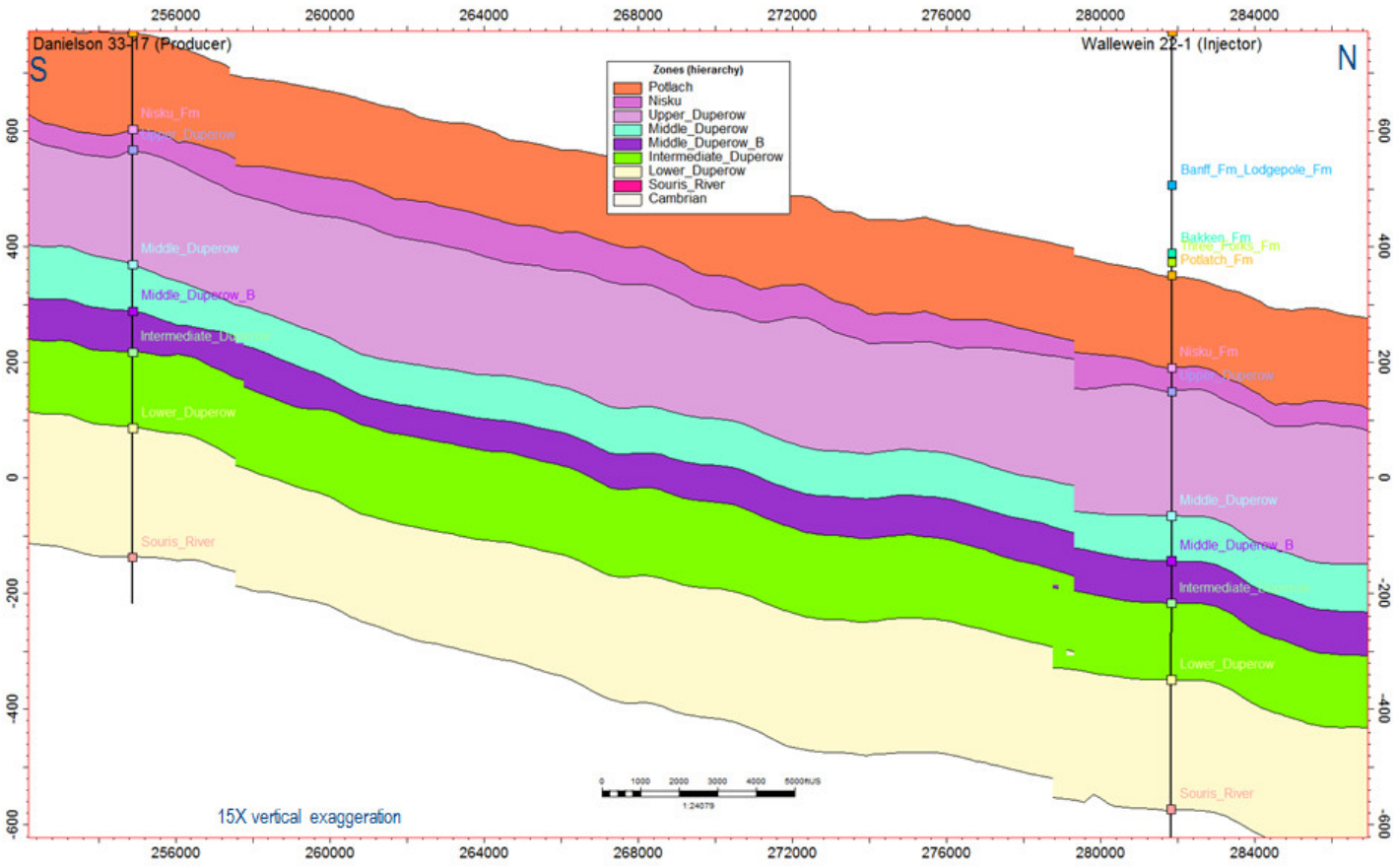

Figure 8: Modeled zones in Geomodel Version 3. View from east. Cross section line indicated on Figure 7.

Table 3: Geomodel formation layering

Zones	Layer Thickness (ft)
Carlile_Fm	Not modeled as properties. Model surfaces only
Blackleaf_Fm	
Bow_Island_Mbr	
Kootenai_Fm	
Sunburst_Mbr	
Morrison_Fm	
Swift_Fm	
Rierdon_Fm	
Sawtooth_Fm	
Madison_Grp	
Banff_Fm_Lodgepole_Fm	
Bakken_Fm	
Three_Forks_Fm	
Potlatch_Fm	4
Nisku_Fm	4
Upper_Duperow	4
Middle_Duperow	3
Middle_Duperow_B	3
Intermediate_Duperow	3
Lower_Duperow	4
Souris_River	Not modeled as properties
Cambrian	

4.2 Petrophysical Property Modeling Workflow Overview

An essential feature of the petrophysical model is the requirement for properties (porosity and permeability) to be distributed in a geologically and statistically reasonable fashion. The following steps describe the workflow used to generate the final property model. There were two versions of the properties (facies, porosity and permeability) generated for Geomodel 3. Before porosity and permeability properties were generated, a facies log representing facies types was predicted along the Danielson and Wallewein wells. The relationship of elastic properties (P-impedance, S-impedance, and density) between the seismic and the well logs was used to predict facies types in the interwell space using a Bayesian estimator. This was used to generate a facies model in model space which was used to more reliably model the porosity and permeability of each facies type. Two versions of porosity and permeability were generated based on two different facies models (3-Rock Type and 8-Rock Type models). The first facies model, originally as part of Geomodel 2, uses a 3-Rock Type facies classification (dolomite, limestone and anhydrite) which was generated from well logs using an unsupervised neuralnet process. The second method incorporates the 8 class depositional environment core logs, made available during the development of Geomodel 3. A supervised neuralnet process used the well logs to predict depositional environments in the wellbore where core is absent. This 8-Rock Type method is better tied to geology instead of the 3-Rock Type model which is the result of an unsupervised neuralnet process.

1. **Neuralnet Calculation of Rock Type:**
    - 3-Rock Type Method: Using an unsupervised neuralnet process, petrophysical logs were used to calculate a discreet log of the three dominate rock types (dolomite, limestone and anhydrite). This log was upscaled into the model grid.
    - 8-Rock Type Method: Supervised to the depositional environment core log provide by Dave Bowen, a neuralnet process used petrophysical logs to calculate a discreet log of the 8 dominate depositional environments. This log was upscaled into the model grid
2. **Upscale Effective Porosity and Permeability:** Effective porosity and permeability logs from all eight wells within the model area were upscaled into the grid.
3. **Upscale 3D Seismic Attributes and Variogram Analysis**: 3D seismic attributes consisting of P-impedance, S-impedance, and density were upscaled into the grid. Variogram analysis was completed on the P-Impedance property. A variogram is a primary parameter used in geostatistical property modeling to describe the natural variations in the property.
4. **Quantitative Integration Seismic Inversion Attributes for Lithology Classification and Porosity Estimation:** A Litho Analysis and Prediction rock physics based lithology prediction workflow was used to integrate well logs, seismic inversion, and geological modeling data together to provide an estimate of the most probable lithology in the inter-well geologic model space, and the likelihood associated with the prediction (probability property). This process was used on both a 3-Rock Type Model and an 8-Rock Type Model.
5. **Facies Modeling:**
    - 3-Rock Type Method: Sequential Indicator Simulation was used to interpolate the 3-dominant rock types (dolomite, limestone and anhydrite) throughout the model domain. These interpolation methods use the probability properties generated in Step 4.
    - 8-Rock Type Method: Sequential Indicator Simulation was used to interpolate the 8-dominant depositional environment lithofacies. These interpolation methods use the probability properties generated in Step 4.
6. **Effective Porosity and Permeability Modeling:**
    - 3-Rock Type Method: Using geostatistics from the variogram analysis, Gaussian Random Function Simulation (GRFS) was used to interpolate effective porosity within each of the 3 dominant rock types as well as to interpolate permeability co-krigged to effective porosity.
    - 8-Rock Type Method: Using geostatistics from the variogram analysis, GRFS was used to interpolate effective porosity within each of the 8-dominant depositional environment lithofacies as well as to interpolate permeability co-krigged to effective porosity.
7. **Quality Control:** Effective porosity and permeability properties were cross-plotted to ensure that there was a reasonable relationship. Histograms were analyzed to check for consistency between input data and the output properties.

4.3 Neuralnet Calculation of Rock Type Log

The number and definition of litho classes to be used in the Litho Analysis and Prediction workflow (Section 4.6) are a function of multiple factors, such as;

- Geology: What distinct geologic facies or lithologies are present?
- Petrophysical log characteristics: How well may the distinct facies be differentiated with the available logs?

- The number of degrees of freedom available for classification: The number of litho types, which may be uniquely classified, is limited (at best) to the number of elastic properties available for classification.

Two versions of rock type logs were generated. The 3-Rock Type facies classification (dolomite, limestone and anhydrite) was generated from well logs using an unsupervised neuralnet process. The second 8-Rock Type method uses an 8 class depositional environment classification core log in a supervised neuralnet process.

4.3.1 Neuralnet Calculation of 3-Rock Type Log

Although litho classifications may be determined through manual interpretation of well logs for the 3-Rock Types (dolomite anhydrite and limestone), such interpretation is time consuming, subjective, and suffers from poor repeatability. Litho classes were determined through statistical analysis of the five mineral fraction logs using K-means based cluster analysis in which a litho class is defined on the basis of statistical similarity of attribute (log) characteristics. Cluster analysis applied to mineral fraction logs is the task of grouping log samples at each measured depth in such a way that log samples from each of the five mineral fraction logs in the same cluster or class are more similar to each other than to those in other clusters or classes. Cluster analysis is referred to as an “unsupervised” process because the result is purely statistical grouping which, as a result, may or may not reflect actual geologic facies.

For litho classification using seismic inversion, the maximum number of input elastic properties is three (Ip, Is, density, or combinations). Fortunately, inspection of mineral fractions suggests that the geologic section may be largely characterized by three “classes” distinguished by dominance of anhydrite, limestone, and dolomite. Given the very low level of gas present (Figure 9) and the similarity between the two wells available for cluster analysis the gas saturation will be assumed constant and below the resolution for this analysis.

Figure 9 shows anhydrite, dolomite, and limestone mineral fraction logs along with the discrete litho class log created through unsupervised classification using all five mineral fraction logs but constrained to output three litho classes (anhydrite, dolomite, and limestone) using a 10% error limit and 0.9 probability threshold. The cluster analysis is detecting clusters around the three dominant mineral fractions (anhydrite, dolomite, and limestone). Although these classes are purely statistical and are not constrained by geologic interpretation they clearly represent dominant mineral fractions and will hereafter be referred to as “anhydrite”, “dolomite”, and “limestone”. Also shown are the probability estimates for each litho class. This 3-Rock Type log was generated on eight wells within the model domain and was upscaled into the grid. The eight wells upscaled were Wallewein, Danielson, LLLOYD Danielson 2, Allen 14-2, State_1, Suta 1-34, Suta 2-26 and Pace 11-28 (Figure 10).

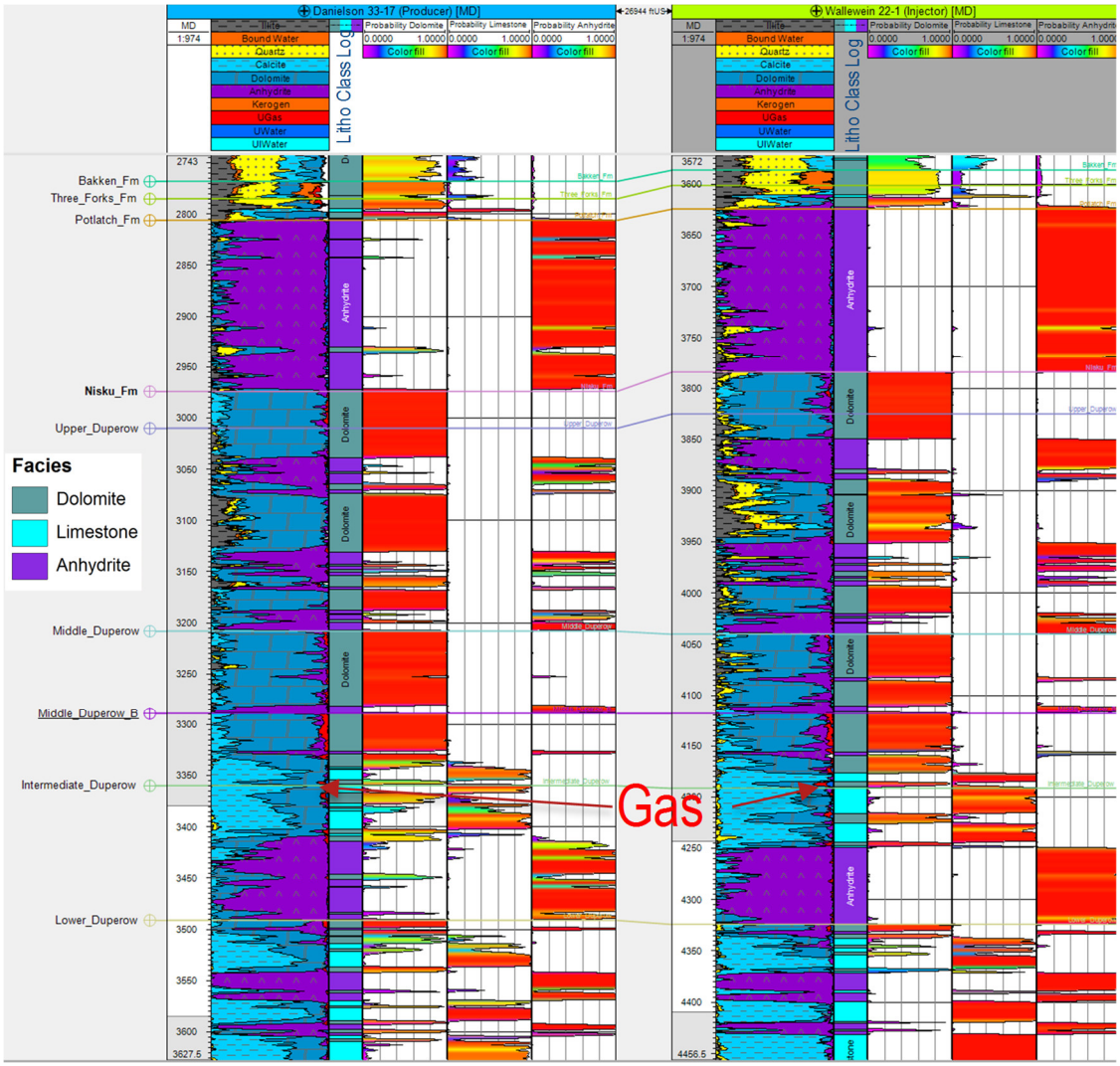

Figure 9: ELAN analysis with 3-Rock Type discrete litho-class log from cluster analysis and probability estimates for each class.

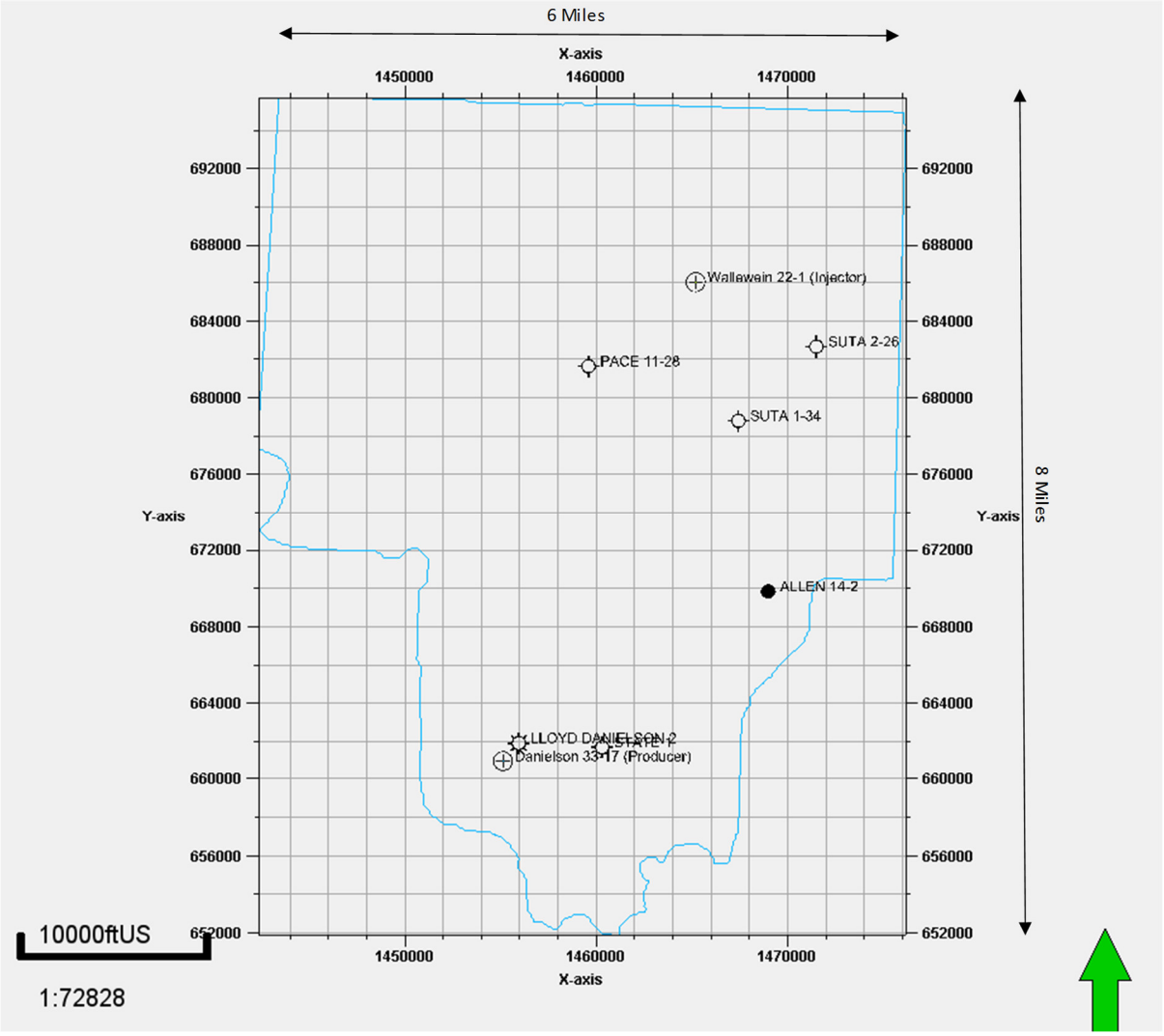

Figure 10: Wells with upscaled rock type, effective porosity and permeability

4.3.2 Neuralnet Calculation of 8-Rock Type Log

There were 8 depositional environments as identified with core logging Dave Bowen completed on the Wallewein and Danielson core (Figure 11). This is very detailed geological information that was not available using the above described 3-Rock Type unsupervised neuralnet method. Using the ELAN analysis, a neuralnet process, supervised to the 8 depositional environment core log, was used calculate a discreet 8-Rock Type log of the dominate depositional environments within each of the wells (Figure 12). The process of "calibrating" classification to geologic interpretation is referred to as "supervised" classification. The match between the predicted depositional environment and the actual depositional environment core log resulted in a reliable match as indicated by the histogram in Figure 13. Figure 14 shows the statistics for depositional environment thicknesses. The Slope and Basin environments were not able to be predicted because the core log data itself was at such a low percentage; therefore, only 6 of the 8 depositional environment logs were used for facies modeling. This discreet 8-Rock Type log was upscale into the model grid. This was completed on eight wells within the model domain were upscaled into the grid. The eight wells upscaled were Wallewein, Danielson, LLLOYD Danielson 2, Allen 14-2, State_1, Suta 1-34, Suta 2-26 and Pace 11-28 (Figure 10).

Facies Model Color Scale

tidal_flat	
lagoon	
high_energy_shoal	
reef	
shallow_reef_front	
fore_reef	
slope	
Basin	
back_reef	

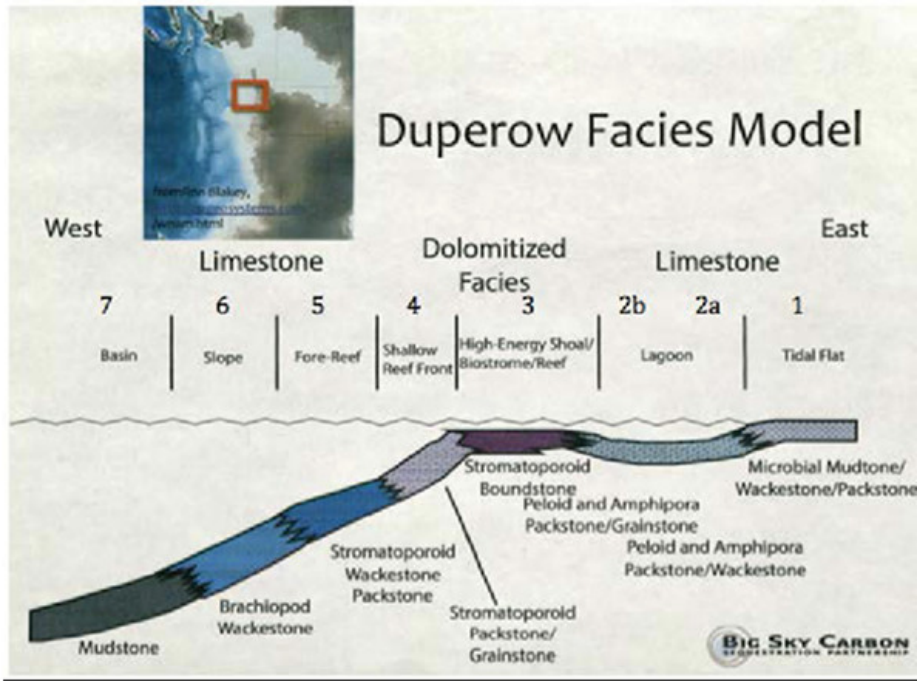

Figure 11: 8 Depositional environment illustration

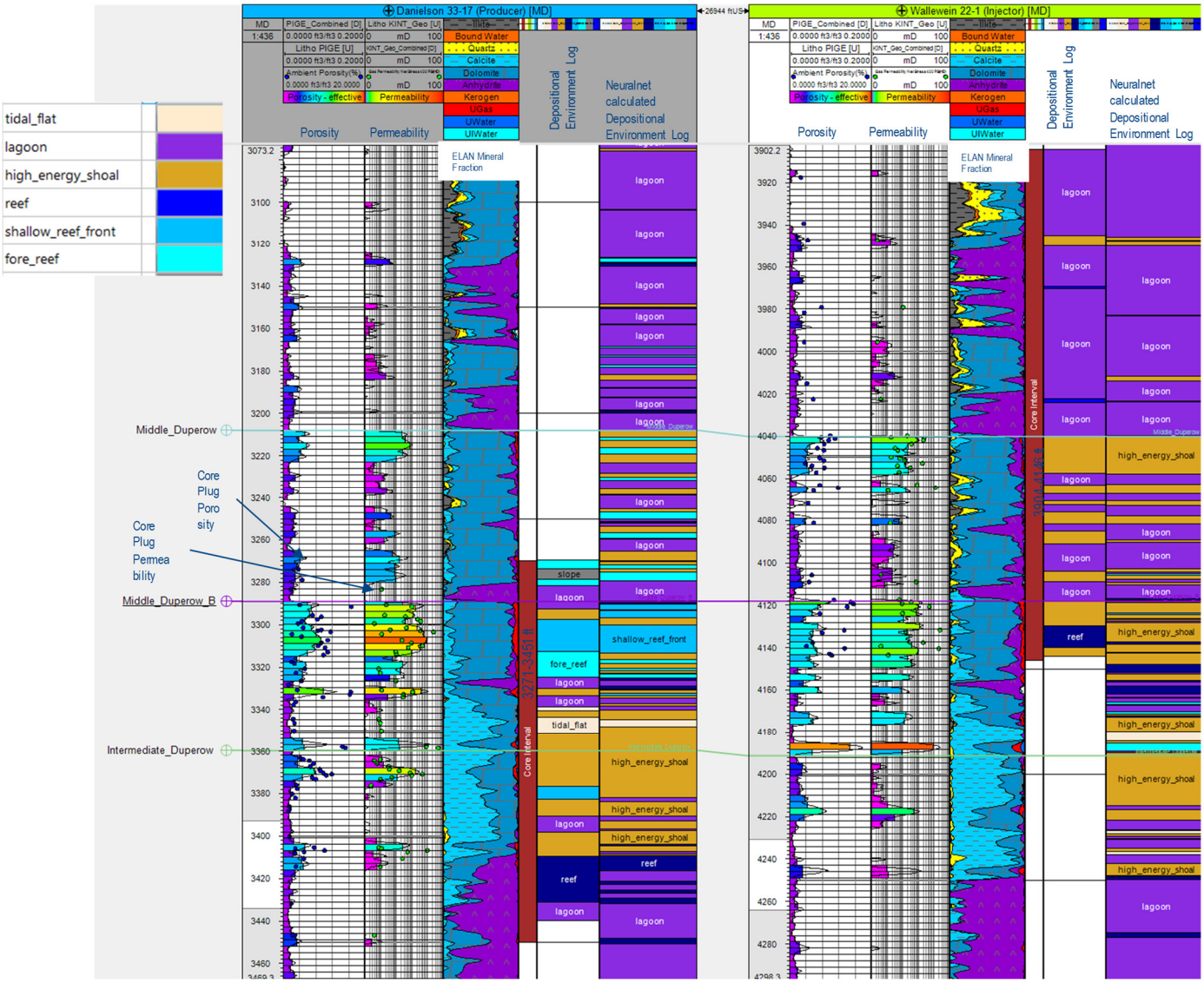

Figure 12: Supervised neuralnet calculation of 8 Rock Type log

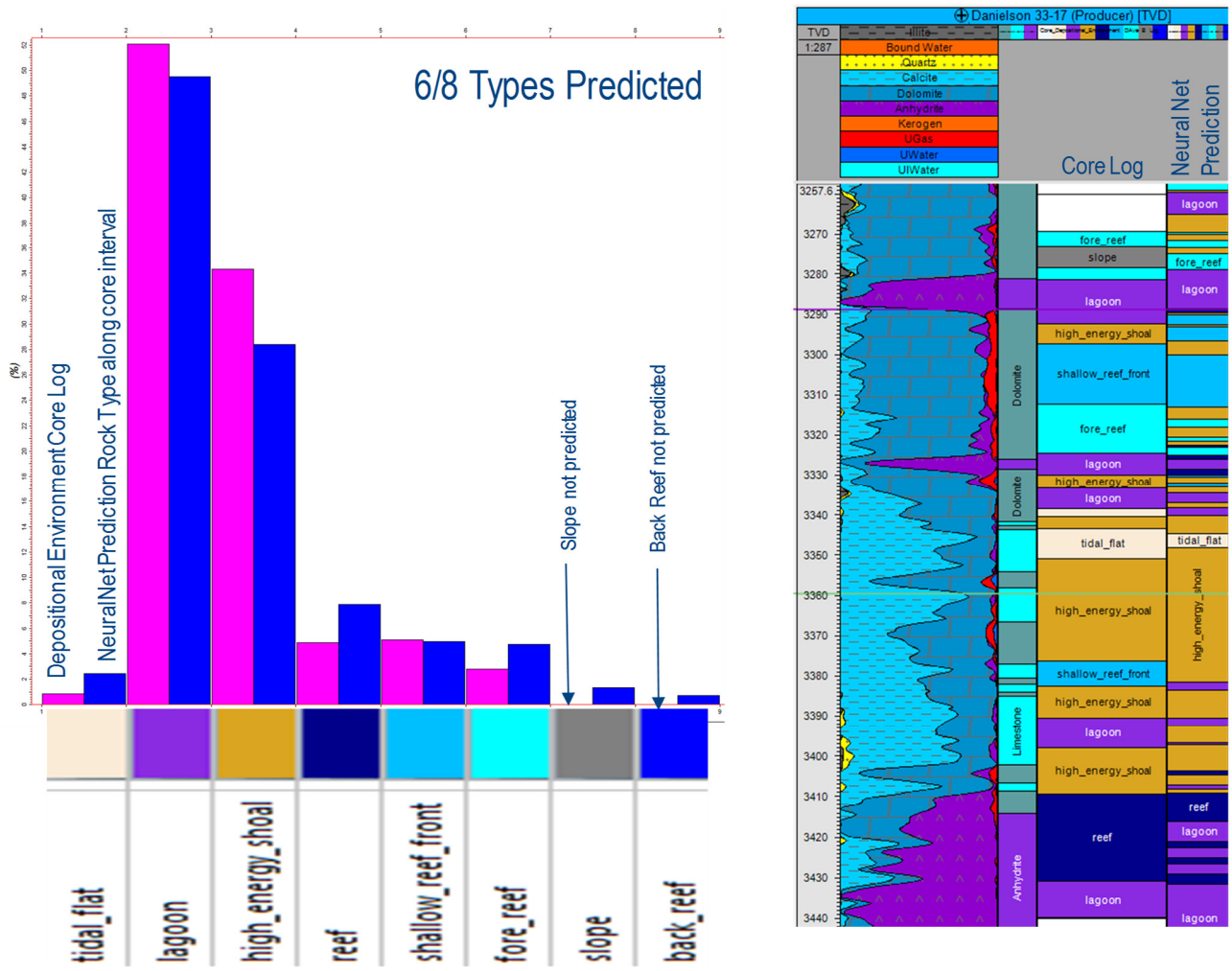

Figure 13: Histogram of 8 depositional environment core log vs the neuralnet predicted 8-Rock Type log (filtered along the core interval only)

		Danielson			Wallewein			Combined	
Code	Depositional Environment	Total Interval Thickness	Total % Thickness	Average Interval Thickness	Total Interval Thickness	Total % Thickness	Average Interval Thickness	Total % Thickness	Total
1	Tidal flat	9.5	5.5%	2.4	0.0	0.0%	N/A	2.3%	9.5
2	Lagoon	0.0	0.0%	5.1	144.7	60.8%	4.5	35.3%	144.7
3	High Energy Shoa	55.6	32.3%	5.1	69.5	29.2%	5.0	30.5%	125.1
4	Reef	62.5	36.3%	5.2	4.0	1.7%	2.0	16.2%	66.5
5	shallow reef fron	20.8	12.0%	3.5	0.0	0.0%	N/A	5.1%	20.8
6	Fore reef	19.0	11.0%	3.8	0.0	0.0%	N/A	4.6%	19.0
7	Slope	5.0	2.9%	5.0	0.0	0.0%	N/A	1.2%	5.0
8	Back reef	0.0	0.0%	N/A	19.9	8.4%	10.0	4.9%	19.9
	Total	**172.3**			**238.2**				410.5

Figure 14: Core Depositional Environment Statistics

4.4 Upscale Effective Porosity and Permeability

Effective porosity and permeability logs for eight wells within the model domain were upscaled into the grid. The eight wells upscaled were Wallewein, Danielson, LLLOYD Danielson 2, Allen 14-2, State_1, Suta 1-34, Suta 2-26 and Pace 11-28 (Figure 10). In 2017, the permeability values at these wells were re-calculated. This was completed because the permeability calculation equations for the LLOYD Danielson 2, Allen 14-2, State_1, Suta 1-34, Suta 2-26 and Pace 11-28 wells were different than what was used for the Wallewein and Danielson. Re-calculation of the permeability of the Wallewein and Danielson was done because an equation error was observed and has been corrected. The effective porosity logs were upscaled using the arithmetic method. Permeability was upscaled using the geometric mean method. The thin 3-foot cell size was sufficient to capture the heterogeneity of the well logs within the formations of interest (Figure 15).

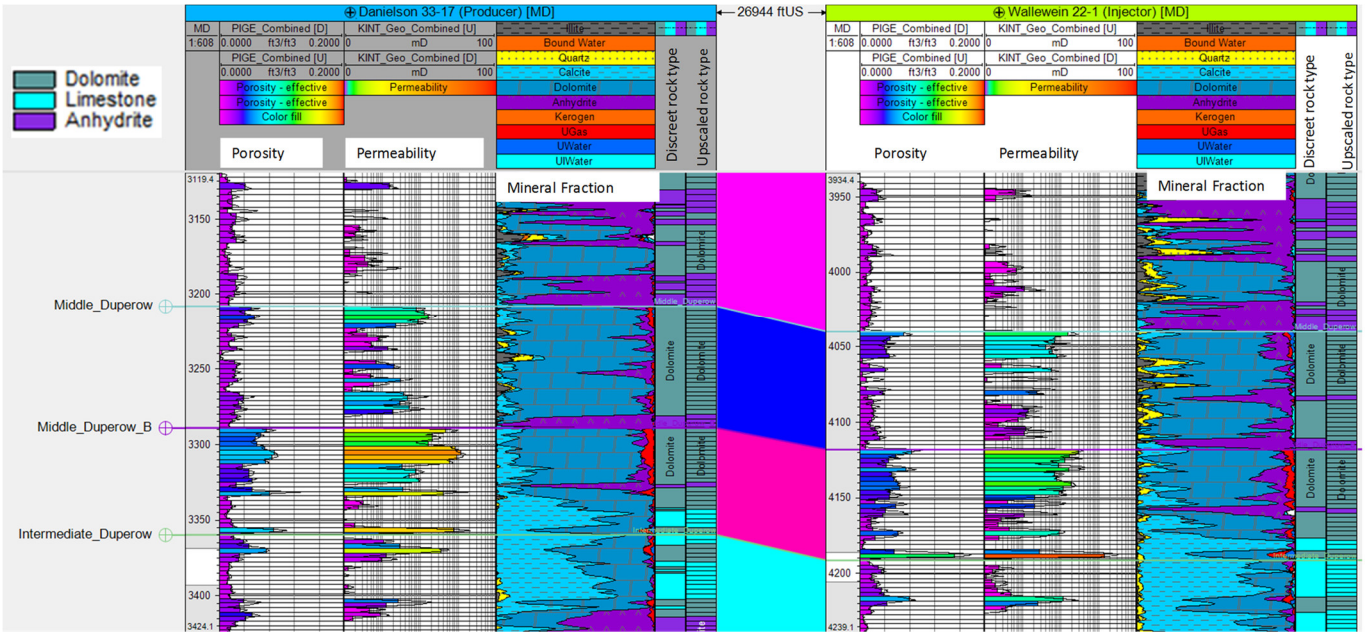

Figure 15: Upscaled effective porosity and permeability well logs with ELAN analysis

4.5 Upscaled 3D Seismic Attributes Variogram Analysis

There were eight wells with porosity and permeability data from ELAN analysis within the model boundary. With geomodel Version 1, there is much uncertainty regarding spatial distribution of porosity and permeability because of the few number of wells and high separation distance between wells; furthermore, not all of these wells penetrated deeper formations. These limitations mean that the variogram function has a high amount of uncertainty making interpolation of porosity and permeability uncertain. The variogram analysis of Geomodel Version 3 has an advantage over Geomodel 1, because, Geomodel 3 had 3D seismic attributes (P-impedance, S-impedance, and density) made available from the 3D seismic survey. Variogram analysis was completed on the 3D seismic P-Impedance, which was upscaled into the model grid.

4.6 Quantitative Integration Seismic Inversion Attributes for Lithology Classification

4.6.1 Workflow Overview

A typical problem in reservoir characterization is the poor constraint of reservoir properties in the model space between wells containing petrophysical data. Commonly used rudimentary forms of well log interpolation leave large amounts of uncertainty away from wells. Litho Analysis and Prediction is a rock physics based lithology prediction workflow that integrates well logs, seismic inversion, and geological modeling to provide an estimate of the most probable lithology in the inter-well geologic model space, and the likelihood associated with the prediction. Litho Analysis is a fully Bayesian approach that integrates different measurements at different scale.

The general Litho Analysis and Prediction approach is to first, develop probabilistic (Bayesian) relationships between elastic properties and litho-class using co-located petrophysical and elastic property well logs. The inverse of these relationships is used to convert seismic elastic inversion output volumes litho-class and associated likelihood volumes. The workflow (illustrated in Figure 16) is comprised of the following main steps:

1. Litho-Class Log Creation - Petrophysical analyses and geological interpretation of available geophysical well logs and core are used to define distinct lithology classes. The outputs of this process are a litho-class log for each well. The methodology for generating a 3-Rock Type and 8 Rock Type version has already been discussed in Section 4.3.
2. Litho Analysis and Estimator Creation - Litho Class logs and co-located elastic property logs are used to develop Bayesian estimators, which define the probabilistic relationships between litho-class and elastic properties at wells. The output of this process is a set of probability density functions (PDF's) defining these relationships.
3. Litho Prediction – Litho Estimators (PDF's) are used to convert seismic elastic inversion property volumes to a litho class volume and likelihood volume for each litho class. These probability volumes are used in future facies modeling.

The following sections describe application of the Litho Estimation and Prediction workflow to the Kevin Dome geologic model using available well logs and seismic elastic inversion products.

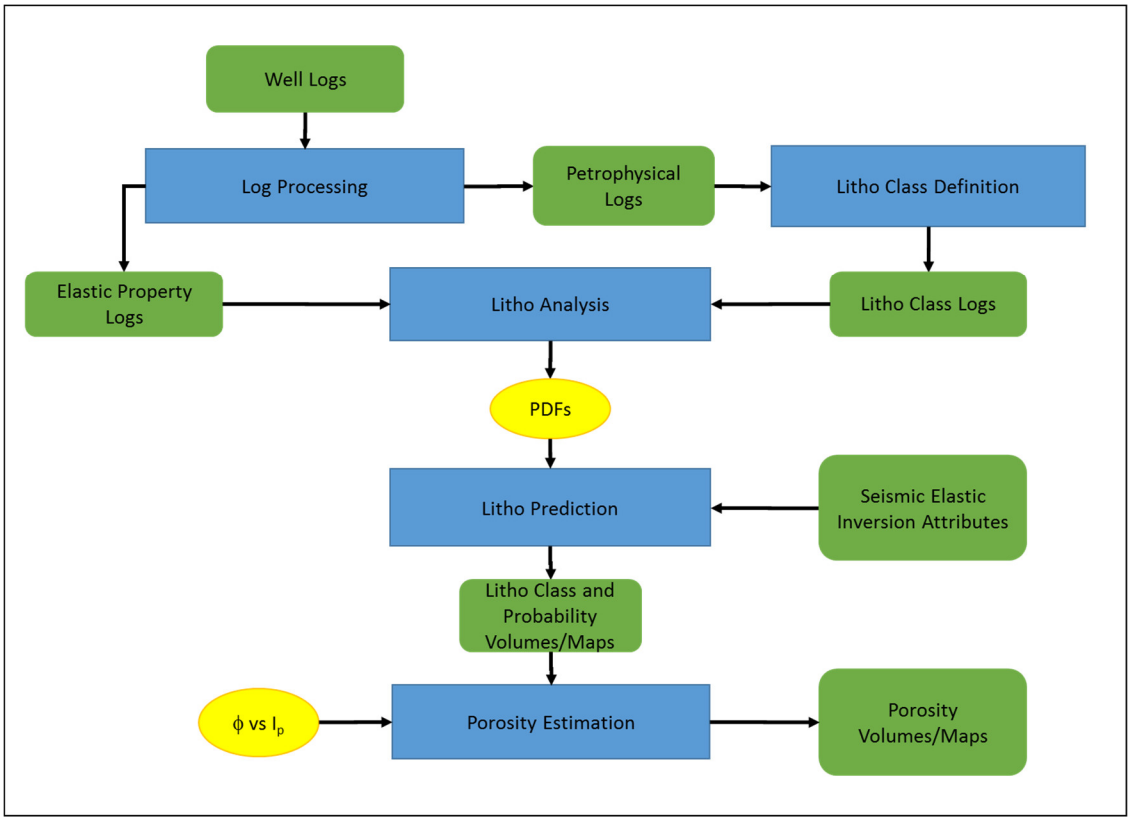

Figure 16: Litho estimation and prediction workflow diagram.

4.6.2 Available Data and Volume of Investigation

The Litho Estimation and Prediction workflow requires the following data:

1. Well Logs - One or more wells with sufficient log data for geological interpretation as well as density, compressional, and shear velocity logs required for litho analysis.
2. Seismic Data - Seismic elastic inversion attribute (Ip, Is, density, Poisson Ratio, etc.) volumes were used for litho prediction.

The data available at Kevin Dome are:

1. Well Logs – Comprehensive advanced well log suites at Danielson and Wallewein. These log suites supported identical petrophysical analysis workflows supporting statistical litho class analysis and had advanced sonic log measurements.
2. Seismic Data –A set of elastic inversion properties (Ip, Is, Density) were extracted from seismic inversion volumes into all modeled zones. The area of investigation is limited to the area of the seismic inversion results. Figure 17 shows seismic inversion property average maps for the Intermediate Dupeorw, cropped to the aerial extent recommended by seismic analysts, along with the two wells with logs used in the workflow.

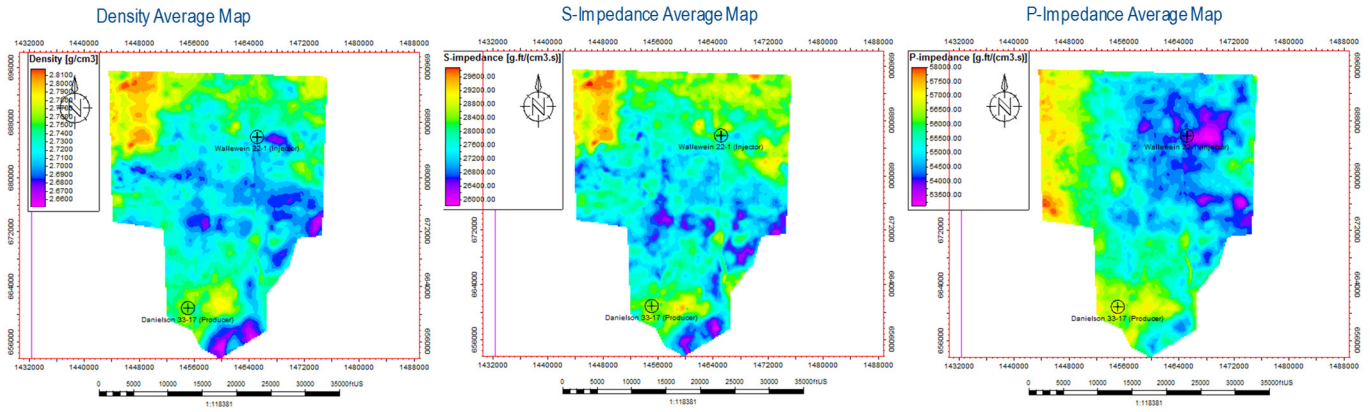

Figure 17: Cropped seismic inversion average maps resampled into Intermediate Duperow zone

4.6.3 Well Log Processing and Analysis

Logs for wells Danielson and Wallewein were processed through ELAN using a model comprising five mineral components and five fluid components. Results of the ELAN analysis is shown in Figure 18. Note the limited porosity and permeability and the low levels of gas saturation generally confined to the Middle Duperow interval in both wells. Gas (red) is the only measurable fluid within this interval. Also shown in Figure 18 are elastic property logs to be used in the litho analysis step discussed in a later section.

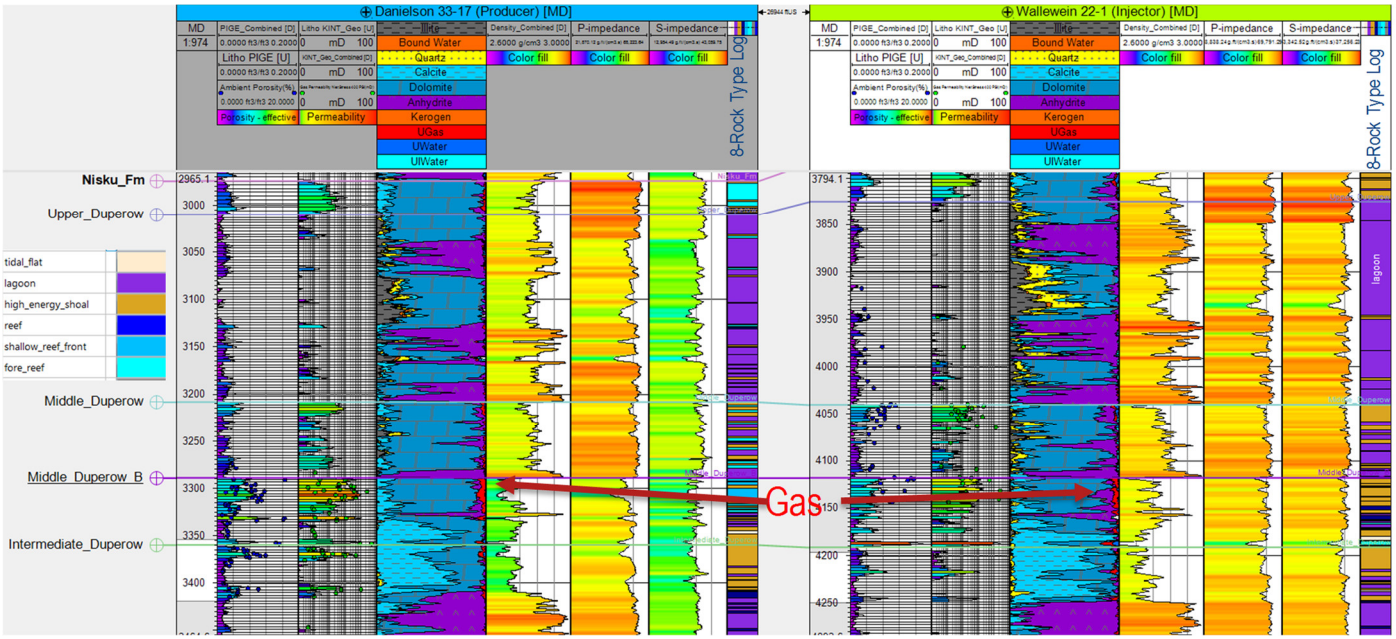

Figure 18: ELAN analysis with elastic logs (P-impedance, S-impedance, and density) on wells Danielson and Wallewein.

4.6.4 Litho Analysis

Litho Analysis is the process of creating a Bayesian litho class predictors from elastic properties using well logs. Inspection of elastic property and mineral fraction logs in Figure 18 suggests that relationships between elastic properties and mineral fractions are non-trivial and non-unique. This is a common condition and is the reason that a probabilistic rather than deterministic process is required. The output of Litho Prediction is a set of probability density function (PDF's) describing the likelihood (or probability) of each litho class as a function of combinations of the three elastic properties (Ip, Is, Density) taking into account appropriate prior constraints and estimated measurement uncertainty.

The Duperow formation is geologically separated into five units representing distinct depositional environments. These are the Upper, Middle, Middle _B, Intermediate, and Lower Duperow units. These units are distinguishable through characteristic mineral content, which controls litho class (Figure 9 and Figure 12) and thus also suggests the need for separate litho analyses for each formation. The variable relative quantities of each litho class in the different units are reflected in prior constraints in the litho analysis.

Litho analysis results are presented as joint litho class PDF's which may be viewed in various dimensions of elastic parameter space. For brevity, only results for the intermediate Duperow unit are shown in Figure 19 and Figure 20. Both the 3-Rock Type and 8 Rock Type methods are summarized here. The probabilities are scaled to the rock type fractions from the well logs. All litho types clearly illustrate the overlap (non-uniqueness) in the classification, hi-lighting the need for probabilistic treatment.

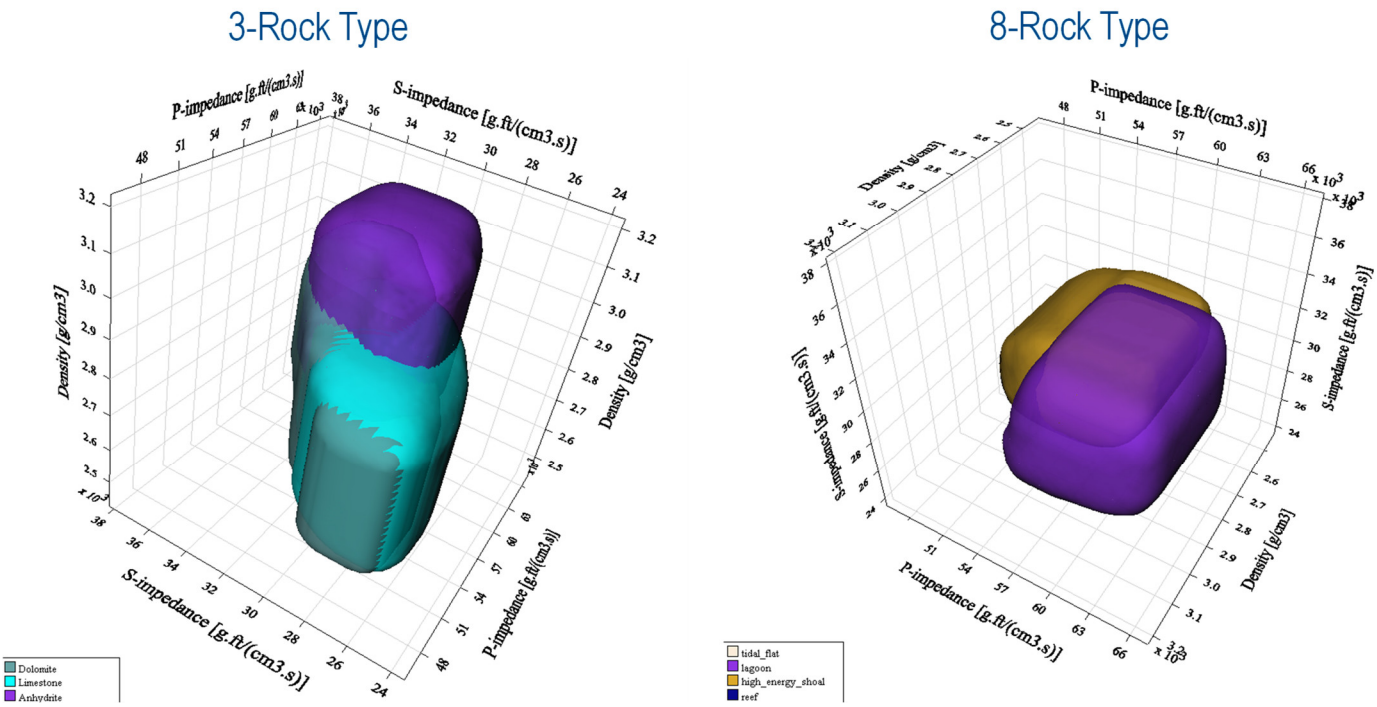

Figure 19: 3-Rock Type and 8-Rock Type; 3D PDF litho class for Intermediate Duperow using Ip, Is, density.

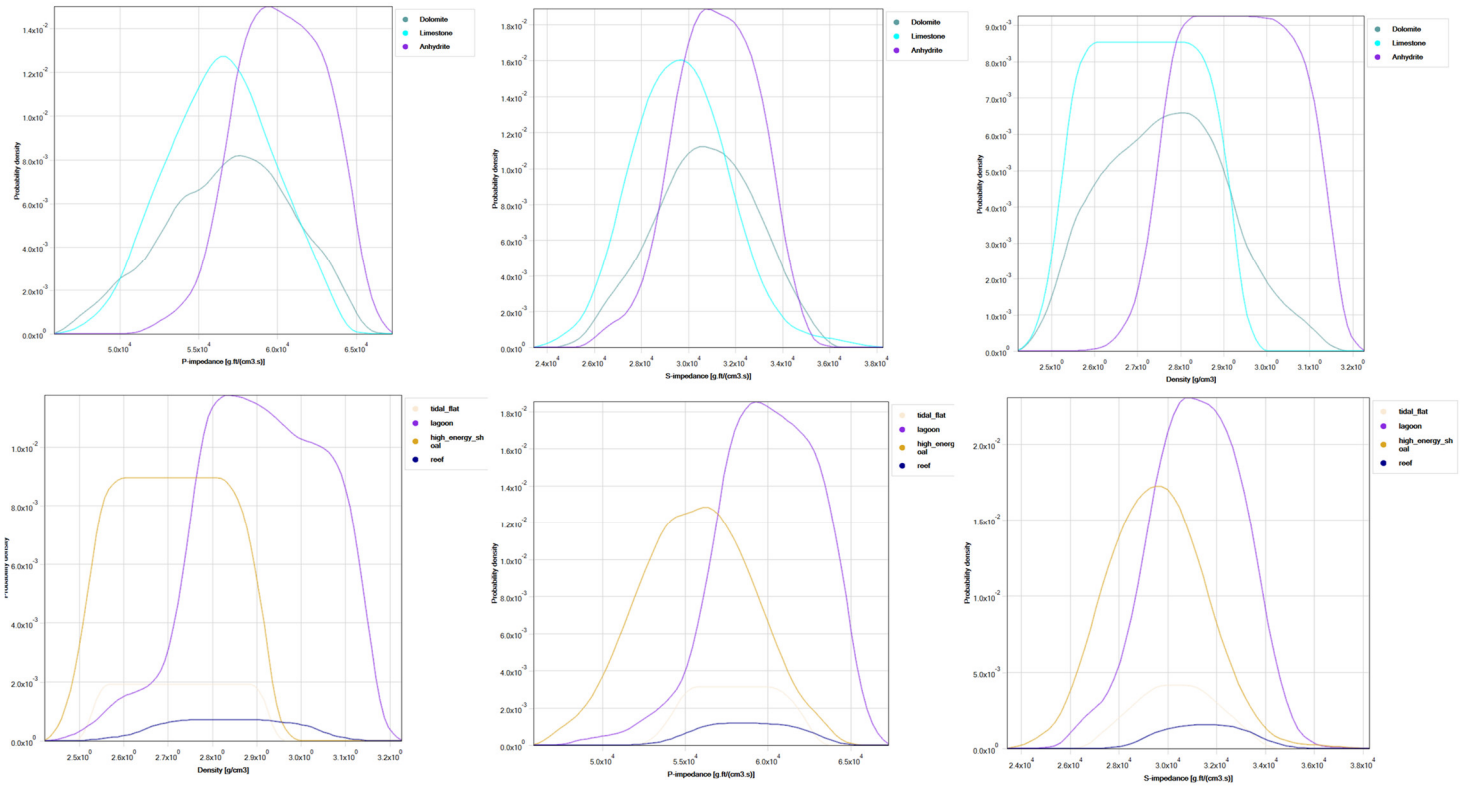

Figure 20: 1D (3-Rock Type) and 1D (8-Rock Type) litho class PDF's for the Intermediate Duperow using Ip, Is, density.

4.6.5 Litho Prediction

In the lithology prediction process, PDF relationships analyzed from the well logs with each formation (Figure 20), were applied to the elastic attribute cubes from the seismic inversion to produce lithology prediction probability volumes. These volumes contain all the litho classes contained in the litho analysis model. The process generated one probability cube per litho class. Each of them contains the probability of a litho class occurring within the seismic volume. This process was completed within each formation for both the 3-Rock Type and 8-Rock Type models. Implementation of these litho prediction products were used to condition facies modeling as described in Sections 4.7.1 and 4.8.1. Figure 21 displays a map view of the top layer of the probability volumes for the 8-Rock Type Method while Figure 22 displays the probability volumes for the 3-Rock Type method.

A key factor that must be considered in litho prediction is the vertical resolution of the seismic inversion results. Using compressional velocity (from sonic logs) of approximately 21,000 ft/s and approximate dominant frequency of 50 Hz, the estimated compressional wavelength of approximately 420 ft. Applying a ¼ wavelength resolution rule of thumb and assuming an improvement in vertical resolution from the inversion process the vertical resolution limit of the available elastic inversion dataset is estimated to be on the order of 100 ft.

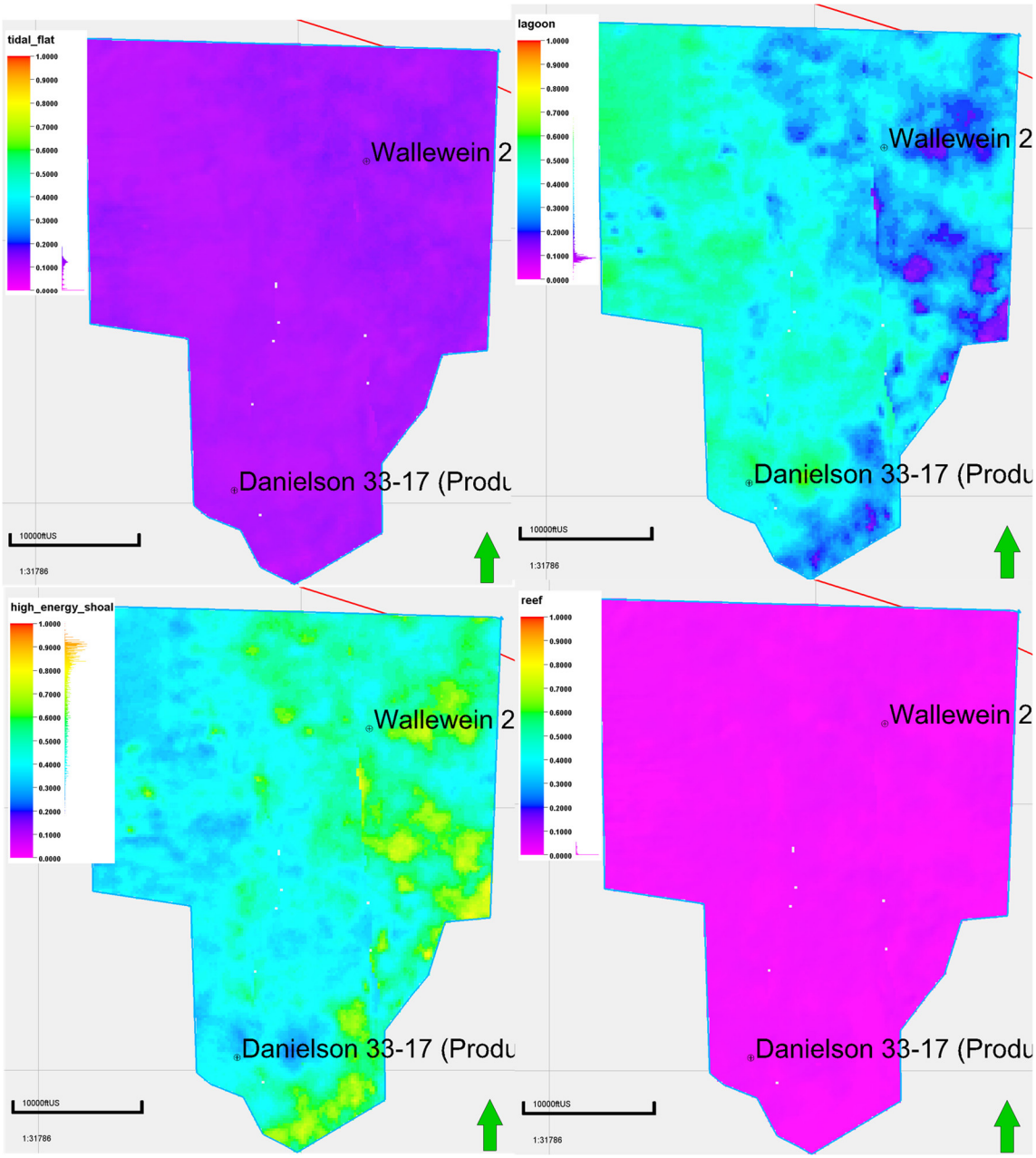

Figure 21: 8-Rock Type probability volumes for the Intermediate Duperow

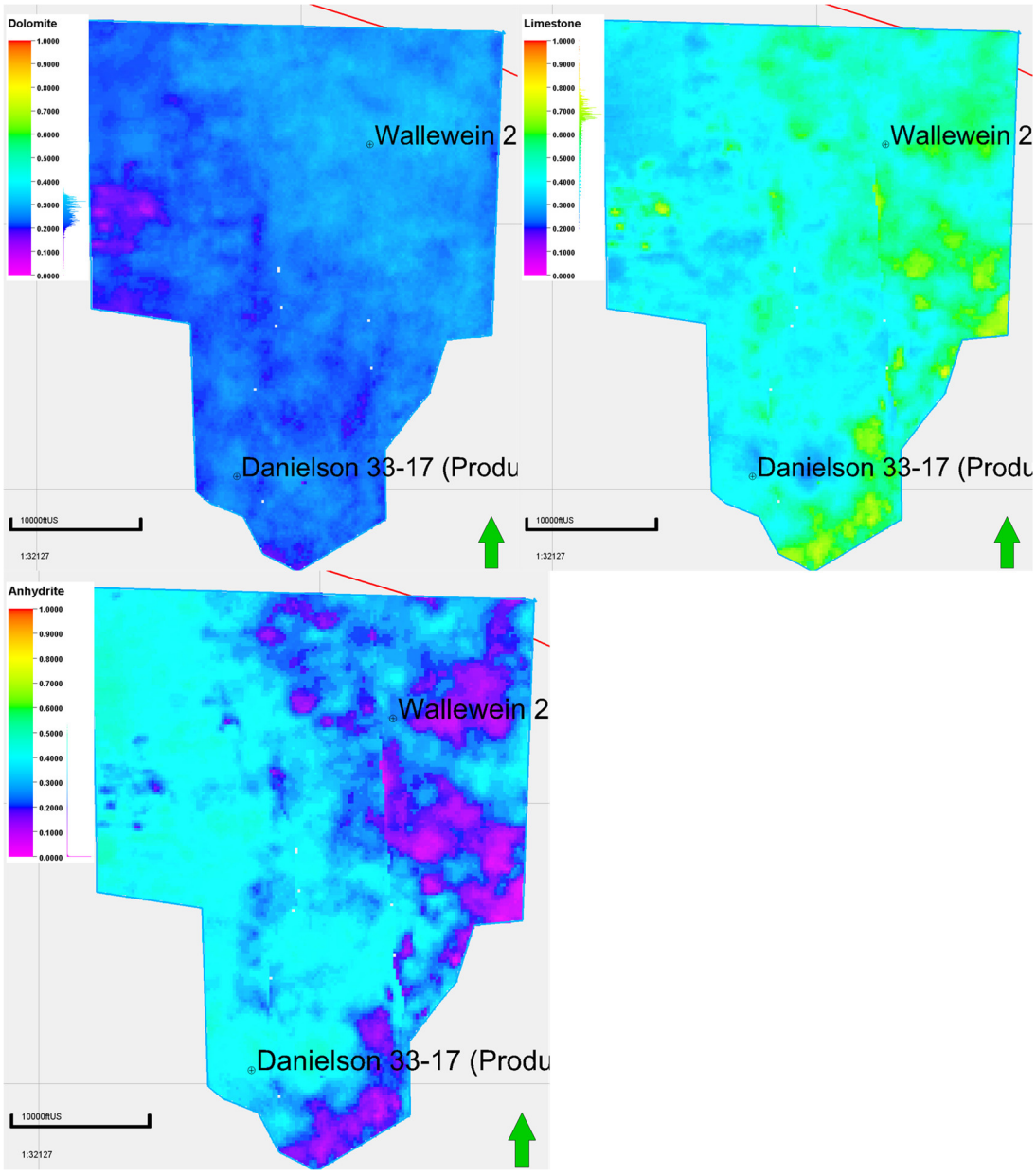

Figure 22: 3-Rock Type probability volumes for the Intermediate Duperow

4.6.6 Litho Class Conditioned Porosity Modeling from Seismic

This section describes how the results from litho prediction have been used in conjunction with the standard P-impedance attribute correlation techniques to create probability-weighted estimates of porosity in each zone. The following 4-step process was applied;

1. Porosity versus Ip relationships for each litho class are extracted from well log data.
2. Using these relationships and seismic Ip, porosity is computed for each litho class in each zone.
3. Individual litho class porosities are combined to form a probability- weighted porosity on a zone-by-zone basis through linear weighting by litho class probability.
4. The probability-weighted porosities were used as support in co-simulation of well log porosity.

Figure 23 shows porosity versus Ip cross plots for logs from wells Danielson and Wallewein. The plot shows that both wells have similar data characteristics but does not exhibit a single distinct linear trend although overlapping trends are evident. The full shaded colors represent log data in the modeled zones while lightly shaded data represents log data above the model zones. Along the core interval, porosity versus Ip cross plots (Figure 24) and porosity vs permeability cross plots (Figure 25) were examined with the 8-class depositional environment log to find linear regression lines for the 8-Rock Type model. Used in conjunction with the results from litho prediction these linear regression lines could be used to calculate porosity and permeability from seismic Ip. Although this process provides valuable information in the inter-well space, the result suffers from a drawback. The resulting porosity population statistics may not honor the well log data. This was the case for these data and other methods (Sections 4.7 and 4.8) for porosity interpolation were used in place of this method.

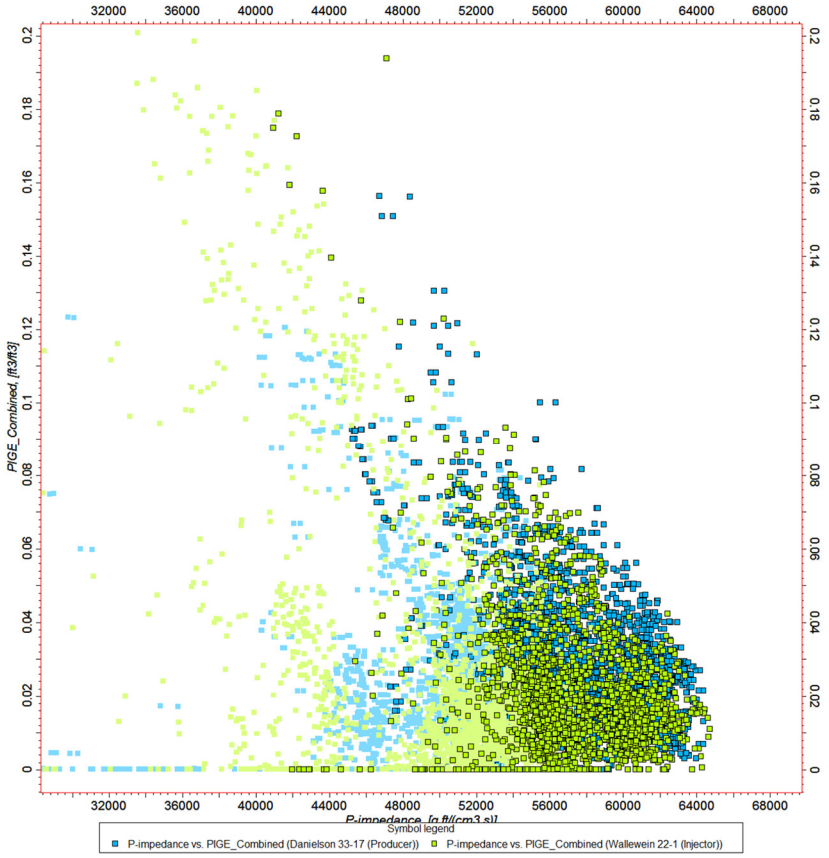

Figure 23: Porosity versus Ip for Danielson and Wallewein 22-1 annotated by well

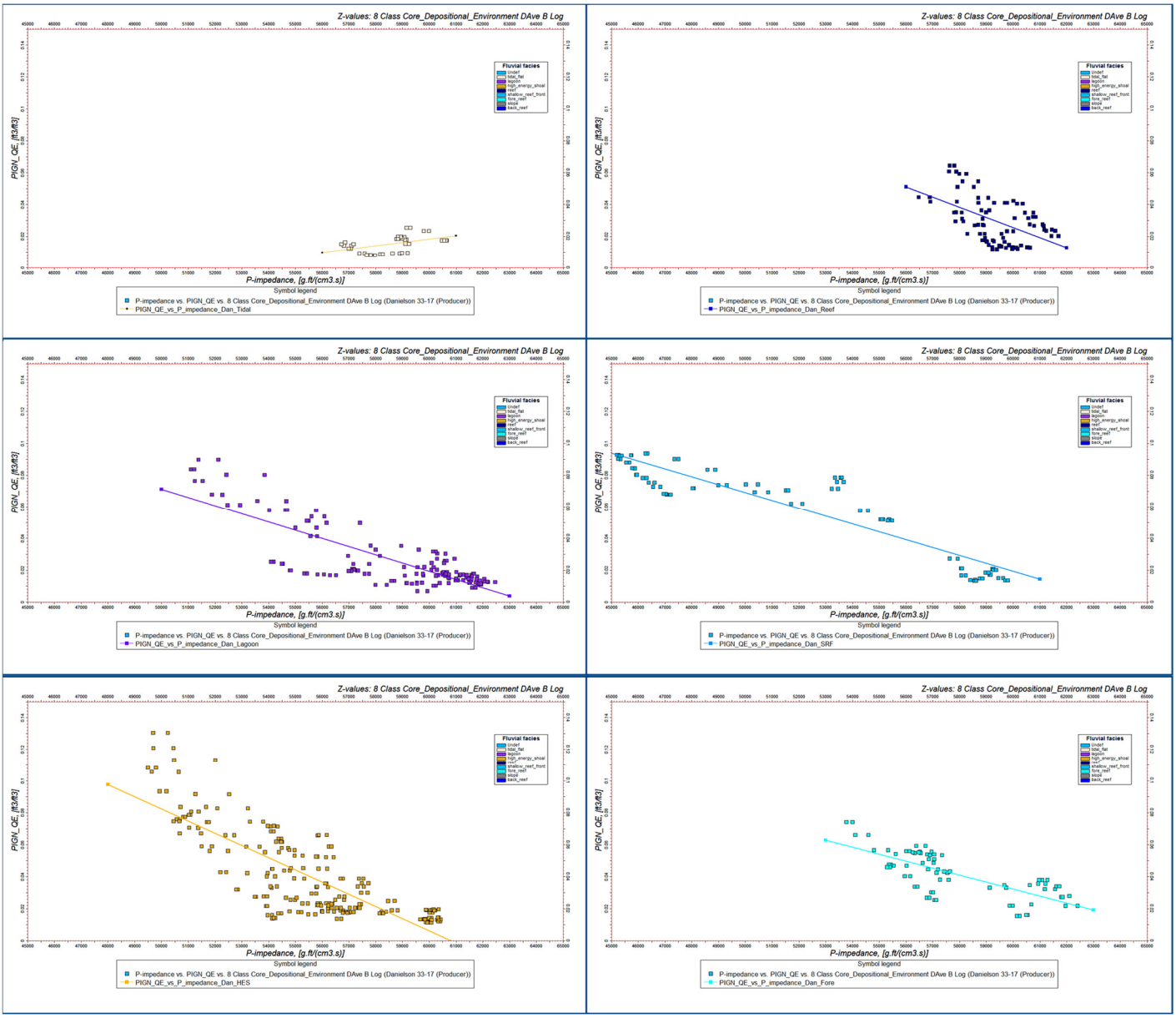

Figure 24: Porosity vs P-Impedance Relationships for the 8-Rock Type model. These data were taken from the Danielson well and are filtered along the core interval

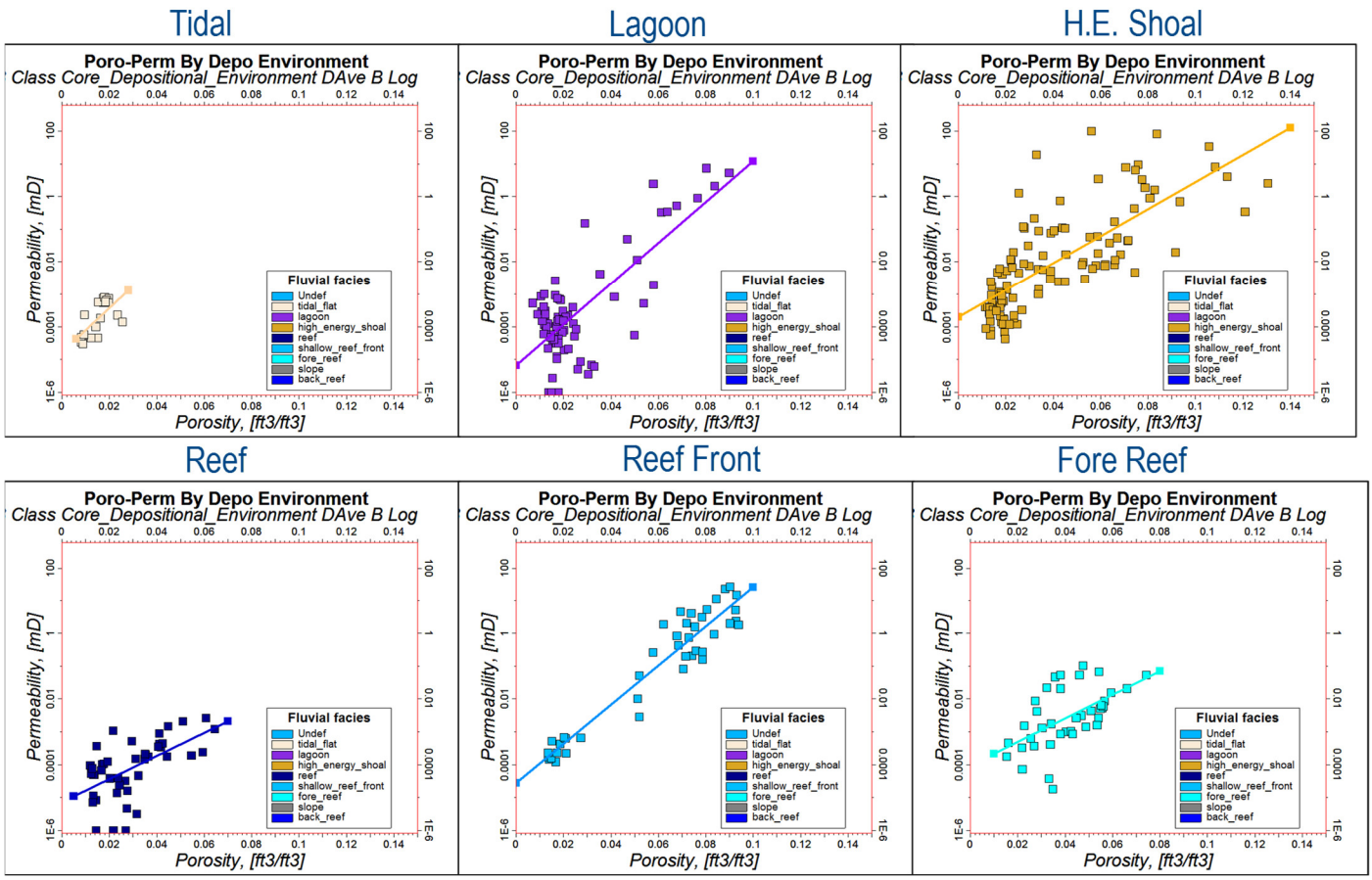

Figure 25: Porosity vs Permeability Relationships for the 8-Rock Type model. These data were taken from the Danielson well and are filtered along the core interval

4.7 Property Modeling 3-Rock Type

4.7.1 Facies Modeling 3-Rock Type

Rock Types for both the 3-Rock Type (Figure 26) method and the 8-Rock Type method were interpolated separately in the interwell space from the upscaled discreet rock type logs using Sequential Indicator Simulation. The 3-Rock Type facies modeling interpolates the rock types from the wells using both the facies probability properties from the results of the Lithology Classification workflow (Section 4.6.5) and the variogram parameters extracted from the upscaled P-Impedance 3D seismic property. The facies modeling carries the lateral spatial structures of the facies probability volumes in the inter-well space while honoring vertical resolution and overall population statistics of the primary variable (well logs). It must be noted that this process, as with all geostatistical methods, contains uncertainties and errors, which are dependent upon the amount and quality of conditioning data. The results of this process are not deterministic. Rather they represent one possible result, which fits the input data under given assumptions, uncertainties, and data errors. This workflow represents a valuable probabilistic approach.

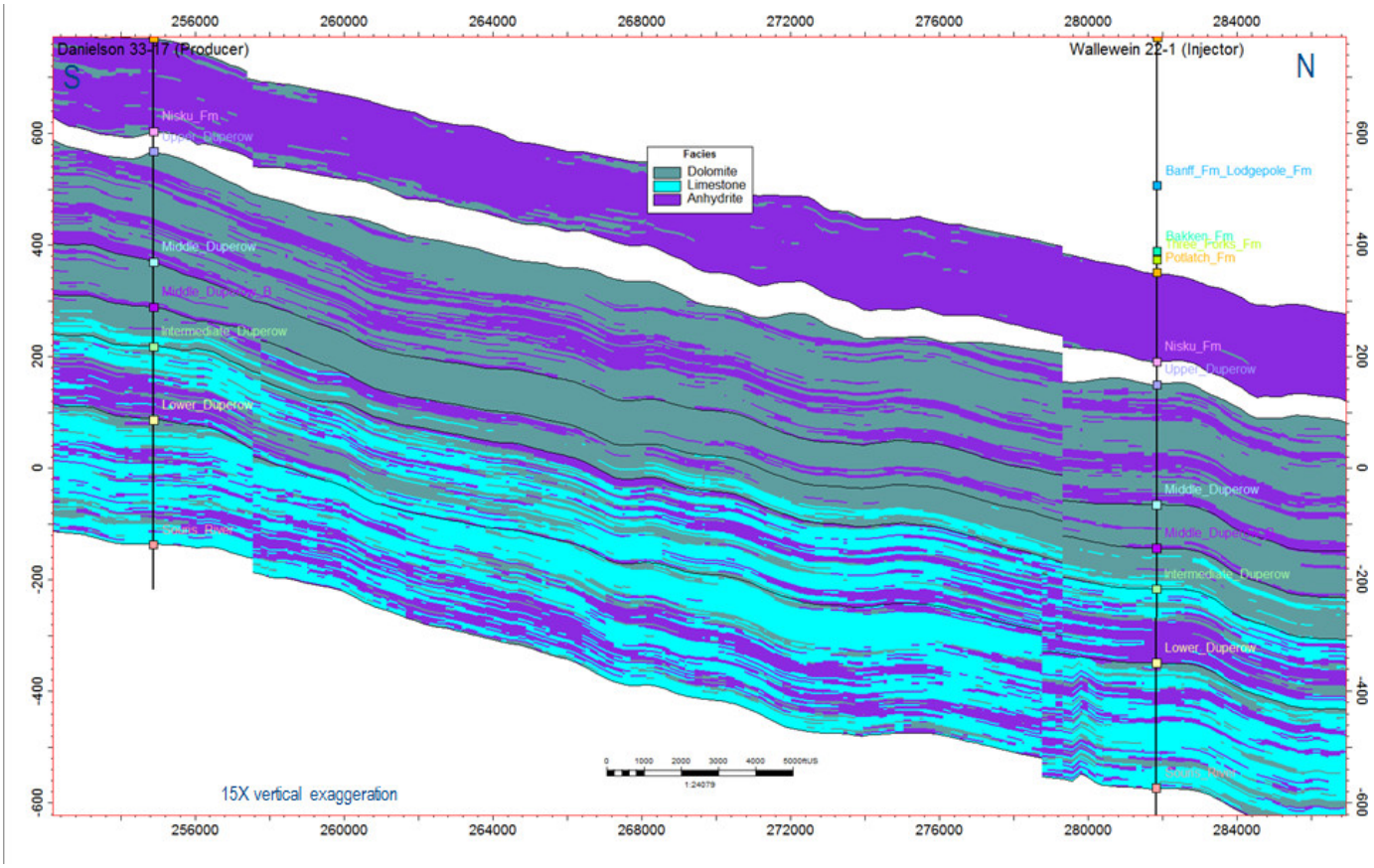

Figure 26: 3-Rock Type Interpolation of rock type (dolomite, limestone and anhydrite). Cross Section view from east. Cross section line indicated on Figure 28.

4.7.2 Effective Porosity and Permeability Interpolation 3-Rock Type

The analysis of the porosity/permeability relationships in the upscaled well logs (Potlach down to Lower Duperow) shows that there are three separate relationships when plotted against rock types (dolomite, limestone and anhydrite) (Figure 27 left side). Figure 27 also colors the porosity vs permeability cross plot by formation showing how each formation has a unique porosity and permeability relationship. Here it is clearly seen most of the higher porosity and permeability is in the dolomite facies of the Middle Duperow_B. Because of this, the porosity and permeability data within each rock type within each zone were analyzed and modeled separately using GRFS. Using the same method, GRFS was used to interpolate permeability. Because of the known functional relationship of increasing porosity representing increasing permeability, permeability was co-krigged at 95% to effective porosity. Using the GFRS method in this way, ensures that the statistical porosity-permeability relationships are honored within in each formation and within each formations' s rock type. Figure 28 shows the average effective porosity for each zone and a cross-section line for Figure 29 (Effective porosity cross-section) and Figure 30 (permeability cross-section).

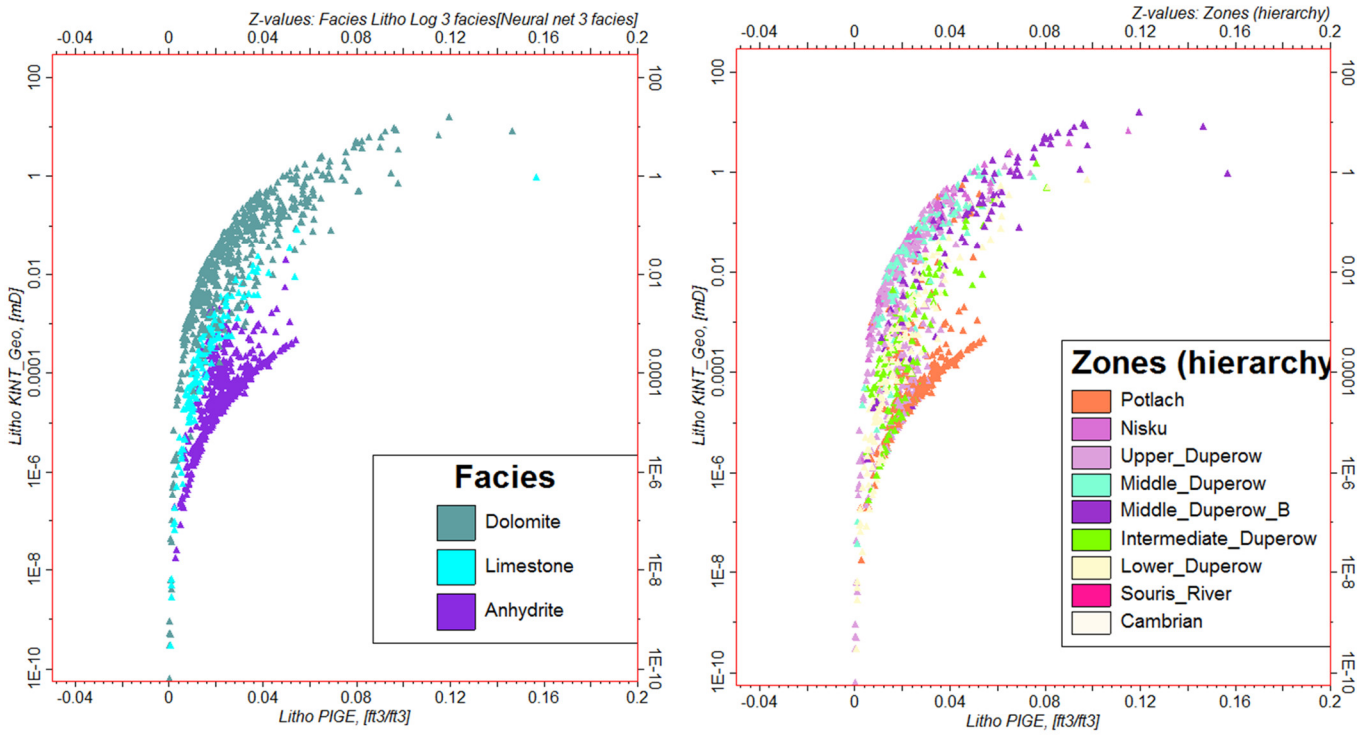

Figure 27: Cross plot of porosity (PIGE) vs. permeability (KINT) (Potlach down to Lower Duperow). On the left, the points are shaded based on the 3-Rock Types which show the three separate relationships for the three dominant rock types. On the right, the points are shaded based on the formations which show the separate relationships for each formation.

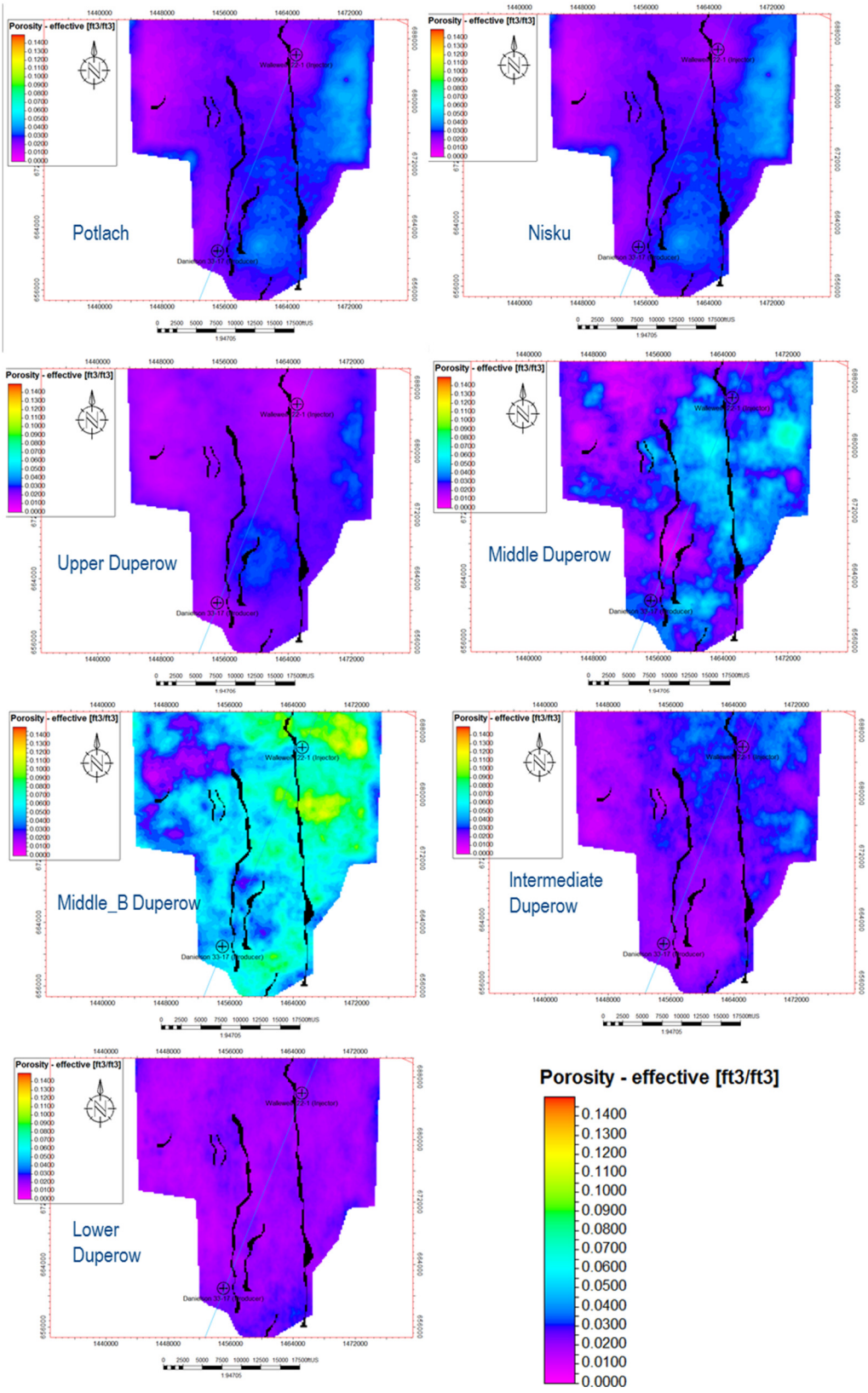

Figure 28: 3-Rock Type average effective porosity for each formation

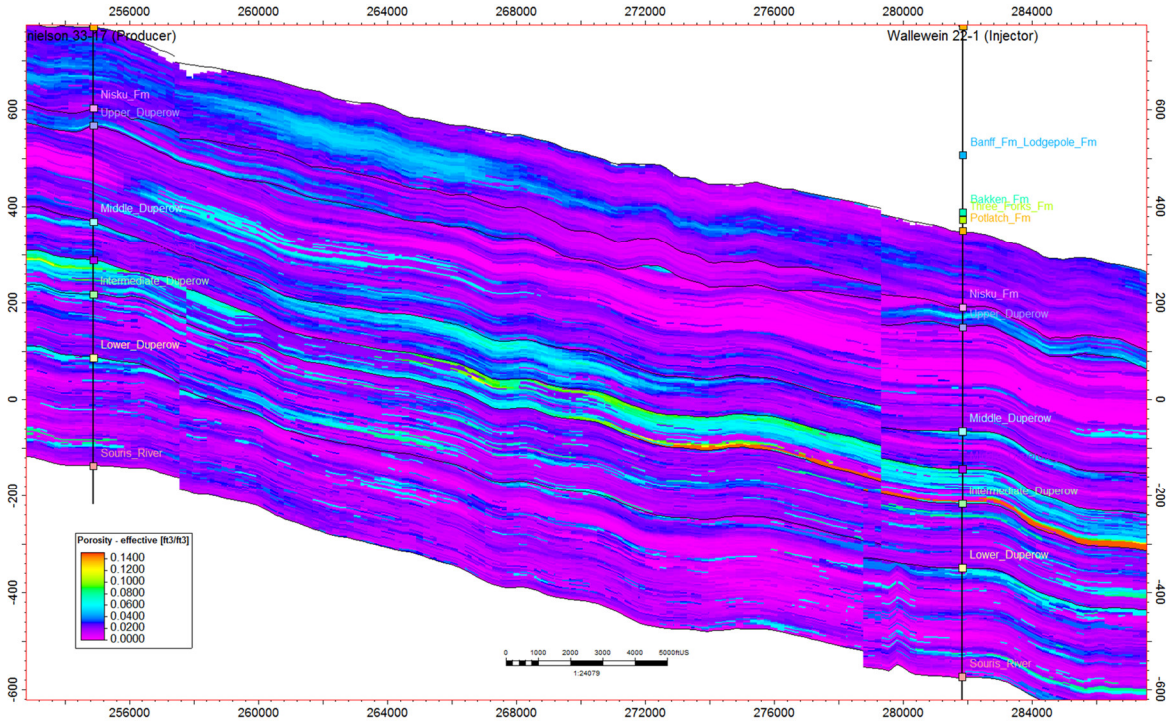

Figure 29: 3-Rock Type Effective porosity cross section. View from east. Cross section line indicated on Figure 28.

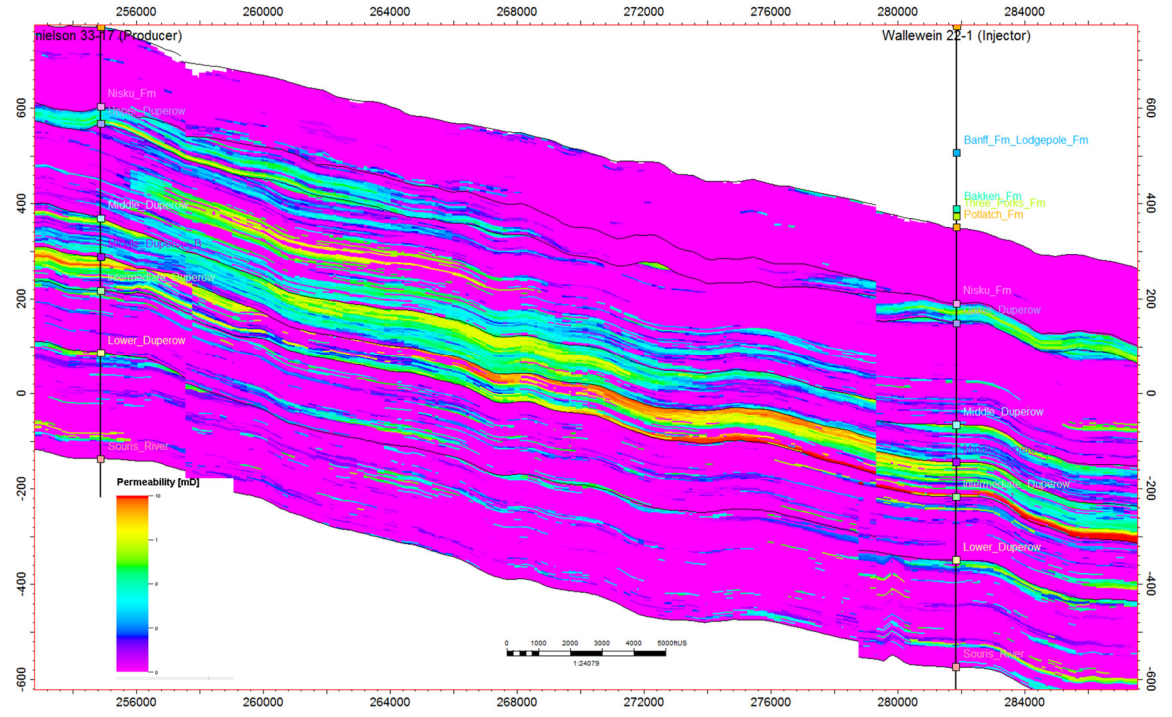

Figure 30: 3-Rock Type Permeability south to north cross-section. View from east. Cross section line indicated on Figure 28.

4.7.3 Property Modeling Quality Control 3-Rock Type

To quality control the effective porosity and permeability interpolation, a crossplot of effective porosity (PIGE) vs permeability (KINT) was analyzed for each zone to see if the relationship observed from the well log data is honored in the well log upscaling and the geocellular interpolation (all cells). Figure 31 is a cross plot that represents all the model zones combined. Histograms of porosity and permeability were examined for each zone to see if the distribution of well log values resemble the associated upscaled cells and final property interpolation (all cells). Figure 32 displays a porosity and permeability histogram that represents the all the model zones combined. The quality control cross-plots and histograms are considered reliable.

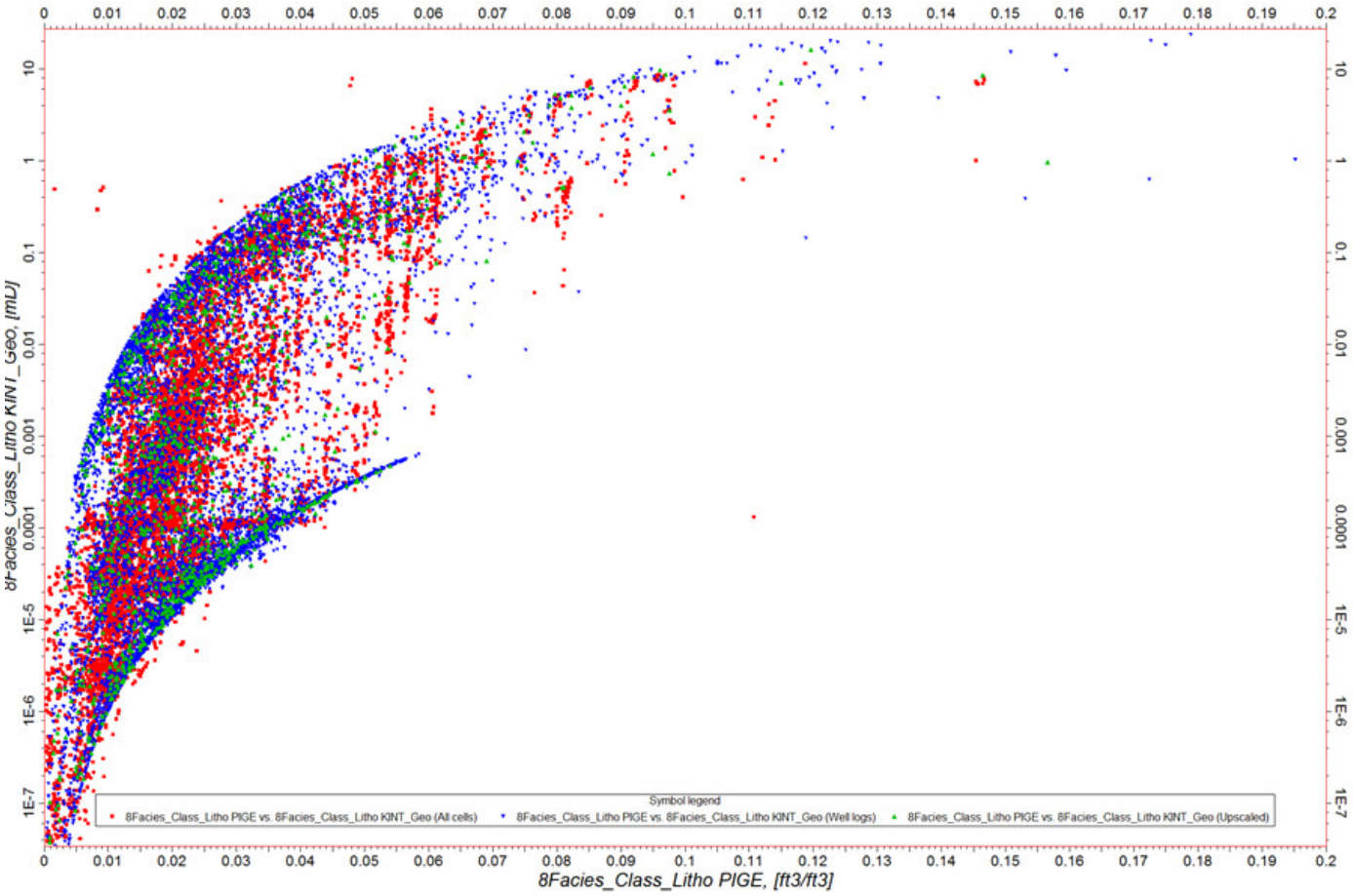

Figure 31: 3-Rock Type Quality control, cross plots of effective porosity and permeability (well logs (blue), upscaled cells (green) and modeled property (red) for all modeled zones

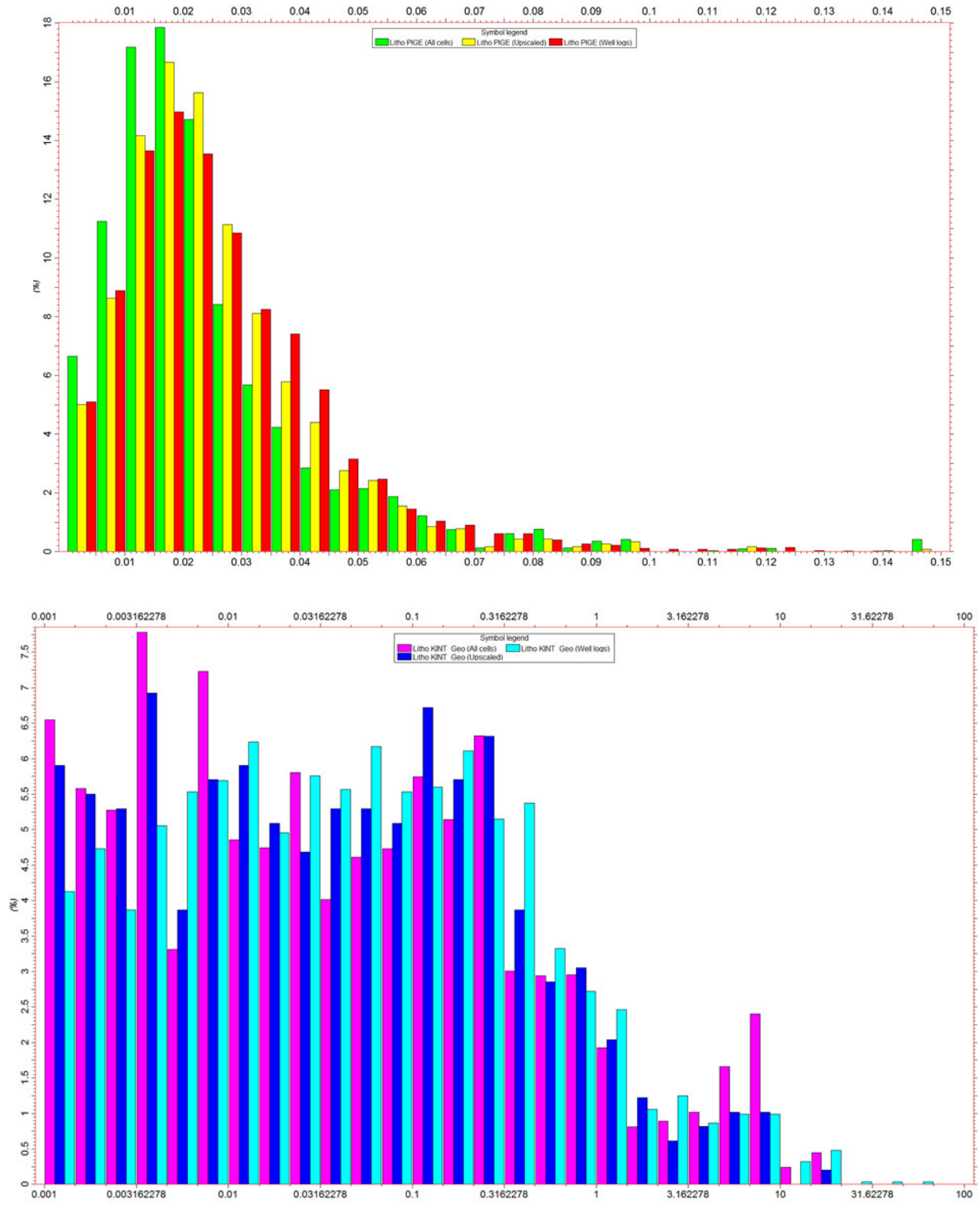

Figure 32: 3-Rock Type Quality control histograms for all modeled zones, porosity (top) and permeability (bottom)

4.8 Property Modeling 8-Rock Type

4.8.1 Facies Modeling 8-Rock Type

Rock Types for both the 3-Rock Type method and the 8-Rock Type (Figure 33) method were interpolated separately in the interwell space from the upscaled discreet rock type logs using Sequential Indicator Simulation. The 8-Rock Type facies modeling interpolates the rock types from the wells using both the facies probability properties from the results of the Lithology Classification workflow (Section 4.6.5) and the variogram parameters extracted from the upscaled P-Impedance 3D seismic property.

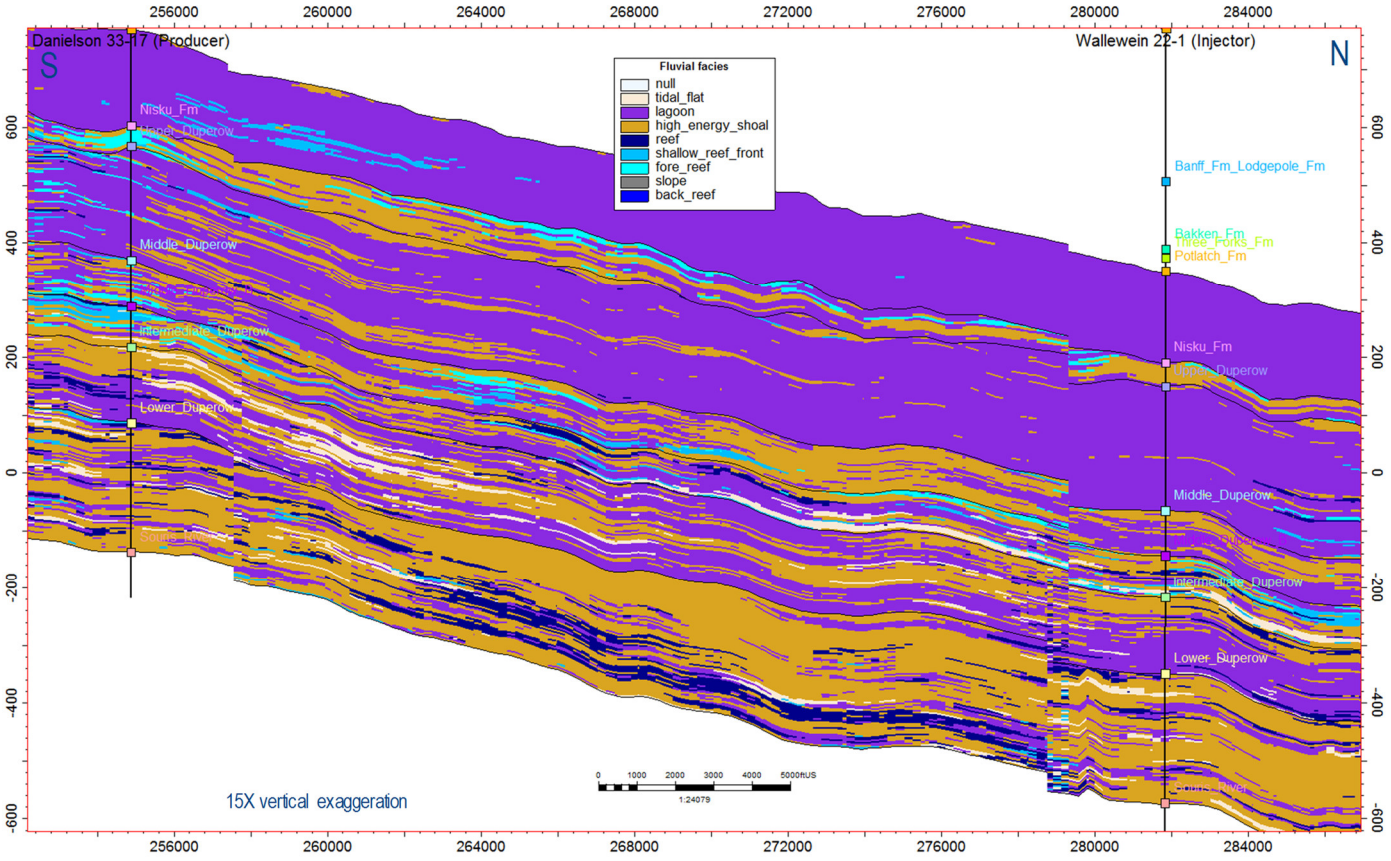

Figure 33: 8-Rock Type Interpolation of rock type. Cross section view from east. Cross section line indicated on Figure 35.

4.8.2 Effective Porosity and Permeability Interpolation 8-Rock Type

The analysis of the porosity/permeability relationship in the upscaled well logs (Potlach down to Lower Duperow) shows that there are separate and overlapping relationships when plotted against the 8 Rock Types (Figure 34 left side). Figure 34 also colors the porosity vs permeability cross plot by formation showing how each formation has a unique porosity and permeability relationship. Here it is clearly seen most of the higher porosity and permeability is in the high_energy_shoal, reef, shallow_reef_front and fore_reef facies of the Middle Duperow_B. Because of this, the porosity and permeability data within each rock type within each zone were analyzed and modeled separately using GRFS. Using the same method, GRFS was used to interpolate permeability. Because of the known functional relationship of increasing porosity representing increasing permeability, permeability was co-krigged at 95% to effective porosity. Using the GFRS method in this way, ensures that the statistical porosity-permeability relationships are honored within in each formation and within each formations' s rock type. Figure 35 shows the average effective porosity for each zone and a cross-section line for Figure 36 (Effective porosity cross-section) and Figure 37 (permeability cross-section).

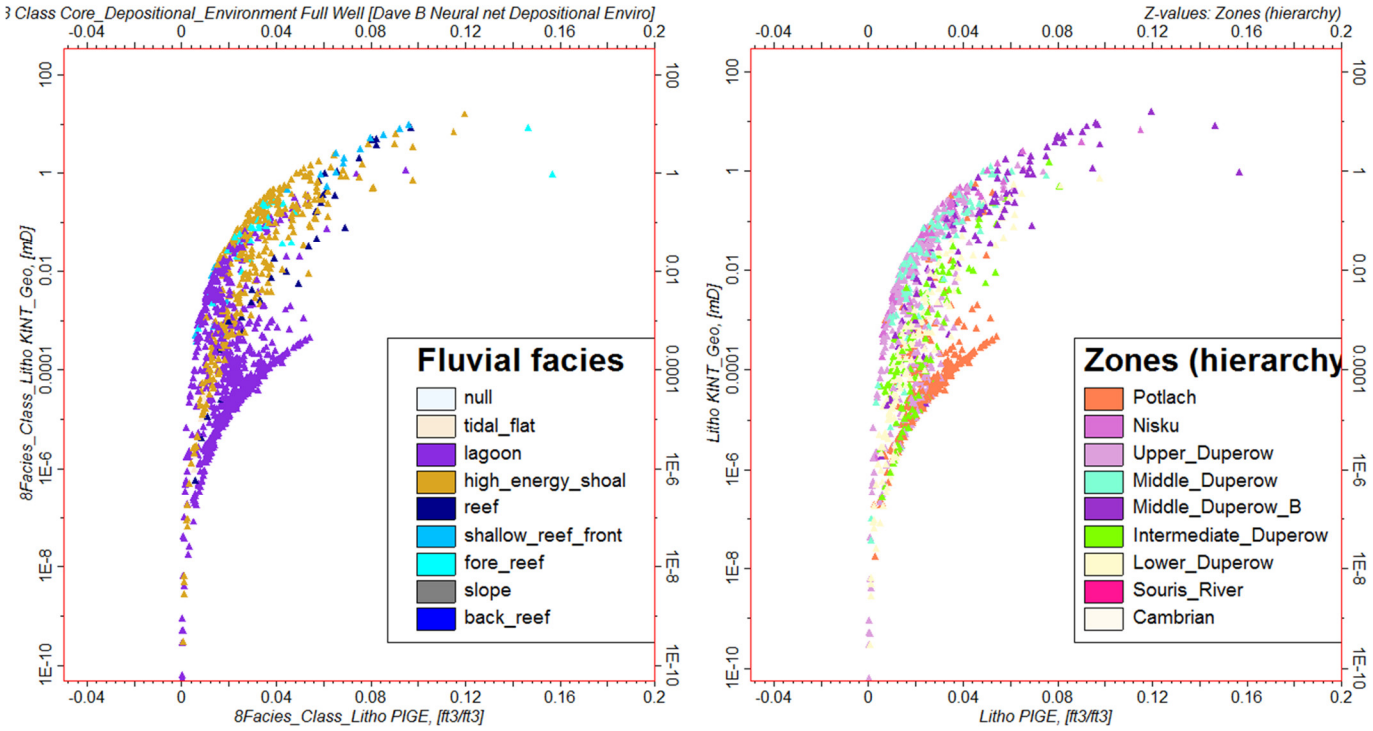

Figure 34: Cross plot of porosity (PIGE) vs. permeability (KINT) (Potlach down to Lower Duperow). On the left, the points are shaded based on the 8-Rock Types which show the three separate relationships for the three dominant rock types. On the right, the points are shaded based on the formations which show the separate relationships for each formation.

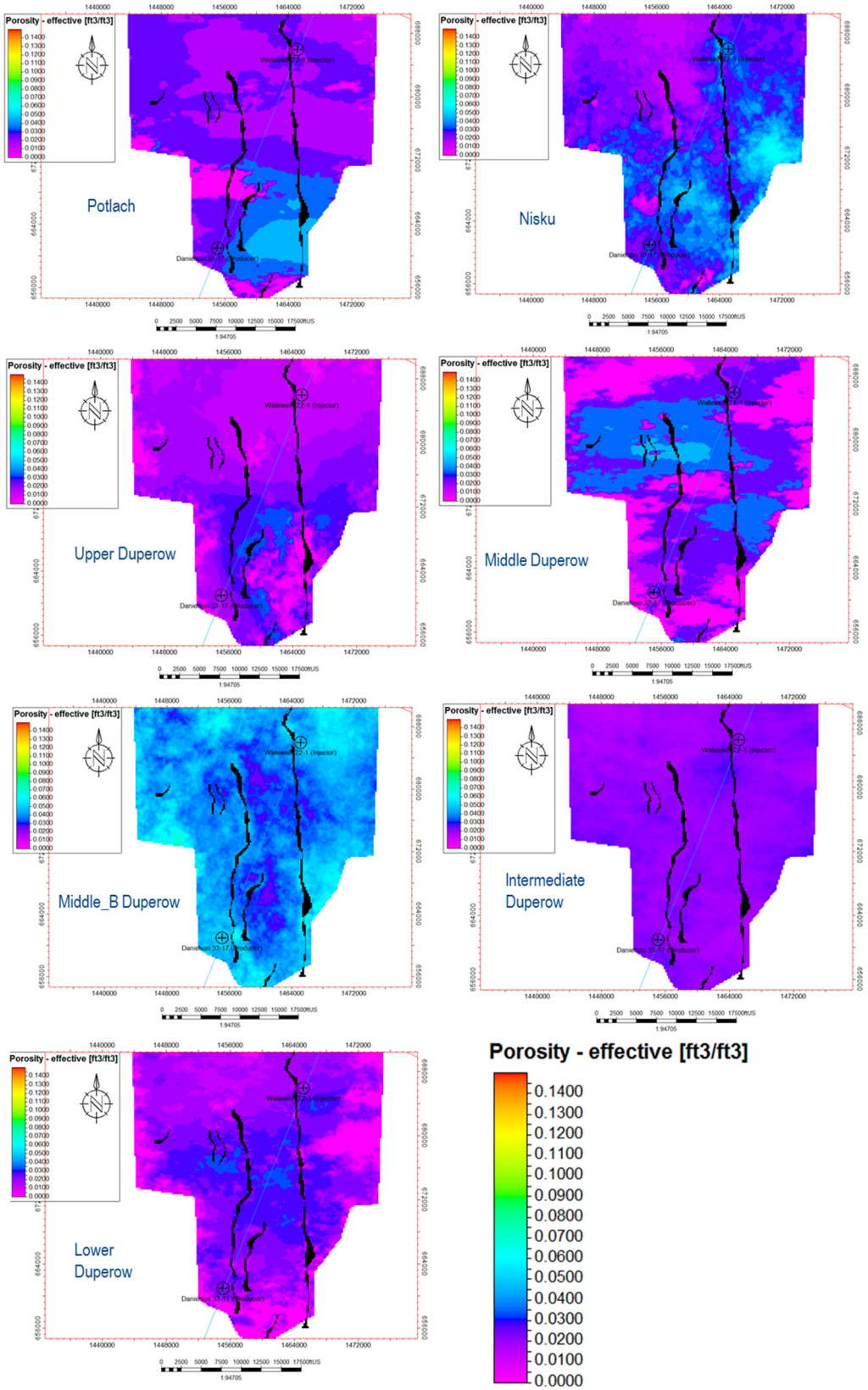

Figure 35: 8-Rock Type Average effective porosity for each formation

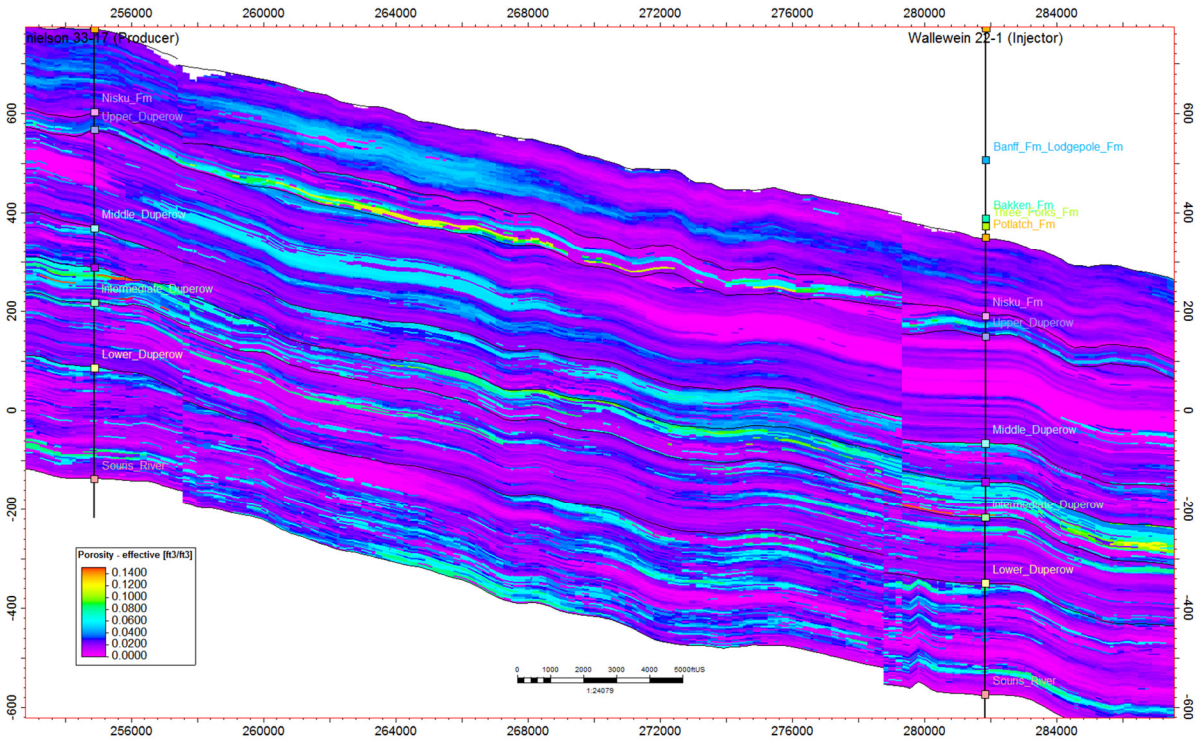

Figure 36: 8-Rock Type Effective porosity cross section. View from east. Cross section line indicated on Figure 28.

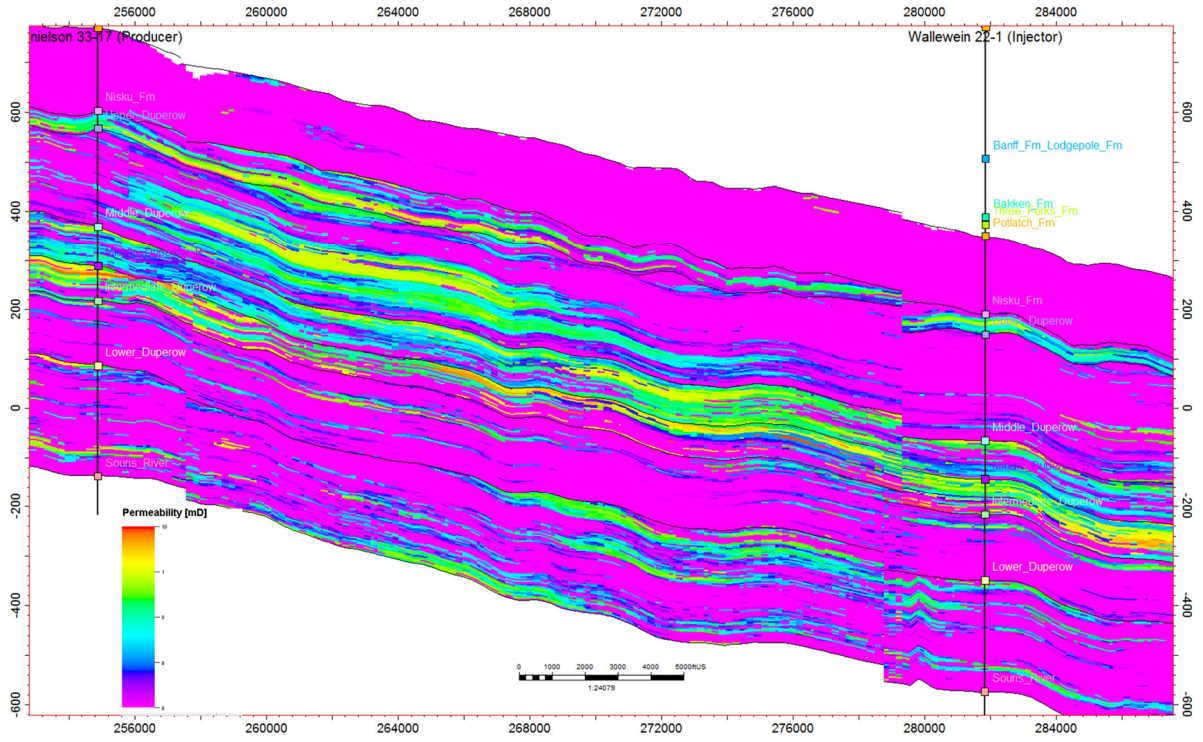

Figure 37: 8-Rock Type Permeability south to north cross-section. View from east. Cross section line indicated on Figure 28.

4.8.3 Property Modeling Quality Control 8-Rock Type

To quality control the effective porosity and permeability interpolation, histograms of porosity and permeability were examined for each zone to see if the distribution of well log values resemble the associated upscaled cells and final property interpolation (all cells). Figure 38 displays a porosity and permeability histogram that represents the all the model zones combined.

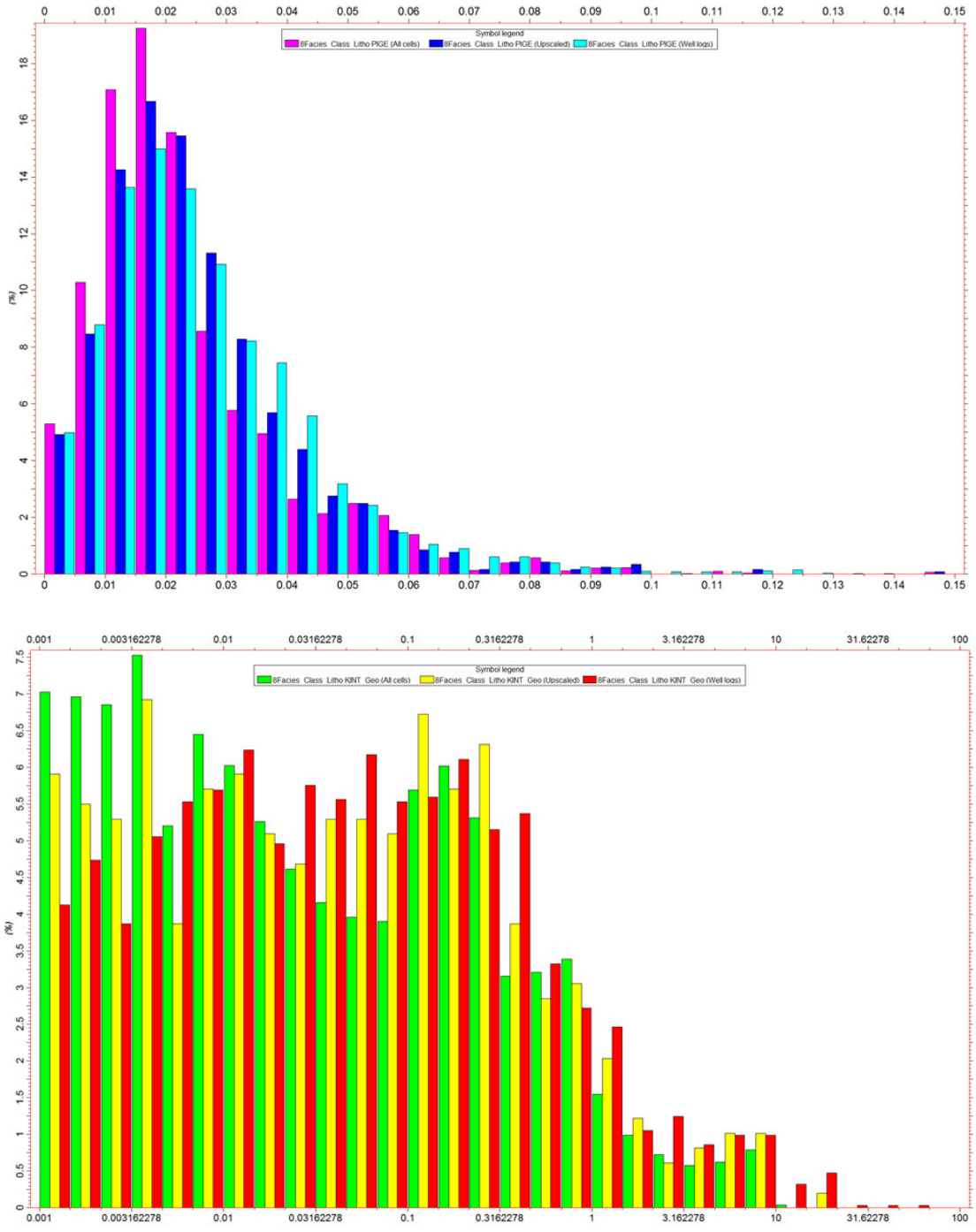

Figure 38: 8-Rock Type Quality control histograms for all modeled zones, porosity (top) and permeability (bottom)

4.9 Probabilistic Site Screening/Risk Assessment Tool

A probabilistic site screening/risk assessment tool was developed to assess likelihood of achieving objectives at any arbitrary hypothetical drilling location within the geomodel. Using an automated litho-prediction workflow with stochastic facies, porosity, and permeability modeling, this method comprehends uncertainties throughout the property modeling workflow. Because, the facies and property modeling used in the above described process is stochastic, the final result represents one of many equally likely results. Running the model multiple times will result in statistically similar results; however, the results at a specific location will vary. When picking a CO_2 injection well location, it is important to understand the uncertainty in pore volume and KH (permeability thickness) in the local area surrounding the well. The following workflow was used to quantify this uncertainty.

1. Using the 8-Rock type model, the facies, porosity and permeability modeling was run 100 times in the Middle Duperow_B. This produced 100 different by equally probable property interpolations.
2. Before each model run, the porosity and permeability model areas were clipped to a 2500ft radius around the Wallewein and a hypothetical pseudo injection well located between the Wallewein and Danielson wells (Figure 39).
3. After each model run, pore volume (PV) and KH were calculated in these clipped areas and used as proxies for storage volume and injectivity.
4. The KH values at the two pseudo wells (One in the Wallewein model and one in the pseudo well model area) were extracted after each model run.
5. A probability density function (PDF) and a cumulative distribution function (CDF) of KH maps, pseudo well KH and PV are summarized in Figure 40. The histograms show the high, low and mid-range possibilities for a 2500ft radius around the Wallewein and the hypothetical pseudo well. The distributions have less uncertainty around the Wallewein well because the localized well data have localized control of the property modeling.

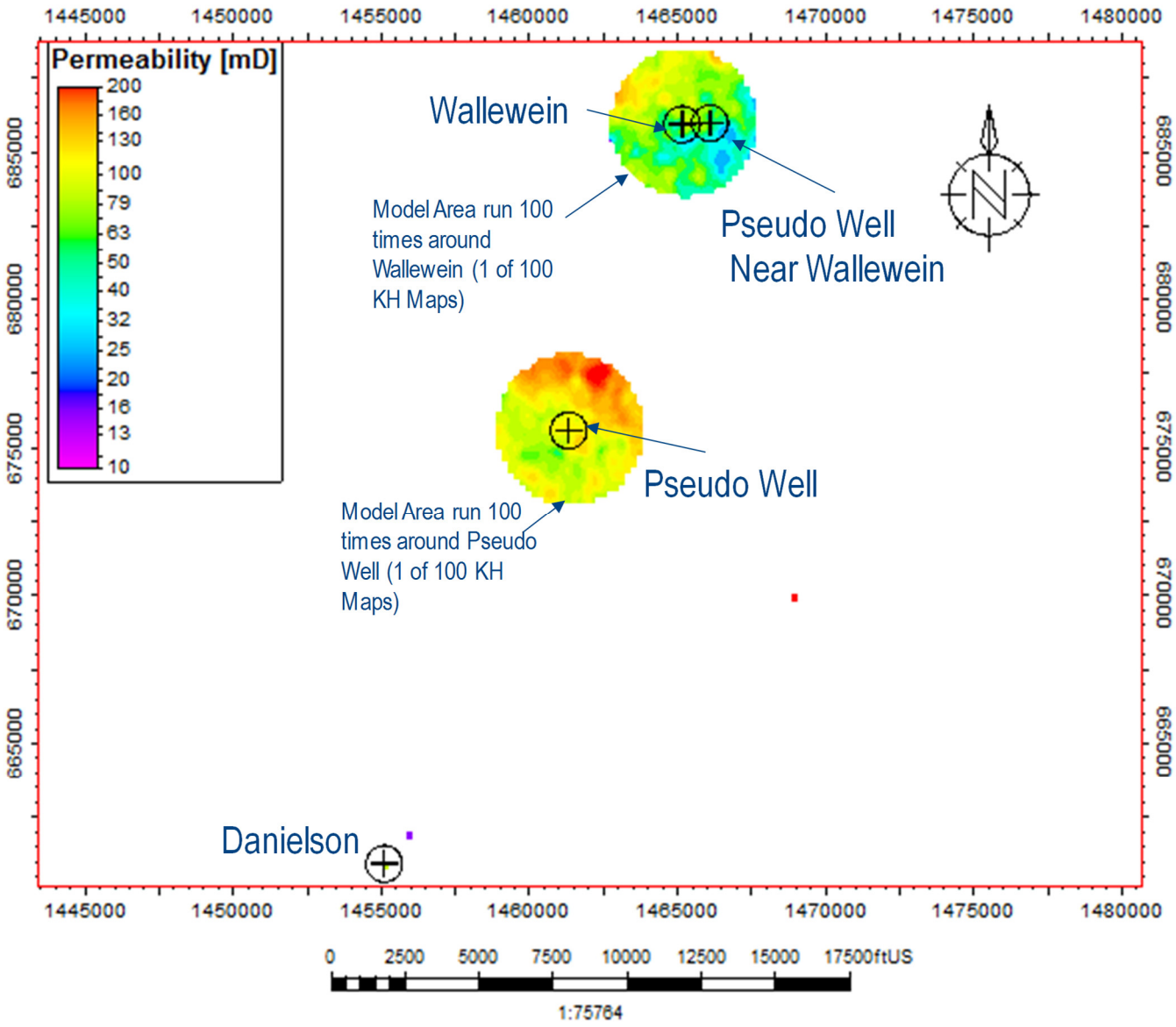

Figure 39:Uncertainty analysis model area

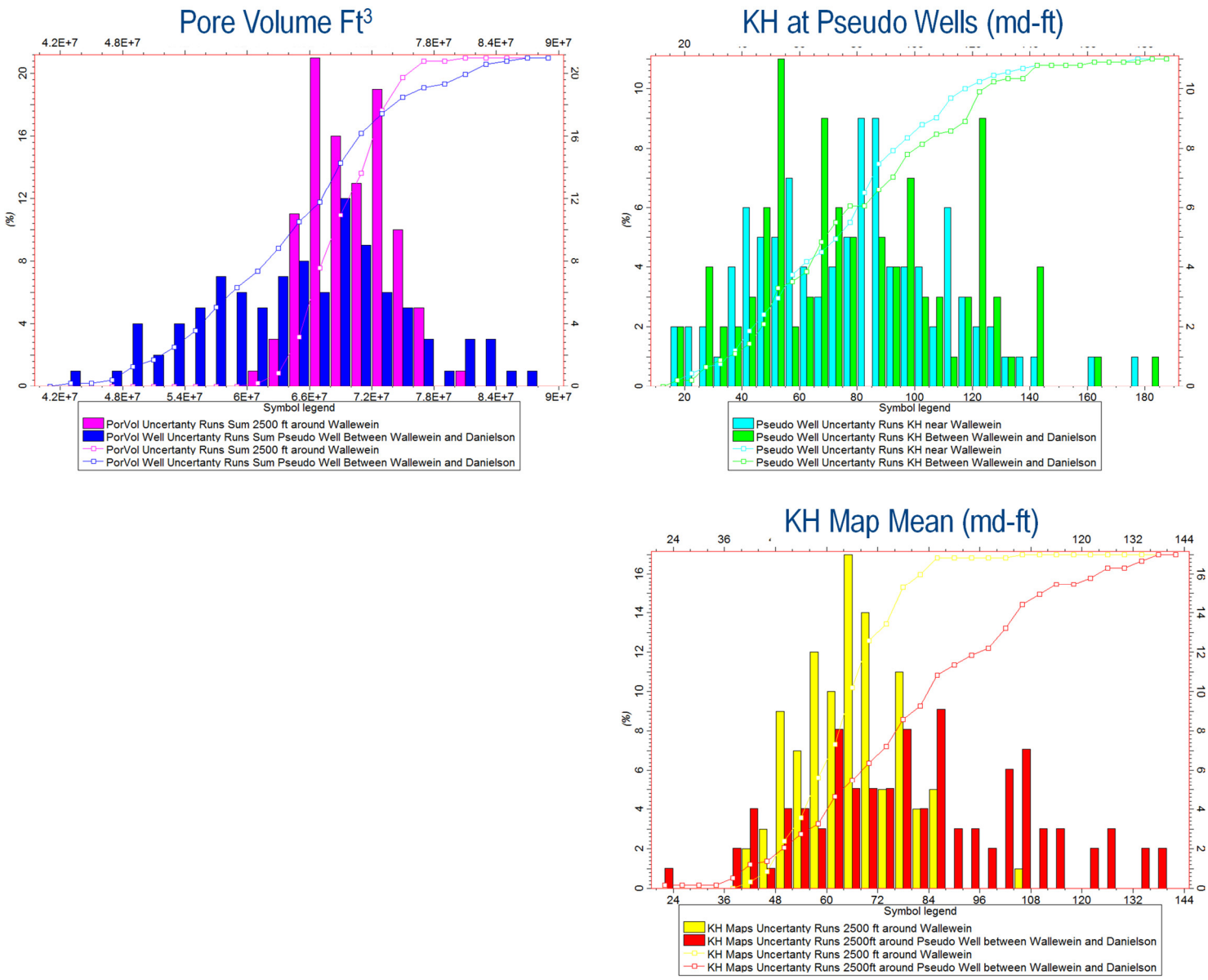

Figure 40: Summary of the 100 Iterations of PV, Pseudo Wells KH and KH average maps within a 2500 ft radius around the Wallewein and Pseudo Well

5 Fracture Modeling

Fracture modeling was completed because a significant amount of fracturing was observed in the core and FMI logs. In addition to the matrix porosity and permeability, these fractures contribute to secondary fracture porosity and fracture permeability. To represent these fractures in the geomodel, a discreet fracture network (DFN) was developed. The DFN used available data from FMI logs and core slab viewing. The DFN was developed to represent the Potlach, Nisku and Upper Duperow, Middle Duperow, Middle Duperow_B, and Intermediate Duperow formations. A DFN is calculated from many fracture attributes and outputs a discreet and implicit fracture network (Figure 41). Discreet fractures are greater than 250 ft and individually represented as a plane in the model. Implicit fractures less than 250 ft are too numerous to be modeled as individual planes; therefore, they are molded as a model property. These two fracture networks are then upscaled into the model grid to provide fracture porosity, permeability and a Fracture Matrix Coupling for each model cell. The details of this process are described in the following sections.

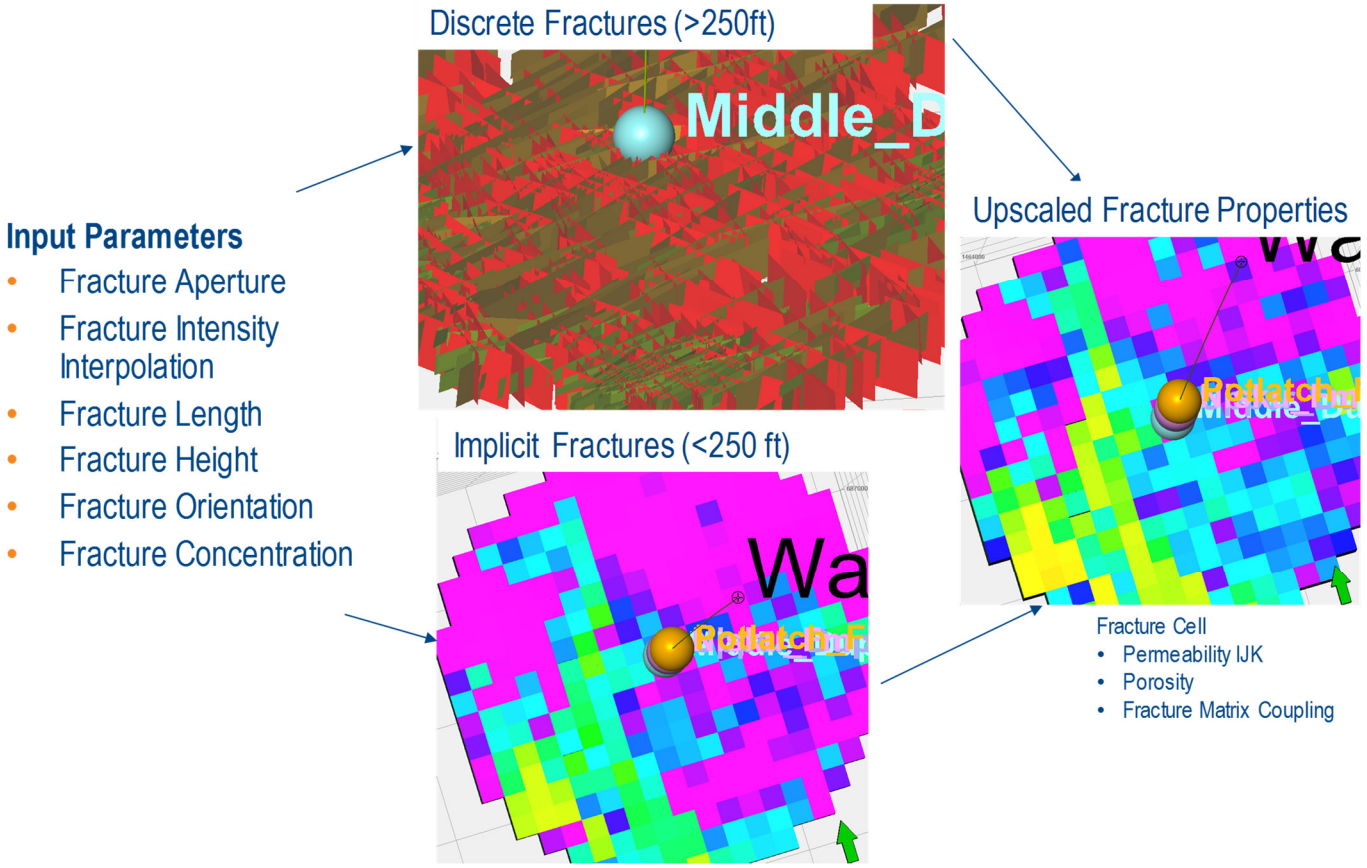

Figure 41: Key fracture parameters inputs, fracture network and fracture upscaling

5.1 Fracture Data

FMI data was collected in the Danielson and Wallewein wells (Figure 42). The following general observations were made from the FMI logs and core observations.

- The Danielson structural bedding (green circles) has a mean dip of 3.3 degrees towards the NE (N 39 degrees).
- The Wallewein structural bedding (green circles) has a mean dip of 1 degrees towards the N (N 14 degrees).
- Danielson borehole breakout indicates the direction of SHmin (N 147) and is oriented perpendicular to SHmax.
- Wallewein borehole breakout indicates the direction of SHmin (N 149) and is oriented perpendicular to SHmax.
- There were 260 open fractures (dark blue tadpoles Figure 42) observed in the Danielson and 183 in observed in the Wallewein. Closed fractures are the light blue tadpoles Figure 42. The fact that more fractures observed in the Danielson is to be expected because it is located up on Kevin Dome and that location would have undergone more structural change resulting in more fracturing.
- The Madison formation is highly fractured. This formation is above the Potlach so was not part of the DNF.
- The base of the Middle Duperow_B is fractured heavily in the Danielson and is likely related to an interpreted micro fault just below this fracture zone. This feature matches what was observed from core slab viewing (Figure 43).
- A student of Dave Bowen's (Thomas Pausch) logged the core with a focus on fractures and prepared a report (Fracture Analysis of Cored Intervals of the Duperow Formation). This report recorded characteristics of all individual fractures observed in the core; however, only summaries of the results were provided. The raw data of a fracture's depth and parent rock type were not made available; therefore, these results could not be compared directly to the FMI results. The summary results of open and closed fracture count did match reliably to the FMI log cropped along the core interval.

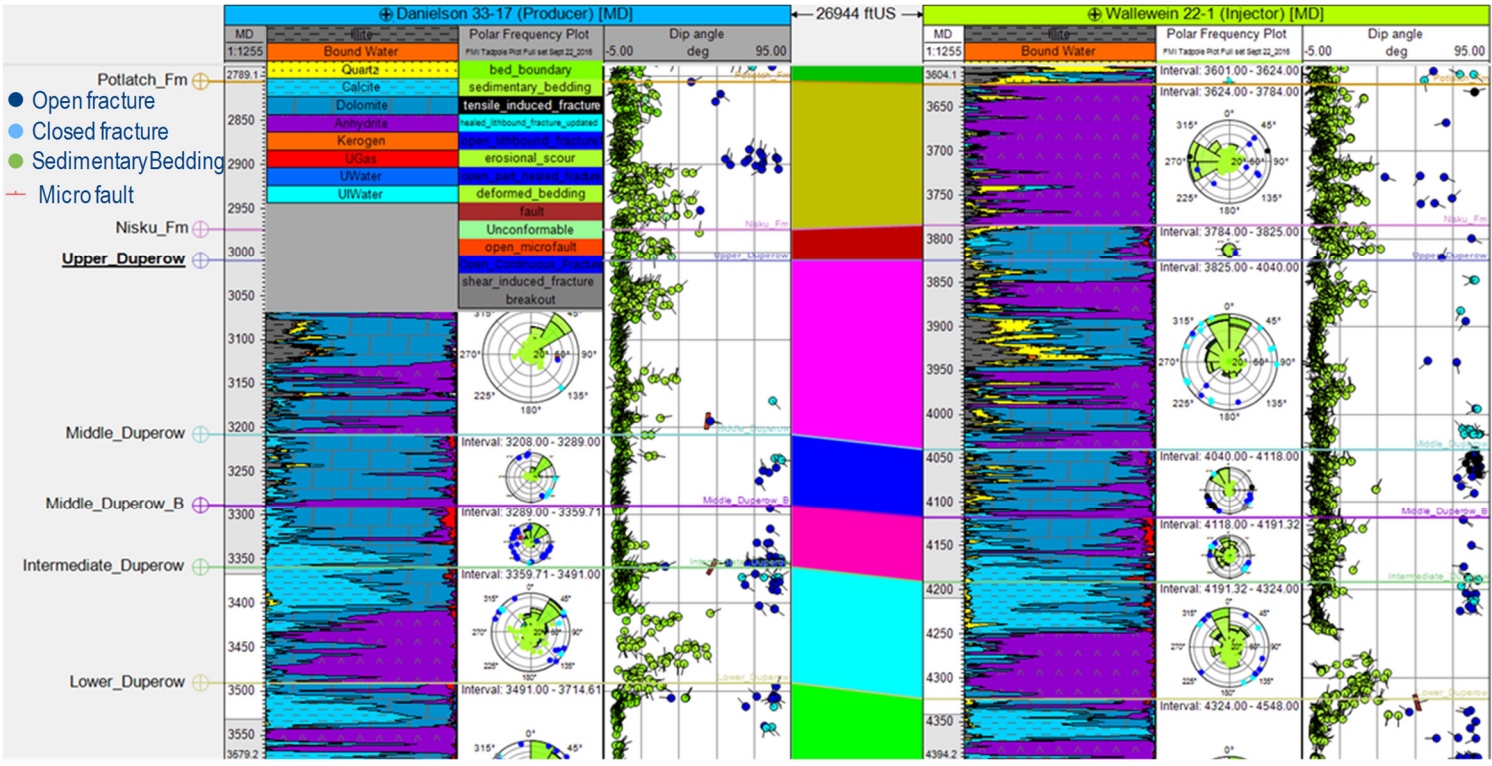

Figure 42: FMI data from the Danielson and Wallewein (stereonet and tadpole plot)

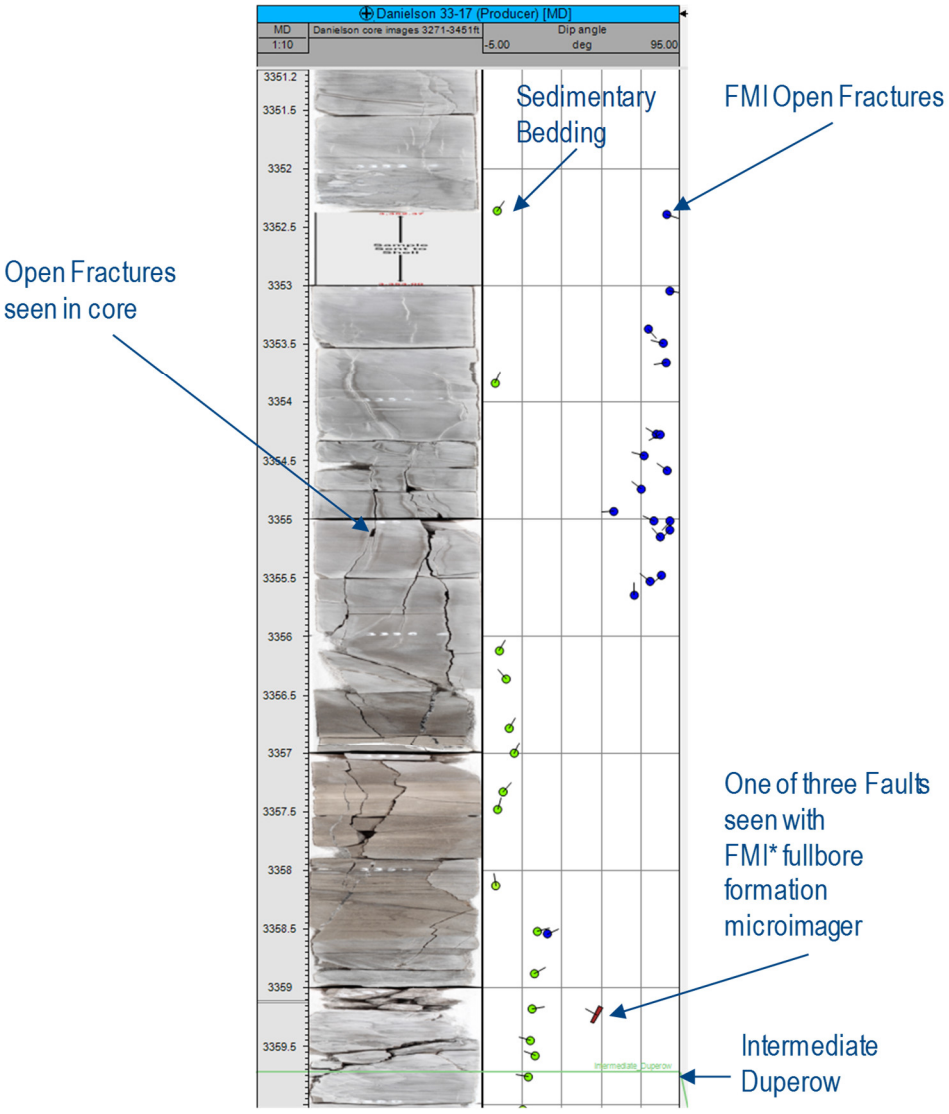

Figure 43: FMI and Core Comparison of an area of high fracture intensity in the Danielson

5.2 Fracture Sets

To keep the model computation time to a minimum, only the open fractures as interpreted from the FMI data were modeled in the DFN. Fracture patterns were observed in the data and fracture sets were grouped into two formation groups. Formation Group 1 consists of the Potlach and Nisku (Figure 44), while Formation Group 2 (Figure 45) consists of the Duperow Formation (Upper, Middle, Middle_B, and Intermediate). Three identifiable fracture clusters were distinguished with within each formation group. When modeling fracture sets, it is necessary to enter the mean dip azimuth, mean dip, and concentration. Table 4 is a list of fracture sets with these parameters as identified from the fracture set analysis.

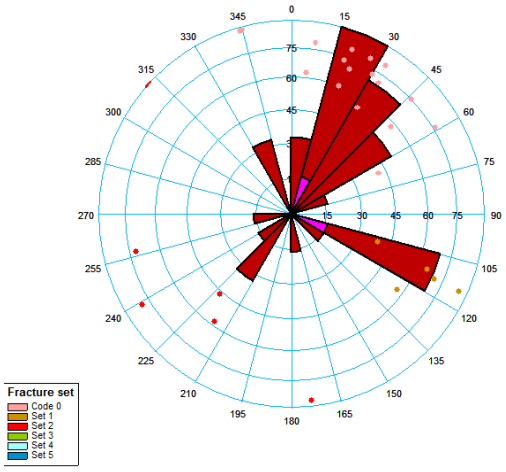

Figure 44: Formation Group 1 stereonet of fracture sets 0, 1 and 2 in the Potlach and Nisku, Wallewein and Danielson Wells

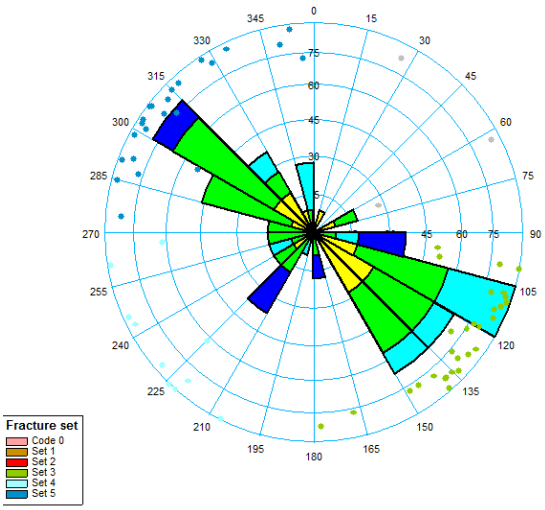

Figure 45: Formation Group 2 stereonet for fracture sets 3, 4 and 5 in the Duperow (Upper, Middle, Middle_B, Intermediate), Wallewein and Danielson Wells

Table 4: Fracture set dip, azimuth and concentration

Fracture Group	Formation	Fracture Set	mean dip azimuth (degree)	mean dip (degree)	concentration
Fracture Group 1	Nisku, Potlach	Set 0	26.8	70.2	7.6
		Set 1	115	63.2	31.4
		Set 2	215	65.2	7.1
Fracture Group 2	Upper, Middle, Middle_B, Intermediate Duperow	Set 3	126.4	78.3	10.5
		Set 4	235	81.7	19.7
		Set 5	311.3	81.4	10.8

5.3 Ant Tracking

Ant Tracking is a process to capture the discontinuities embedded in seismic data. It is particularly powerful in terms of capturing small scale, often subtle discontinuities which normal interpretation cannot realistically capture. The Ant Tracking algorithm follows an analogy of ants finding the shortest path between their nest and their food source by communicating using pheromones, a chemical substance that attracts other ants. The shortest path will be marked with more pheromones than the longest path and so the next ant is more likely to choose the shortest route, and so on. The idea is to distribute many these electronic "ants" in a seismic volume; and let each ant move along what appears to be a fault surface while emitting "pheromone." Ants deployed along a fault should be able to trace the fault surface for some distance before being terminated. Surfaces meeting expectations will be strongly marked by "pheromone." Surfaces unlikely to be faults will be unmarked or weakly marked. The resultant Ant Track attribute cube offers a highly detailed mapping of fault/fracture discontinuities within the seismic data.

The Ant Track seismic attribute volume was created from the final Chaos attribute volume (Figure 46). The ant paths or subtle discontinuities are highlighted in blue. Using this Ant Tracking volume, an automatic fault extraction process was run to generate fault planes along the ant paths or subtle discontinuities highlighted in blue. The dip azimuth of these extracted faults and the dip azimuth observed from the FMI fractures were compared in a histogram filtered for the Potlach to Intermediate Duperow (Figure 47). A good correlation of dip direction was observed with dip directions being concentrated around 120 degrees, 240 degrees and 320 degrees in both data sets. This correlation demonstrates that the Ant Tracking Attribute is a reliable way to identify subtle discontinuities related to fracturing at Kevin Dome. This Ant Tracking attribute was used an input for generating a fracture driver for fracture network interpolation. At the wellbores, there is also a reasonable correlation between Fracture Intensity and the Ant Tracking attribute.

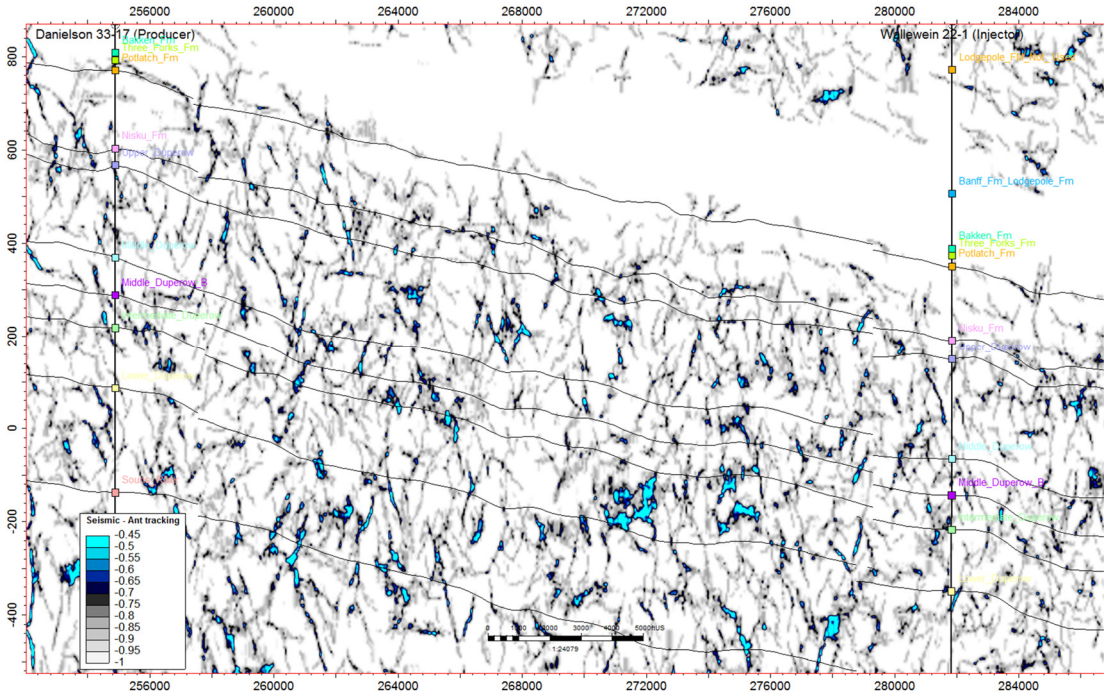

Figure 46: Ant Tracking south to north cross-section. View from east. Cross section line indicated on Figure 28.

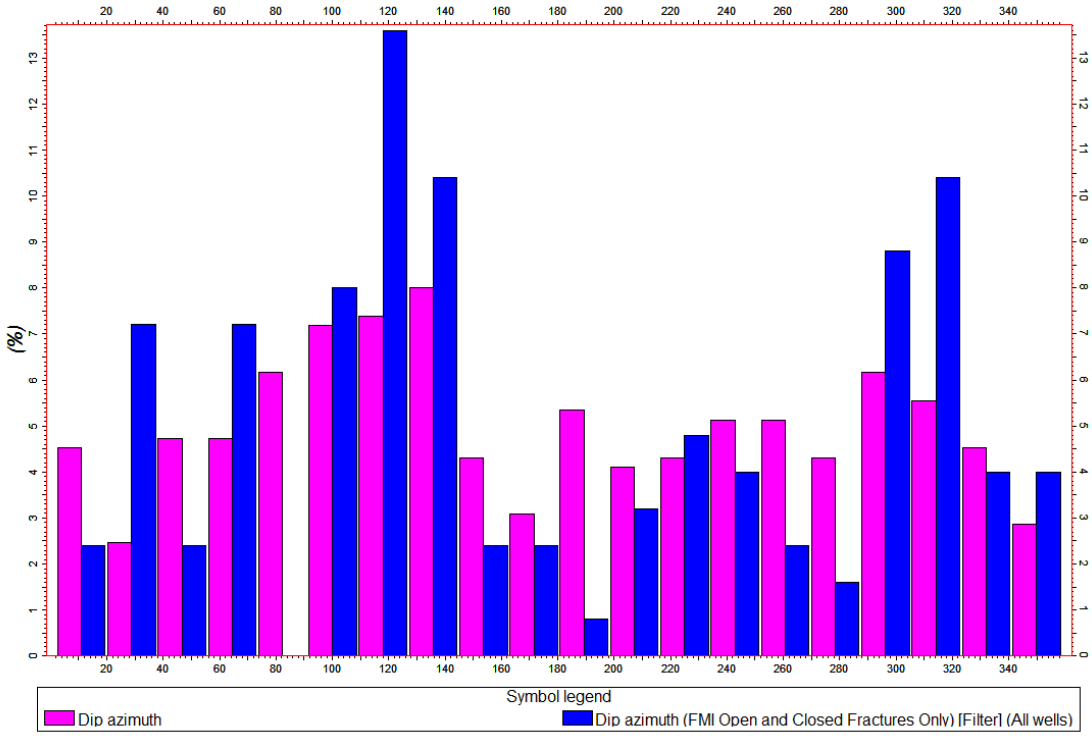

Figure 47: Ant Tracking dip azimuth of extracted faults (pink) and the dip azimuth observed from the FMI fractures (blue). These data are filtered for the Potlach to Intermediate Duperow

5.4 P32 Fracture Intensity

For each fracture set, logs of fracture intensity were generated from the FMI open fractures. This fracture intensity P32 log is fracture area per volume. This process outputs a P10, P50 and P90, which represent lower, middle and an upper end estimation of P32 fracture area per volume. These logs were upscaled at the borehole. The mid case P50 fracture intensity P32 logs were used in following fracture modeling. Because fracturing is typically observed along faults, a P32 value was assigned to an area along the faults.

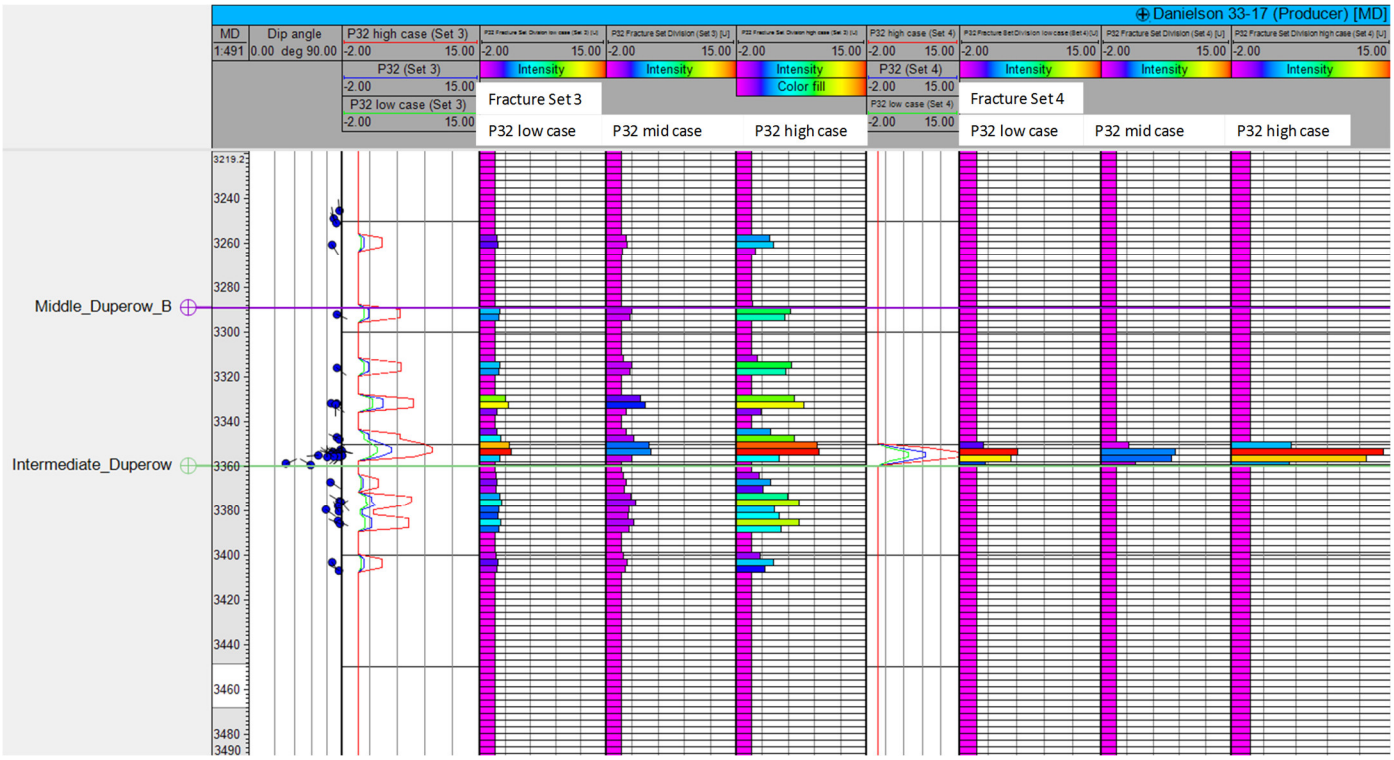

Figure 48: P32 fracture intensity logs and upscaled cells for fracture sets 3 and 4 at the Danielson well

5.5 Fracture Driver

FMI data provides detailed information about fractures at the wellbore but nothing in the inter-well space. To resolve this, a fracture driver was needed to guide the P32 fracture intensity property interpolation. Volume attributes were extracted from the 3D TVD seismic data and used in a neuralnet process supervised to the P32 fracture intensity mid case at the wells. This supervised process attempted to find a correlation between the seismic attributes and the well log P32 intensity. The neuralnet included the following seismic attributes:

- Density
- S-Impedance
- P-Impedance
- Ant Tracking
- Variance
- Chaos
- Gradient
- Frequency
- Curvature
- Sweetness
- 3D edge Enhancement
- Brittleness index

Given the data availability for this project, the brittleness component of the fracture driver was a combination trend of a brittleness index and formation curvature. Brittle rock is more likely to fracture therefore a brittleness index property was calculated from the elastic inversion products. The brittleness index was calculated using the equation in Figure 49. Because rock that is more deformed is more susceptible to fracturing, a formation curvature property was calculated from the formation surfaces. A process to extract a curvature attribute from the formation surfaces was completed.

E Young's Modulus
υ Poisson's ratio

Calculated Attributes
V_p P Wave Velocity
V_s Shear Wave Velocity

Available Data
I_p P-Impedance
I_s Shear-Impedance
ρ Density

Brittleness Index;

$$\frac{E}{\upsilon}$$

Where;

$$E = 2\mu(1+\upsilon)$$

$$\upsilon = \frac{(V_p^2 - 2V_s^2)}{2(V_p^2 - V_s^2)}$$

$$V_p = \frac{I_p}{\rho}$$

$$V_s = \frac{I_s}{\rho}$$

$$\mu = \rho I_s$$

Figure 49: Brittleness index equation

The results of the seismic attribute neuralnet predicted P32 intensities and the P32 intensities at the wells were cross plotted and a not ideal but useable correlation (0.41) was found (Figure 50 and Figure 51). The P32 fracture intensities for each fracture set were interpolated from the wells using the seismic neuralnet prediction P32 property and extracted variogram parameters. The result was a P32 fracture intensity property for the six fracture sets.

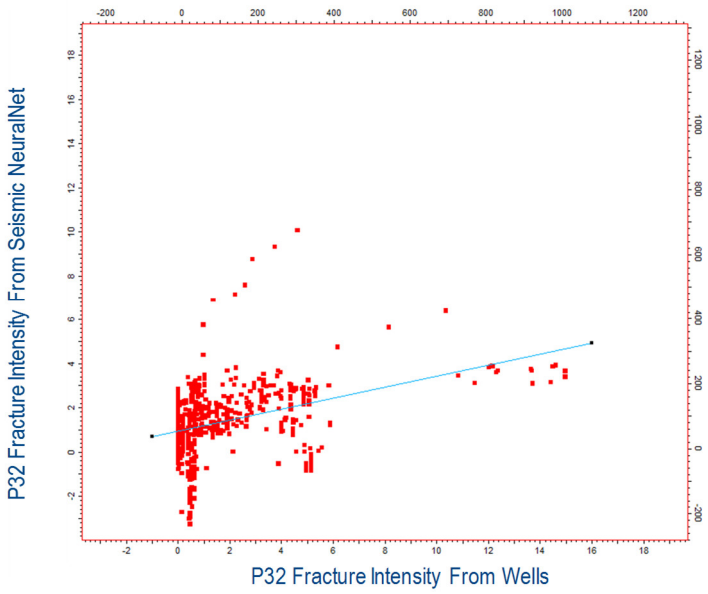

Figure 50: Cross plot of Fracture P32 intensity; log fracture intensity vs neuralnet predicted seismic fracture intensity and correlation coefficient

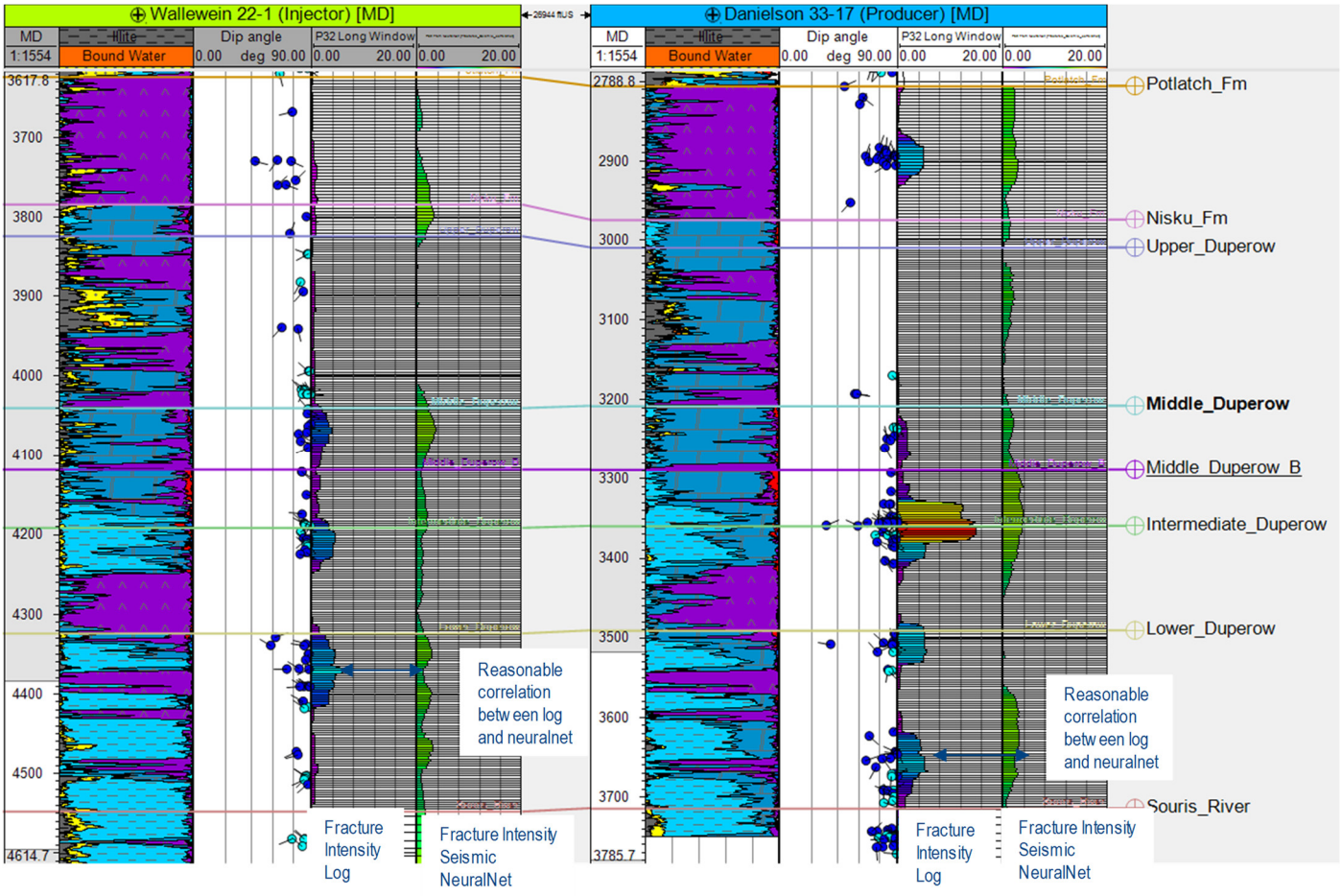

Figure 51: Well scale comparison of the well log fracture P32 intensity and the neuralnet predicted seismic fracture intensity

5.6 Fracture Aperture

A Mean Hydraulic Fracture Aperture (FVA) log was provided that represents the aperture width of open fractures in the wellbore. The aperture width observed from the FVA log (green) has a lognormal distribution and the modeled fractures (blue) were scaled with a similar log normal distribution to match the FVA log (Figure 52).

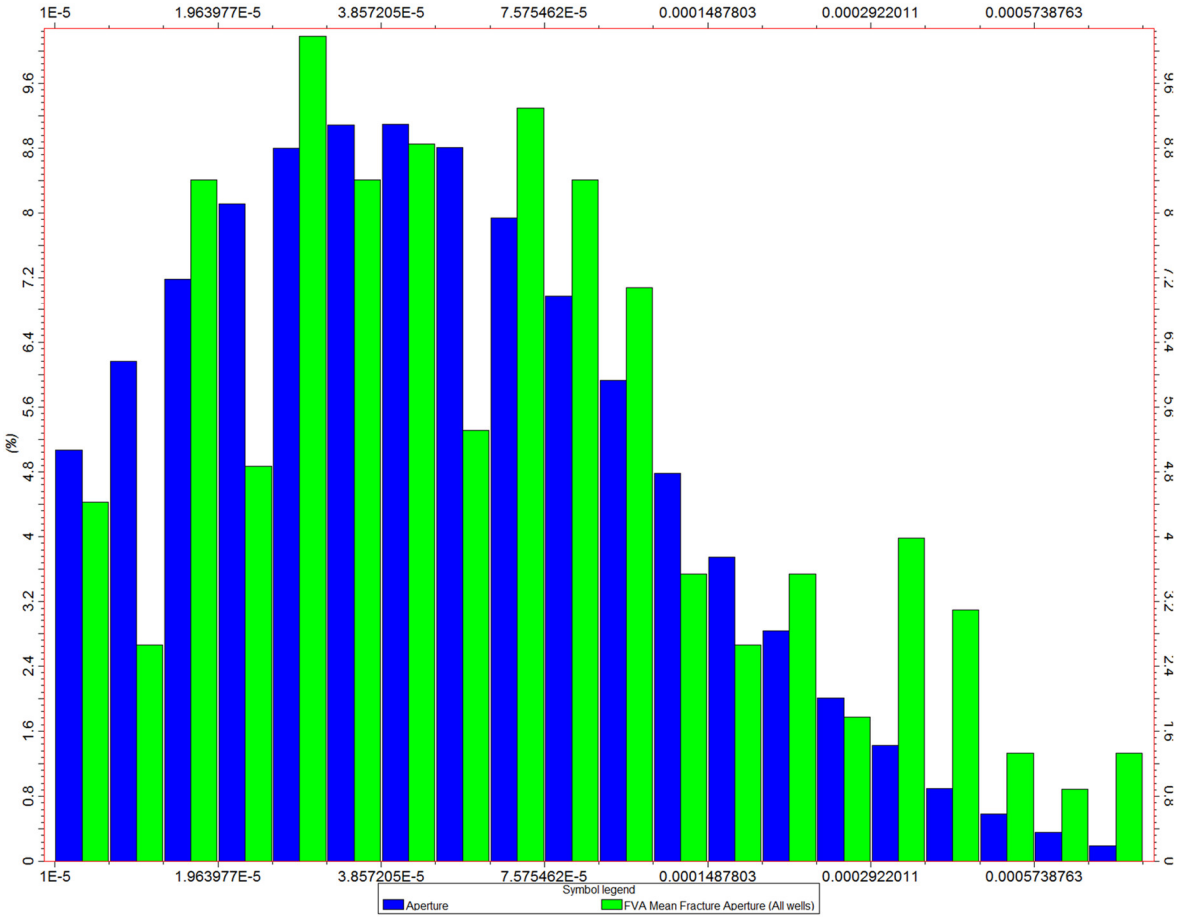

Figure 52: Histogram of fracture apertures (ft) from the FMI analysis (green) and the model results (blue)

5.7 Fracture Length and Height

When modeling fractures, the following input parameters were used to control length, height, shape and distribution:

- Observed fractures in the whole core slabs indicated that fractures are up to 10 feet high and mechanically bound within the originating rock type.
- The length of fractures is difficult to determine from FMI logs alone. Fractures lengths were entered to be ten times as long as they are high. MSU geologist Dave Bowen estimated this parameter.
- Using a power law distribution, fracture length was modeled with a minimum length of 100ft up to a maximum length of 400ft.
- Fractures were modeled implicitly and discreetly. Discreet fractures are greater than 250 ft and individually represented as a plane in the model. Implicit fractures less than 250 ft are too numerous to be modeled as individual planes; therefore, they are molded as a property.

5.8 Fracture Network

Using the previously described input parameters, a fracture network was generated for each formation for all six-fracture sets. Figure 53 is an of how the discreet fracture sets 3, 4, and 5 are orientated within the Middle Duperow_B.

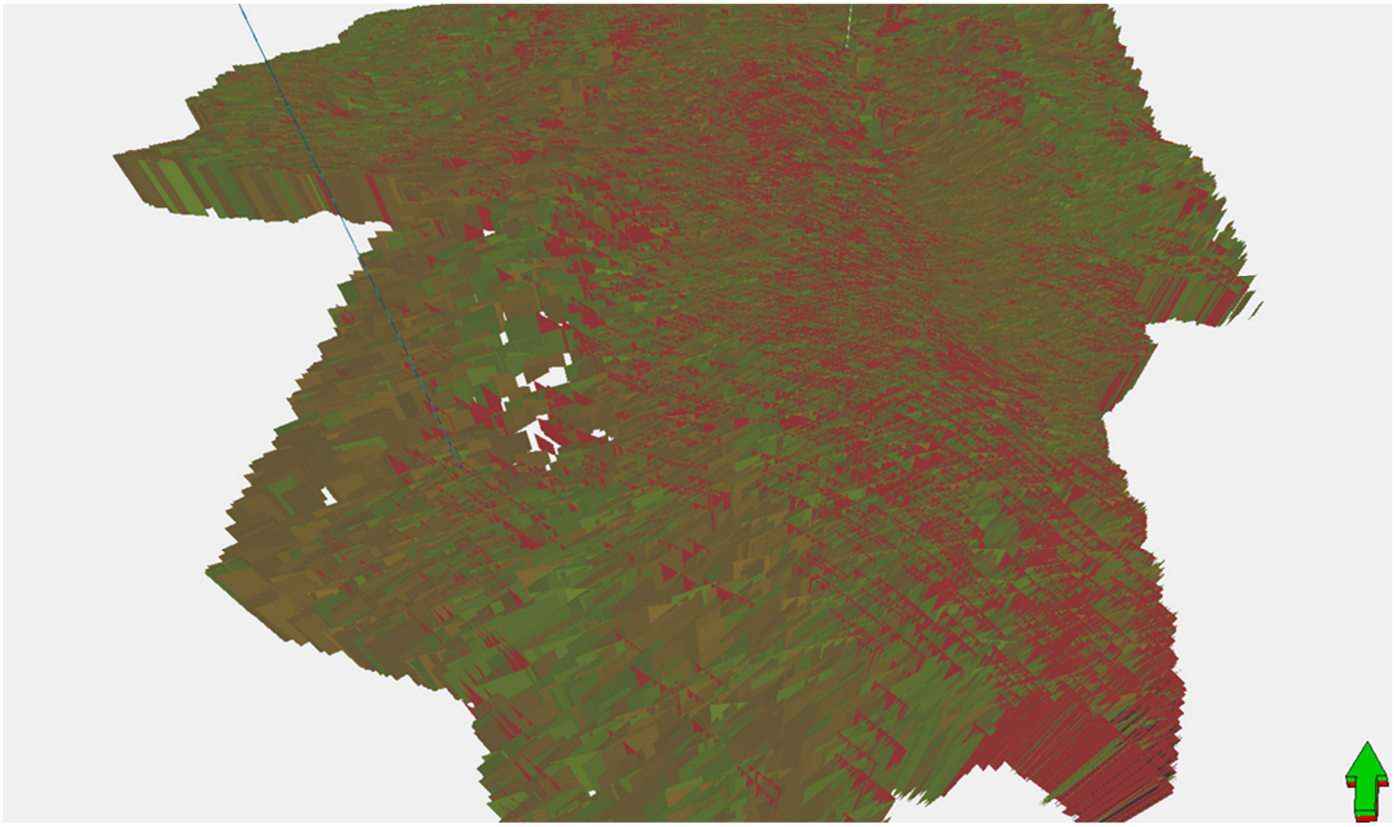

Figure 53: Fracture network of Middle Duperow_B, fracture set 3, 4 and 5.

5.9 Scale Up Fracture Network Properties

To incorporate the discreet and implicit fracture model into the 3D grid, the scale up fracture network process was used to scale up the DFN to grid porosity and permeability properties. Three steps were used to do this:

1. The Oda upscaling method, a statistical calculation of permeability based on the geometry and distribution of fractures in each cell, was used. This method runs quickly and incorporates both the implicit and discreet fracture network; however, it assumes that all the discreet fractures are connected and therefore often overestimates permeability.
2. The Oda Corrected upscaling method was run because it calculates the connectivity or lack of connectivity of the discreet fractures unlike the Oda method. This method provides a more reliable calculation of permeability for the discreet fractures. The limitation to the Oda Corrected method is that it can only be run on the discreet fracture network and excludes the implicit fracture network.
3. An Oda Calibrated technique was used to compensate for the limitations of both upscaling methods.
    a. The Oda method was run only on the discreet fracture network.
    b. The factor between the discreet fracture permeability values for Oda and Oda Corrected methods was calculated at each grid cell. This quantifies how much the Oda method overestimated permeability compared to the Oda Corrected method. The Oda method overestimated permeability by a mean factor of approximately 1.4.
    c. An Oda Calibrated version of permeability was generated by applying the above factor to reduce the original Oda results. The Oda Calibrated version of fracture permeability now incorporates the non-connectivity of the discreet fractures.

d. The fracture permeability values from the Oda Calibrated method are reasonably close to what was observed in the step-rate injection and pressure fall-off test conducted at the Wallewein well on March 18, 2015 (Middle Duperow perforation interval). The well test results described a heterogeneous reservoir with good permeability to the injected water, with effective permeability of 19 md to the injected water, and a skin factor of -1.3, which is a normal skin value for a naturally-fractured reservoir. The average permeability that the Oda Calibrated method calculated over the Wallewein perforation interval where the test was conducted was 30md. Notwithstanding the uncertainty in these methods, these fracture permeability results are a reasonable match to the well test; therefore, the Oda Calibrated method is considered to have calculated a reliable result with respect the to the magnitude of fracture porosity and fracture permeability. Histograms of fracture permeability in the I, J and K directions were analyzed (Figure 54 and Figure 55).

e. To better visualize where the fracture permeability results are most concentrated, the I, J and K direction permeabilities were summed for each formation. Permeability thickness maps (Kh maps) were then calculated from these permeability totals (Figure 56). In Figure 56, warm colors indicate areas of more fractured rock.

Figure 54: Histogram of the fracture network permeability (md) in the I, J and K directions (Nisku and Potlach)

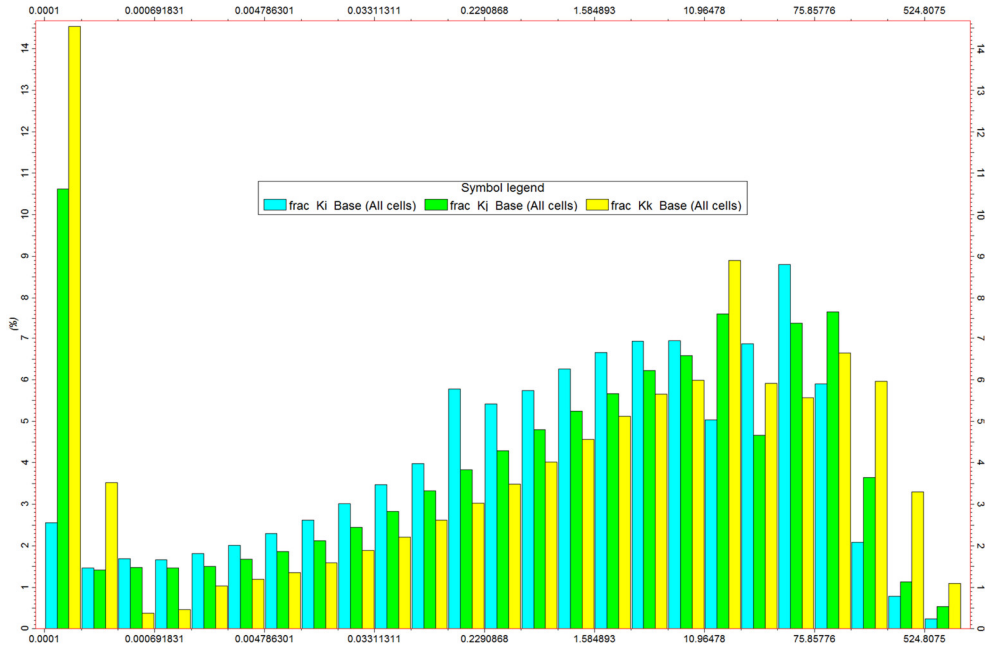

Figure 55: Histogram of the fracture network permeability (md) in the I, J and K directions (Upper, Middle, Middle and Intermediate Duperow)

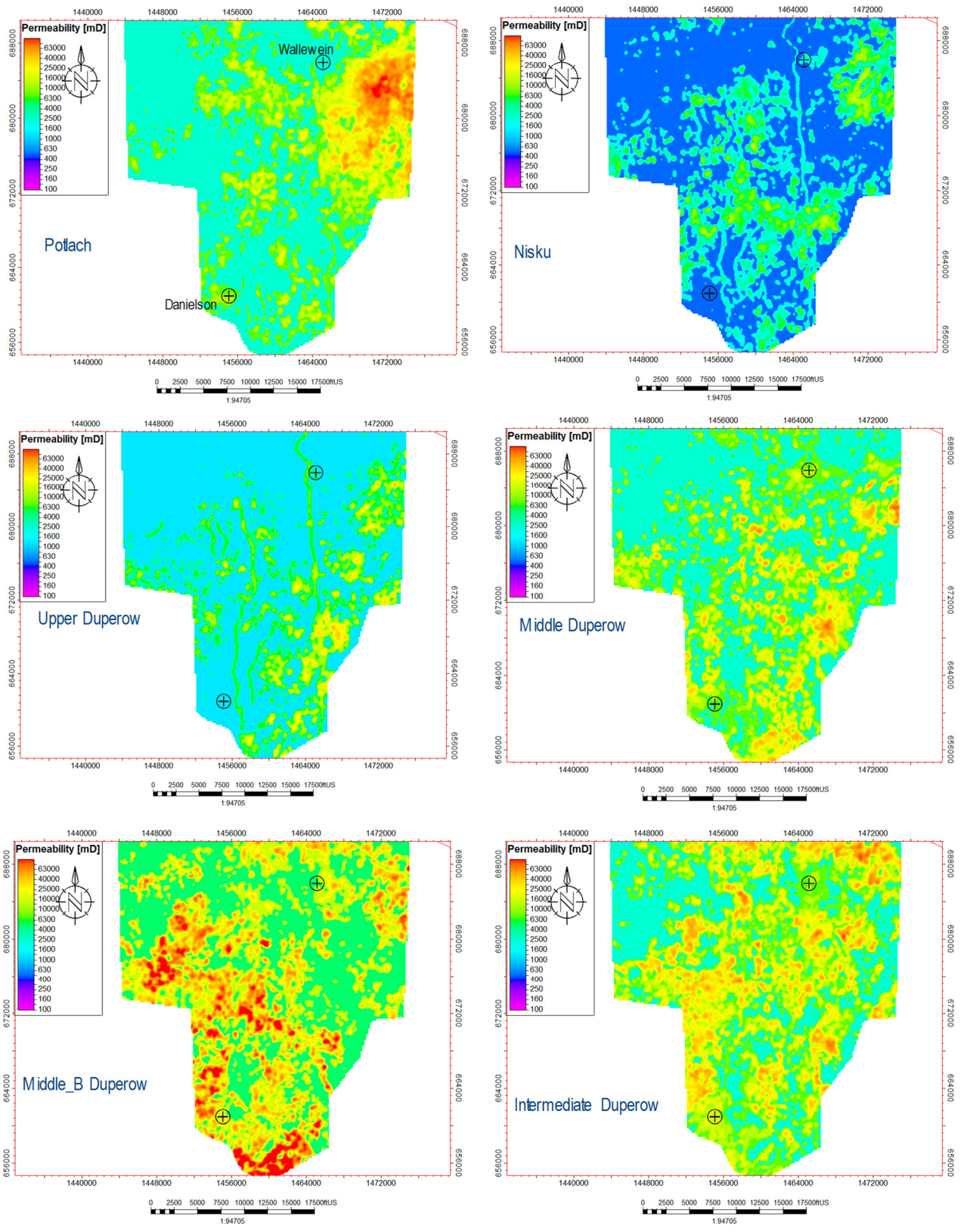

Figure 56: Permeability thickness maps (Kh) of the total of IJK fracture permeability

5.10 Fracture Parameter Sensitivity

With most fracture modeling, there is a high degree of sensitivity to certain input parameters. There is detailed fracture information at the Danielson and Wallewein wells but limited fracture information between the wells. To handle this, a sensitivity analysis was completed on input parameters. This analysis used a tornado chart to illustrate how the high, low and mid-range input parameters affect the outcome of the fracture modeling. Four variables consisting of P32 intensity, fracture length calculated with the Oda method, fracture length calculated with the Oda corrected method and fracture aperture diameter were adjusted one at a time to quantify the variation in the calculated fracture cell permeability. The sensitivity analysis was only completed on the Middle Duperow_B and on a smaller model with a 3000ft diameter centered on the Wallewein.

Tornado diagrams (Figure 57) deterministically analyze the sensitivity and relative importance of input variables. For each of these input variables considered, an estimate for what the low, base, and high outcomes where determined. Base case values were already discussed in the above sections; high and low ranges for these input data (P32 intensity, fracture length and fracture aperture diameter) were then determined based on available data. The metric used to quantify the sensitivity with these varying parameters, the mean of the fracture permeability within the Middle Duperow B, was determined to be a reliable metric. For each cell in the model, a fracture permeability value is calculated which represents how much fractures contribute to the permeability of each cell in the model. This is not to be confused with the matrix permeability. Both the fracture permeability and matrix permeability are to be used in future reservoir simulations. The mean fracture permeability is the average of the I, J and K direction fracture permeability for each cell in the model.

The base case for fracture aperture diameter was determined by picking the average aperture value from the log-normal distribution from the histogram (Figure 52) of the apertures measured from the FMI log of the Danielson well (Section 5.6). Likely high end and low-end cases were also chosen from the histogram. Fracture length was the most difficult input parameter to determine because no direct measurements of fracture length were available. A base, low and high value were determined based on what was considered reasonable for carbonates in the area. The base, high and low values for P32 fracture intensity was easier to determine because the Petrel* Fracture density process calculates these automatically and exports a base (P50), low (P10) and high (P90) range for this parameter.

Analyzing the results of Figure 57 shows that a small change in fracture aperture or the choice which P32 case to use, has a large impact on the output fracture permeability. Discreet fracture length used by the Oda corrected method has a significant effect on the final permeability results. Discreet fracture length used by the Oda method had little effect on the final permeability results.

Variable Input	Low	Base case	High
Aperture (ft)	0.00004 (0.012mm)	0.00007 (0.021mm)	0.00014 (0.042mm)
P32	P10	P50	P90
Fracture Length Oda Corrected Fracture Upscale method (ft)	10	100	200
Fracture Length Oda Fracture Upscale method	10	100	200

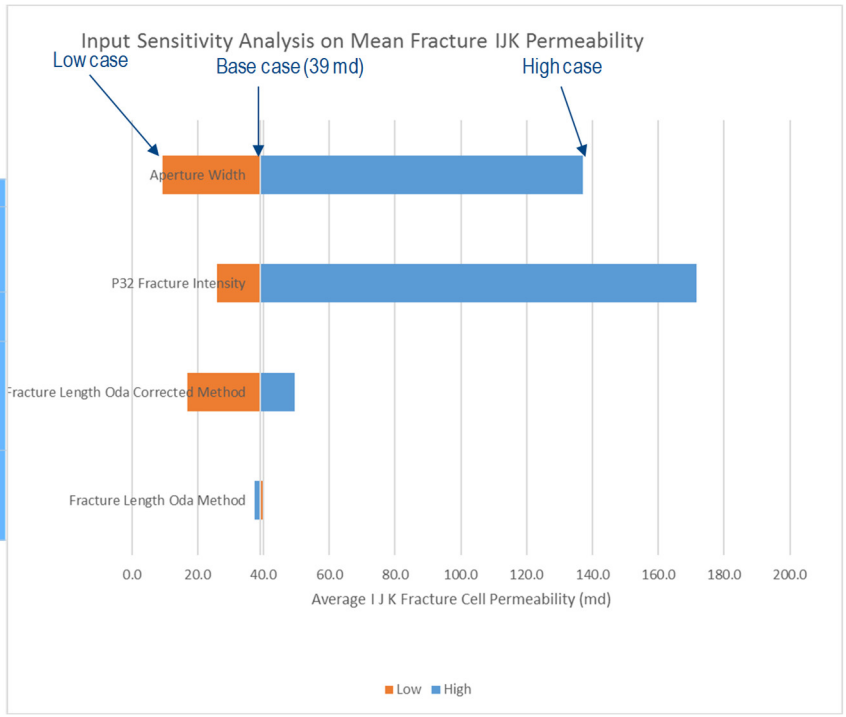

Figure 57: Tornado plots illustrating the sensitivity of input parameters on mean fracture IJK permeability

5.11 Fracture Permeability Uncertainty

The above described fracture modeling process is stochastic and the results that were finalized are one result of many possibilities. Running the process multiple times results in slightly different outcomes. Because of this, the uncertainty in these final upscaled results (fracture porosity and fracture permeability) was explored. The following steps were used:

1. The model domain was cut to a 3000ft diameter around the Wallewein well and isolated to only the Middle Duperow so to save on computation time.
2. The above described input parameters used in the final DFN were kept the same.
3. The seed variable used when generating the implicit and discreet fracture network was randomized and the model was run 17 times producing a slightly different result each time. This seed change resulted in the expected statistically similar result for each of the 17 model runs with a mean IJK permeability ranging from 39.00 to 40.75md; however, results at a specific location showed an expected variation.
4. The difference between these model runs was explored directly at a pseudo well that was placed in the model domain. When each model was generated, the permeability (IJK) values were extracted locally at the pseudo well.
5. At the pseudo well, for each model run, the IJK permeability values were averaged and displayed in a histogram. It was found that at any location within this model domain, the average permeability (IJK) values in the Middle Duperow could range from 32 to 47md (Figure 58). This range is significant; however, it is within tolerable ranges.

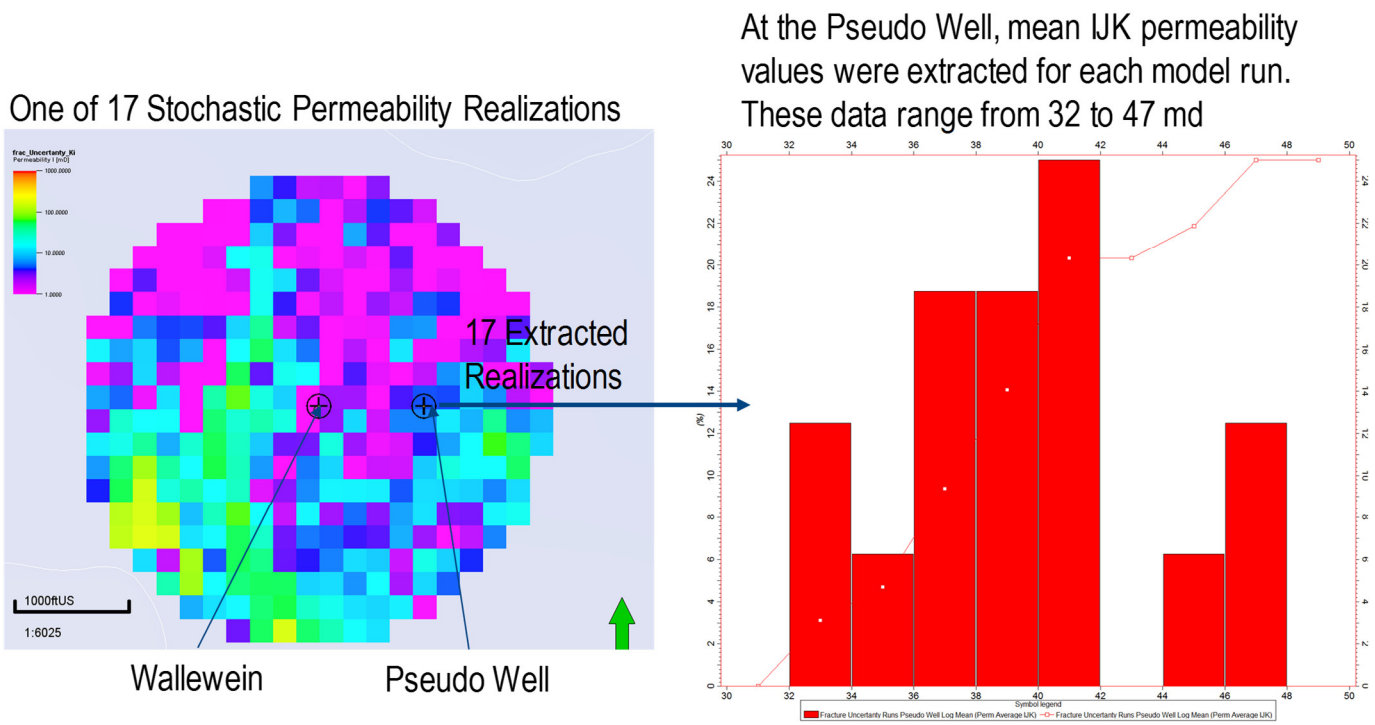

Figure 58: Pseudo well uncertainty analysis of 17 realizations of mean IJK permeability

6 Property Extrapolation

All of the above modeling processes were limited to the footprint of the 3D seismic, the challenge was to then extrapolate the model properties into the rest of the 20km*20km model domain (Figure 59). The model space outside the seismic footprint needs statistically identical properties (range, sill, nugget, function type and data distribution) populated for reservoir simulation efforts; if this was not completed, the boundary of the 3D seismic would have acted as a boundary condition for dynamic simulations. The extrapolated properties outside the seismic footprint are not conditioned to any other data, however, they do honor the statistics of the model. For the 3-Rock Type and 8-Rock Type methods, a facies model was generated without using the seismic data for conditioning. A merged facies model was generated at the 3D seismic boundary, the facies model conditioned to the seismic was used within the seismic boundary and the version without seismic was used outside the boundary. The fit between the two methods was reasonable. The following properties were extrapolated:

- 8-Rock Type Properties
    - 8-Rock Type Facies
    - Porosity
    - Permeability
- 3-Rock Type Properties
    - 3-Rock Type Facies
    - Porosity
    - Permeability

The extrapolation of the fracture properties was more difficult. To do this, for each property and for each formation, the property statistics were extracted (range, sill, nugget, function type and data distribution). Synthetic properties were generated that use these extracted statistics. These synthetic properties are not conditioned to any local data and only honor the property statistics. At the 3D seismic boundary, the synthetic properties and calculated properties were blended together over a 600 feet distance. The following fracture properties were extrapolated:

- Fracture Properties
    - Porosity
    - I-Permeability
    - J-Permeability
    - K-Permeability
    - Sigma (Matrix coupling factor)

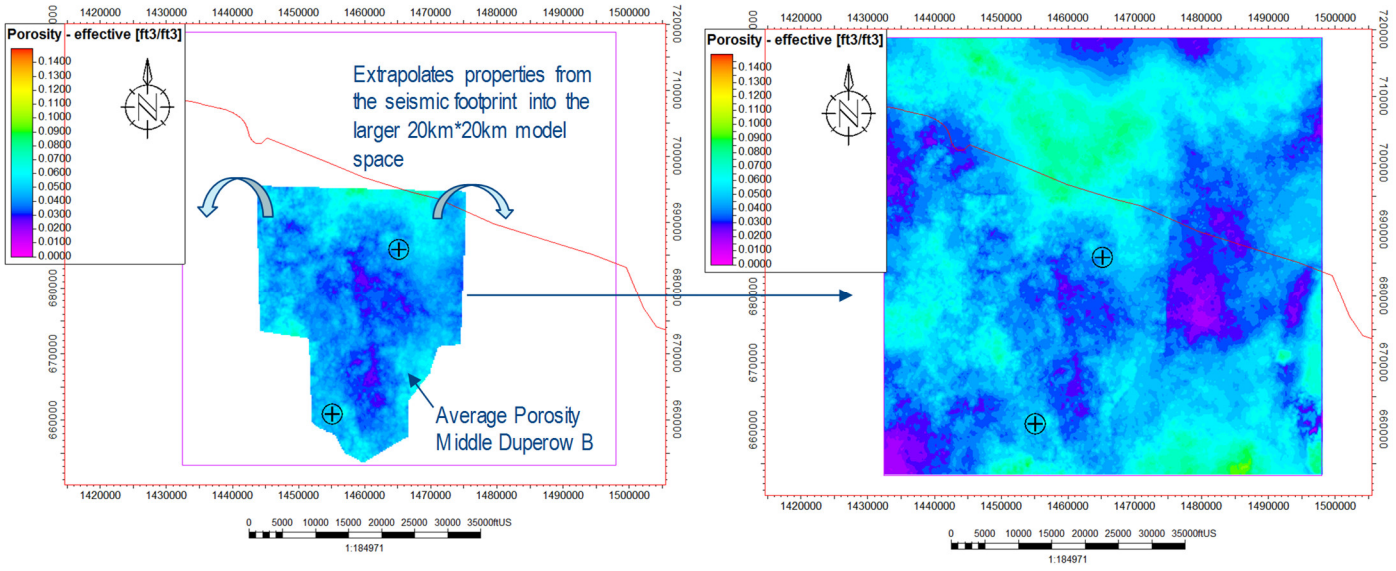

Figure 59: Model property extrapolation average porosity example

7 Kevin Dome Scale Model

A coarser resolution model was also generated that extrapolates the facies, porosity, permeability and fracture properties from the detailed model domain to cover the Kevin Dome (Figure 60). The surface area of the model covers the Kevin Dome limited to the spill point of the Intermediate Duperow. This coarser model contains only a million cells and only covers the Middle Duperow and Middle Duperow_B.

For the 8-Rock Type method of property distribution, additional wells with ELAN petrophysics were used for facies porosity and permeability modeling because they are within this larger Kevin Dome scale model domain. The seismic lithology prediction workflow was not used on this larger coarser model; however, the geospatial statistics were used to guide facies and property interpolation.

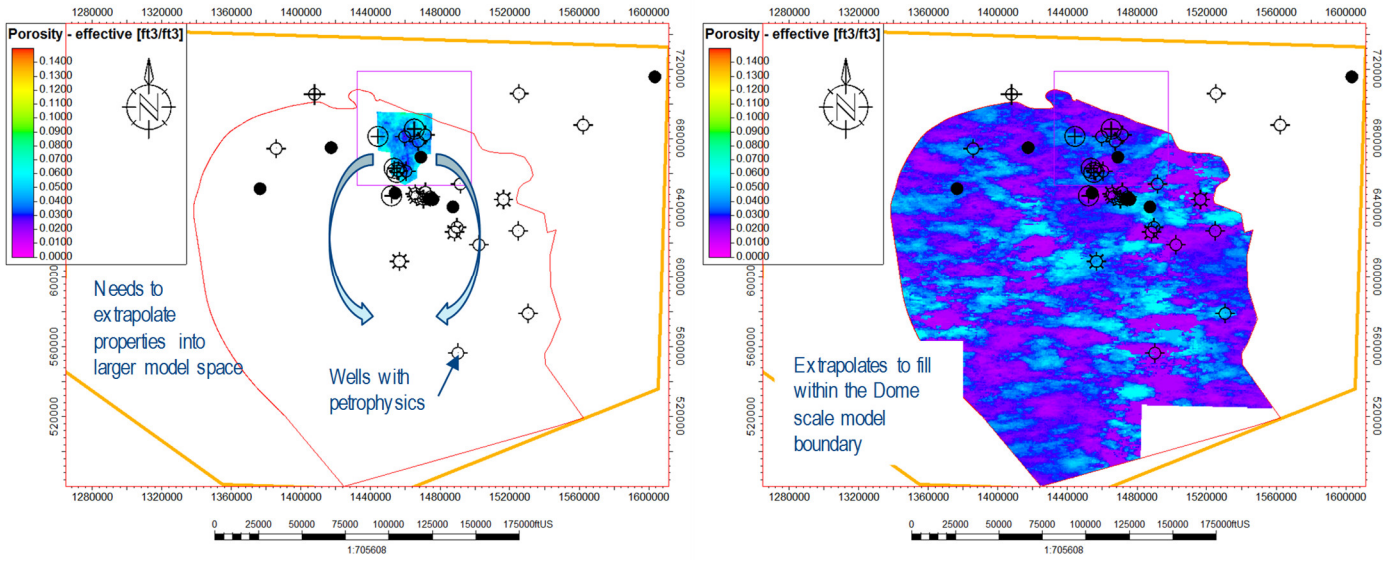

Figure 60: Kevin Dome scale model extrapolation average porosity for Middle Duperow_B

For fracture modeling across the Kevin Dome scale model, the below fracture properties were upscaled from the detailed model (described in Section 5) into this larger model and extrapolated to the model boundary using the techniques discussed in Section 6. The below properties were upscaled and extrapolated:

- Porosity
- I-Permeability
- J-Permeability
- K-Permeability
- Sigma (Matrix coupling factor)

8 Discussion

Progressive development of the Kevin Dome geomodel may be generalized into three versions, Geomodel Version 1, Geomodel Version 2 and Geomodel Version 3. Geomodel Version 1 was a preliminary model that incorporated all data available in late 2014 and was built over a larger regional area (64 miles east to west and 44 miles north to south). This was to be a preliminary version of the model until the 3D seismic data could be incorporated. This model comprises the first comprehensive regional data integration and geomodeling effort and represents a major milestone in the development of the understanding of the Kevin Dome and surrounding regions. Many hurdles were encountered regarding quality and completeness of legacy well log and seismic data and associated meta-data. While porosity and permeability estimates were poorly conditioned due to sparse well control, the consolidation of all available geologic and geophysical data and development of the regional geologic framework provided a valuable tool for advancing regional geological studies and a served as a framework for further improvement through later integration of 3D seismic data.

Geomodel Versions 2 and 3 were generated in 2016-2017 and was developed based on the framework from Geomodel Version 1. Because the scope of Geomodel Version 2 was focused on 3D seismic integration, the model extent was limited to the lateral limits of the 3D seismic footprint (6 miles in the east west and 8 miles north south) and vertically within the Devonian section. Seismic inversion attributes were used to better interpolate rock type, porosity, permeability and fracture intensity properties in the inter-well space. Key updates to Geomodel Version 3 include improvements to stratigraphic horizon interpretation, two methods for porosity interpolation (3-Rock Type and 8-Rock Type) and fracture modeling. Model properties were later extrapolated outside the seismic footprint to the 20km*20km model domain.

A 3-Rock Type model was developed, because porosity and permeability cross plots showed three trends, which are related to three dominate rock types (dolomite, limestone and anhydrite), a discreet log of these rock types was calculated at each well using an unsupervised neural network. A rock physics based lithology prediction workflow was used to provide an estimate of the most probable lithology in the inter-well geologic model space, and the likelihood associated with the prediction. These probability volumes were used to interpolate rock types between the wells. To complete this, seismic elastic inversion attributes were incorporated for lithology and porosity mapping using a Bayesian estimator based technique. This workflow represents a valuable probabilistic approach. To represent the porosity and permeability trends for these three rock types, porosity and permeability were interpolated separately within each rock type within each formation.

An 8-Rock Type model was also developed because Dave Bowen at MSU provided a depositional environment core log which was used to supervise a neuralnet process which predicted a depositional environment discreet log along the wells. As described above in the 3-Rock Type method, a rock physics based lithology prediction workflow was used to estimate of the most probable 8-Rock Type depositional environment in the inter-well geologic model space, and the likelihood associated with the prediction. These probability volumes were used to interpolate rock types between the wells. To represent the porosity and permeability trends for these three rock types, porosity and permeability were interpolated separately within each rock type.

A significant amount of fracturing was observed in the core and in the FMI logs; therefore, a discreet fracture network (DFN) was developed to quantify the fracture network's porosity and permeability. With most fracture modeling, there is a high degree of uncertainty; therefore, a sensitivity analysis was completed on three specific input parameters (aperture width, fracture intensity and fracture length. It was found that fracture aperture and the fracture intensity had a significant impact on the calculated fracture permeability while fracture length had a relatively minor impact. An uncertainty analysis was also completed to quantify how calculated permeability values can vary at specific locations with multiple model runs.

As part of Geomodel Version 3, a Dome Scale model version was developed. This coarser resolution model extrapolates the facies, porosity, permeability and fracture properties from the detailed model domain to cover the Kevin Dome. The surface area of the model covers the Kevin Dome limited to the spill point of the Intermediate Duperow. This coarser model only covers the Middle Duperow and contains only a million cells.

9 Signature Page

Report Prepared By:

Wade Zaluski. P.Geo.
Senior Geologist
Schlumberger

The Association of Professional Engineers, Geologists and Geophysicists of Alberta
Permit to Practice Number: P3551 (Schlumberger Canada)